



HAL
open science

From peridotite to listvenite – perspectives on the processes, mechanisms and settings of ultramafic mineral carbonation to quartz-magnesite rocks

Manuel D Menzel, Melanie J Sieber, Marguerite Godard

► To cite this version:

Manuel D Menzel, Melanie J Sieber, Marguerite Godard. From peridotite to listvenite – perspectives on the processes, mechanisms and settings of ultramafic mineral carbonation to quartz-magnesite rocks. *Earth-Science Reviews*, 2024, 255, pp.104828. 10.1016/j.earscirev.2024.104828 . hal-04637453

HAL Id: hal-04637453

<https://hal.science/hal-04637453v1>

Submitted on 6 Jul 2024

HAL is a multi-disciplinary open access archive for the deposit and dissemination of scientific research documents, whether they are published or not. The documents may come from teaching and research institutions in France or abroad, or from public or private research centers.

L'archive ouverte pluridisciplinaire **HAL**, est destinée au dépôt et à la diffusion de documents scientifiques de niveau recherche, publiés ou non, émanant des établissements d'enseignement et de recherche français ou étrangers, des laboratoires publics ou privés.



From peridotite to listvenite – perspectives on the processes, mechanisms and settings of ultramafic mineral carbonation to quartz-magnesite rocks

Manuel D. Menzel^{a,*}, Melanie J. Sieber^b, Marguerite Godard^c

^a Instituto Andaluz de Ciencias de la Tierra (CSIC – IACT), Av Palmeras 4, 18100 Armilla, Granada, Spain

^b Institute of Geosciences-Mineralogy, University Potsdam, 14476 Potsdam-Golm, Germany

^c Géosciences Montpellier, Université de Montpellier, CNRS, Montpellier, France

ARTICLE INFO

Keywords:

CO₂-fluid-rock interactions
Mineral carbonation
Peridotite alteration
Listvenite
Thermo-hydro-mechanical-chemical processes
Deep carbon cycle
CO₂ sequestration
Thermodynamic modelling
Ophiolites

ABSTRACT

Listvenites form by metasomatic transformation of variably serpentinized peridotites to carbonate-quartz rocks due to extensive reaction with CO₂-bearing aqueous fluids. This transformation sequesters large amounts of carbon since listvenites commonly contain >30 wt% CO₂. Although volumetrically a rare rock type, they occur in many ophiolites throughout much of the geological record, with preserved examples from the Archean to the present. Listvenites are highly interesting because they can form in the forearc mantle wedge, modulating deep carbon cycling. They further are natural analogues for optimal carbon sequestration by mineral carbonation.

Here we elucidate the influence of different controlling variables and feedback mechanisms on natural listvenite formation, investigate which prerequisites and geodynamic settings are favorable, and discuss related implications for the deep carbon cycle and engineered CO₂ storage by mineral carbonation. Using thermodynamic fluid infiltration-fractionation models that simulate idealized, step-wise carbonation flow-through experiments, we quantify expected changes in volume, mass, solute transfer (e.g. Mg, Si mobility), redox conditions and pH with reaction progress in dependence of protolith composition, infiltrated fluid composition, temperature and pressure. The models agree well with experiments and natural observations of high-*T* carbonation but have limitations at low temperature ($T \lesssim 130\text{--}150\text{ }^{\circ}\text{C}$) where kinetic effects in experiments limit the approach to equilibrium. Our modeling and assessment of typical CO₂ concentrations in metamorphic/hydrothermal fluids highlight that listvenite formation requires high time-integrated fluid flux, which in turn requires dynamic renewal of permeability despite reactive volume expansion. As most known listvenites crop out along tectonic contacts between crustal and ultramafic rocks in ophiolites that delineate major orogenic sutures, key factors controlling CO₂ supply are deviatoric stress and related deformation. Listvenite microstructures indicate that important hydro-mechanical-chemical feedback processes allowing continued fluid flux during carbonation are brittle fracturing and vein formation, reaction-enhanced ductile deformation, and local mass redistribution due to solute transfer. These feedback processes critically influence carbon flux pathways and the extent of CO₂ sequestration, but are not yet well understood as they are challenging to reproduce experimentally and by modeling. The CO₂ source for listvenite formation is most commonly inferred to be metamorphic devolatilization and/or dissolution of carbonate \pm organic carbon bearing meta-sediments. Less commonly reported are mantle or magmatic CO₂ sources. First-order thermodynamic modeling indicates that listvenites may be a direct consequence of meta-sediment devolatilization in subduction zones, while their formation at low pressure conditions requires rapid, large scale ascent and cooling of deep sourced fluids along shear or fault zones. The latter setting is reminiscent of induced mineral carbonation by subsurface CO₂ injection. The microstructural and chemical record of listvenites thus provides a means to investigate hydro-mechanical-chemical feedbacks during carbonation reaction progress at scales that cannot be achieved in laboratory experiments. Understanding these mechanisms is crucial for developing and validating strategies of engineered subsurface CO₂ sequestration by mineral carbonation.

* Corresponding author.

E-mail address: manuel.menzel@csic.es (M.D. Menzel).

1. Introduction

Two pressing research topics in Earth system sciences are (i) to understand the factors that maintained Earth as a habitable planet throughout its geological history, and (ii) to find ways to prevent climate from becoming human-hostile in the near future due to past and current industrial greenhouse gas emissions. For both of these questions, CO₂-fluid-rock interactions in ultramafic lithologies may play a significant role, because they can lead to geologically fast and extensive sequestration of mobile aqueous CO₂ into solid carbonate (e.g., [Beinlich et al., 2020a](#); [Kelemen et al., 2011](#)).

Earth's long-term habitability depends, among other factors, on the carbon flux balance between surface (atmosphere, oceans, biosphere, sediments and weathered rock) and the volumetrically much larger deep Earth reservoirs (Earth's mantle and mid to lower crust) ([Dasgupta, 2013](#)). Over the last two decades, much progress has been made to constrain the deep carbon cycle with respect to carbon inputs into subduction zones, modeling of carbon release from subducted slabs, and volcanic and metamorphic outgassing (e.g., [Galvez and Pubellier, 2019](#); [Müller et al., 2022](#); [Plank and Manning, 2019](#); [Sverjensky, 2019](#)). The "cold nose" of the forearc mantle wedge of subduction zones acts as a carbon trap for CO₂-bearing fluids released from the subducting slab due to peridotite carbonation, but the extent of this process is essentially unknown despite potentially being very high ([Barry et al., 2019](#); [Kelemen and Manning, 2015](#)). Another major uncertainty in the carbon cycle of subduction zones is the role of slab-parallel ascent of CO₂-bearing fluid (e.g., [Epstein et al., 2021](#)). For instance, CO₂ released from the slab may rise along the plate interface into the forearc instead of vertical infiltrating the subarc mantle wedge, thereby escaping the return flux via arc magmatism. Peridotite carbonation along the subduction plate interface can trace this process.

Prolonged interaction of aqueous CO₂-bearing fluid with peridotite can form listvenite, a carbonate-quartz rock that sequesters >30 wt% CO₂ ([Halls and Zhao, 1995](#); [Hansen et al., 2005](#)). Experiments have shown that listvenites can in principle form at high pressure conditions (1.0–2.5 GPa, 350–750 °C) in the forearc mantle wedge and within the subducted slab if CO₂ concentrations in fluids are high ([Sieber et al., 2018](#); [Sieber et al., 2020](#)). A volume of 1 km³ forearc peridotite fully carbonated to listvenite (230–290 Mt. C) represents a carbon storage equivalent to 4–7 times the annual carbon input into global subduction zones (40–66 Mt. C) ([Kelemen and Manning, 2015](#)). Carbonation of forearc peridotite thus has a large potential to modulate deep carbon fluxes, but the extent of this is unknown.

After being of interest mainly for gold exploration ([Aydal, 1990](#); [Buisson and Leblanc, 1985](#); [Emam and Zoheir, 2013](#); [Qiu and Zhu, 2015](#)), listvenites received increasing scientific attention throughout the last two decades following the proposition that they are natural analogues for carbon sequestration by mineral carbonation ([Goff and Lackner, 1998](#); [Hansen et al., 2005](#); [Kelemen and Matter, 2008](#)). Greenhouse gas emissions have led to substantially higher global atmospheric CO₂ concentrations than ever experienced before by humans ([IPCC, 2021](#)) and CO₂ concentrations are still rising as of 2020–2023 ([NOAA, 2023](#)). While not suitable to justify further burning of fossil fuels, negative carbon emission methods such as carbon sequestration and geological storage comprise a necessary part of the efforts to alleviate climate breakdown even if the transition to a net zero greenhouse gas economy is faster than expected ([IPCC, 2023](#)). Subsurface geological carbon storage by mineral carbonation of ultramafic rocks may be one promising strategy since peridotite carbonation safely stores CO₂ in solid carbonates, through a reaction that is exothermic and geologically fast ([Beinlich et al., 2020a](#); [Kelemen and Matter, 2008](#); [Kelemen et al., 2011](#); [Sanna et al., 2014](#)). Artificially induced formation of 1 km³ listvenite theoretically has the potential to store about 1.5% of annual global greenhouse gas emissions (the latter being >15,000 Mt. C/yr in 2015–2019 across all sectors; [IPCC, 2023](#)). Main hindrances besides economic factors are however the low permeability of peridotites, the

tendency of volume-increasing reactions like hydration and carbonation to clog porosity, and that subsurface reactive systems are not accessible to direct observation, with laboratory experiments necessarily being limited by time and size. Fossil natural listvenite occurrences prove that pervasive, complete carbonation of ultramafic rock by interaction with CO₂-bearing aqueous fluid is possible, likely in a variety of contexts ([Table 1](#)). These natural analogues provide important insights into the interplay between permeability and reaction during carbonation at temporal and spatial scales that are not accessible in experiments.

Although much knowledge has been gained throughout the past decades, various fundamental questions about listvenite formation remain open and are subject to debate. For example, which processes are the most relevant to allow complete transformation into carbonate-quartz despite mass addition and volume increase? In which geodynamic settings do listvenites form in nature? How fast is peridotite carbonation in different tectonic contexts, and which are the rate limiting processes? Which processes are important at the nanometer, hand-specimen to outcrop scales, and which meso-scale insights from natural examples of peridotite carbonation are transferable to technical applications of carbon capture and storage? To address these questions, among others, we critically discuss the state of knowledge of listvenite formation combining a review of natural field, experimental and theoretical studies with new thermodynamic modeling, with a particular focus on the conditions, feedback processes and tectonic environments.

1.1. Definitions and preferred nomenclature

The term listvenite (also spelled listwanite or listwaenite in literature) refers to a rock composed of magnesian carbonates and quartz that is formed by metasomatic reaction of an ultramafic protolith with CO₂-bearing fluids ([Halls and Zhao, 1995](#); [Hansen et al., 2005](#)). Carbonate typically is magnesite with variable Fe content along the magnesite-siderite solid solution or less frequently dolomite (± calcite). Alteration of relict Cr-spinel is commonly linked to the formation of Cr-bearing muscovite (fuchsite, occasionally mariposite), if fluids are potassium bearing. Interaction of CO₂-bearing fluid with ultramafic rock causes a typically stepwise replacement reaction sequence forming with increasing reaction progress carbonate-bearing serpentinite (termed ophicalcite in the following), talc-carbonate rock (soapstone), and carbonate-quartz rock (listvenite) if CO₂ concentrations and fluid replenishment are high enough ([Frost, 1985](#); [Halls and Zhao, 1995](#); [Klein and Garrido, 2011](#)). We favor a genetic-compositional definition of listvenite as fully carbonated ultramafic rock, where most divalent cations are contained in carbonate, most silica is in quartz, chalcedony or opal, and an ultramafic protolith is evidenced by Cr-spinel relicts or other criteria, but, in contrast to [Halls and Zhao \(1995\)](#), we do not consider Cr-bearing muscovite a required phase.

The reaction sequence leading to listvenite formation is characterized by predominantly reactive replacement. This feature distinguishes listvenites from other carbonated peridotites that mainly form by additive carbonate precipitation and that are usually not genetically related to listvenites. The latter include (i) ophicalcites, formed by calcite and/or aragonite precipitation in vein networks, breccias and as a cement between ultramafic clasts in serpentinitized peridotites exposed at the seafloor (e.g., [Schwarzenbach et al., 2013](#)); (ii) carbonate veins cross-cutting serpentinitized peridotites at the sub-seafloor (e.g., [Schroeder et al., 2015](#); [Ternieten et al., 2021a](#)) or in the weathering horizon of ophiolites (e.g., [Noël et al., 2018](#); [Ternieten et al., 2021b](#)); (iii) subaerial magnesite deposits that lack co-genetic quartz, formed in playa environments ([Power et al., 2019](#)); and (iv) carbonate travertine deposits of serpentinite-hosted (hyper)alkaline springs (e.g., [Chavagnac et al., 2013](#); [Giampouras et al., 2019](#)). Similar to the ophicalcite-soapstone-listvenite carbonation sequence, magnesite-enstatite rocks (sagvandites) form by reactive replacement during CO₂ metasomatism, but at higher temperatures of 500–600 °C ([Schreyer et al., 1972](#)).

Some authors further distinguish between carbonate-rich and

Table 1

Selected examples of listvenite occurrences from different ages and settings and some of their (known/interpreted) characteristics.

Abbreviation	Cenozoic			Mesozoic			
	SAF	App	Tin	BT1	Sis	Atl	Lou
Host rock unit; context; location	San Andreas fault California, USA	Ligurian ophiolite, Northern Appenines, Italy	Tethyan exhumed metamorphic terrane, Cyclades, Tinos, Greece	Samaï ophiolite, Oman Drilling Project Hole BT1B, Oman	Birjand ophiolite, Sistan Suture Zone, Iran	Canadian Cordillera ophiolites, Atlin, British Columbia	Loubusa ophiolite, Tibet, China
Inferred tectonic setting of carbonation	active transform fault (a-seismic creeping section)	syn-tectonic during post-obduction extensional faulting of Tethyan ophiolite	post-peak metamorphism and thrusting (?) but before post-collisional magmatism	during thrusting coeval with mature subduction, ophiolite emplacement, or post-obduction extension	forearc subduction transitioning to continental collision	carbonation during/ after ophiolite emplacement?	Supra-subduction zone ophiolite (175 Ma), carbonation context unclear
Structural context	aseismic sections along strike-slip fault branches	along deep rooted, crustal-scale extensional faults	close to or along faulted contact with lower HP/LT metamorphic unit	along basal thrust between basal peridotite and metamorphic sole; coeval with deformation	along or close to large scale fault branch(es)	along faulted contact to meta-basalts and accretionary units; along faults	along boundary fault of ophiolite. Sharp fault contact to triassic flysch
Timing of carbonation (method)	present-day (inferred from spring fluid compositions)	Late-Miocene-Early Pliocene (based on tectono-metamorphic context)	16 Ma / 19 Ma (internal Rb-Sr isochron of fuchsite/ magnesite separates & bulk rock)	97 ± 29 Ma (internal Rb/Sr isochron)	uncertain; Eocene-Oligocene if during ophiolite obduction	168–172 Ma? (Ar-Ar in Cr-muscovite)	unknown; during or after tectonic emplacement of ophiolite?
Protolith	lizardite-chrysotile serpentinite	fully serpentinized harzburgite	fully hydrated and sheared Atg-dominated serpentinite	serpentinized banded harzburgite / lherzolite	partially serpentinized harzburgite	mostly harzburgite-lherzolite, some dunites, rare websterite	serpentinized dunite; Cpx-bearing harzburgite
Listvenite assemblages	Mgs-Qtz, ±opal/chalcedony	Mgs-Dol, opal/chalcedony, smectite	Mgs-Qtz, CrSp, Fuchs, Chl, Ab, Mag	Mgs-Qtz-CrSp-Fuchs Dol-Mgs-Qtz-CrSp	Mgs-Qtz ± Dol, Py, CrSp, FeOx, Fuchs	Mgs-Qtz-CrSp	Mgs-Tlc-Qtz ± Dol, CrSp, Py, FeOx
Associated carbonated rocks	dolomite-quartz veins Tlc-Mgs at depth? (inferred)	dolomite-bearing serpentinite, ophicarbonate breccias	none (isolated listvenite bodies embedded in meta-sediments)	Mgs-bearing serpentinite Dol-bearing serpentinite Mgs-Tlc-Serp (rare) Mgs-Serp-Qtz (rare)	Carb-bearing Atg-serpentinite Mgs-Tlc-Atg (rare) birbirite	Mgs-bearing serpentinite Tlc-Mgs rocks	Tlc-Mgs rocks
Carbonation temperature	at depth 100–300 °C? spring fluids: < 55 °C	< 100 °C? (presence of opal-CT)	250–350 °C? (Chl thermometry)	100 ± 46 °C; early veins possibly up to 250 °C? (clumped isotopes)	uncertain, < 280 °C	210–280 °C (fluid inclusions in quartz-carbonate veins)	unknown
Inferred CO₂ source	mantle & metamorphic devolatilization of crustal lithologies	mantle CO ₂ mixed with meteoric water	deep hydrothermal infiltration of seawater-originated fluid?	partially subducted / underthrust meta-sediments	metasediments?	unkown	unkown
Main references	Barne/s et al., 1973; Klein et al., 2022	Rielli et al., 2022	Hinsken et al., 2017	Kelemen et al., 2022; Falk and Kelemen, 2015; Beinlich et al., 2020a; de Obeso et al., 2022; Menzel et al., 2022a; Godard et al., 2021	Aftabi and Zarrinkoub, 2013; Boskabadi et al., 2020	Hansen et al., 2005 (& references therein) Cutts et al., 2021; Tominaga et al., 2023	Zhang et al., 2015; Robinson et al., 2005

Abbreviation	Paleozoic				Proterozoic		Archean	
	Tia	Sar	Adv	Lin	WAS	ANS	Abi	Bar
Host rock unit; context; location	Tianshan orogenic belt, Western China	Sartohay ophiolitic melange; Xinjiang, China	Baie Verte Ophiolites, Advocate Complex, Newfoundland, Canada	Norwegian Caledonides, Linnajavri Norway	Neoproterozoic Western Arabian Shield, Saudi Arabia	Arabian-Nubian Shield, Egypt	Abitibi greenstone belt, Superior Province, Canada	Barberton greenstone belt, South Africa
Inferred tectonic setting of carbonation	during late stage of exhumation of subducted high-pressure units	possibly related to coeval magmatism. Listvenite is variably deformed / mylonitized.	during/after subduction of Laurentian margin beneath ophiolite (?) analogous to forearc setting; or during post-collisional magmatism	during caledonian orogenic thrusting of exhumed metamorphic terrane?	interpreted as 2-step process from forearc supra-subduction setting to ophiolite obduction	during ophiolite obduction?	Accretion of Abitibi and Pontiac subprovinces and related intrusive porphyries and albitite dikes (?)	deformation and multi-stage fluid infiltration along a basal thrust zone
Structural context	along contact of serpentinites to carbonate meta-sediments	in ophiolitic melange along faults at contact to and in basaltic rocks	along major fault zone separating mantle and crustal ophiolite fragments	along tectonic (?) contact of mantle fragments and meta-sediments	along imbricate thrust faults in the mantle ophiolite section	along shear zones	along local faults and shear zones	in banded/ mylonitic zone between gabbros and meta-pyroxenite
Timing of carbonation (method)	uncertain, < 300 Ma (HP peak metamorphic age)	296–304 Ma? (U–Pb in Zrn) or 280–277 Ma? (Zrn rims)	uncertain; if during obduction of Baie Verte ophiolite: 481–456 Ma	uncertain; during Caledonian orogeny?	uncertain, possibly Neoproterozoic	uncertain, possibly Neoproterozoic	<2704–2719 Ma (komatiite); ≥ 2617–2633 Ma (Ar/Ar in Fuchs & Pb/Pb in Rt)	Archean (possibly ≈ 3.23 Ga)
Protolith	metamorphic Atg-serpentinite	fully serpentinized harzburgite	partially serpentinized harzburgite	Atg-serpentinite (lherzolithic)	variably serpentinized harzburgite ± dunite	serpentinite; serp. Harzburgite	serpentinized komatiite	komatiite (?), partly basalt/gabbro (?)
Listvenite assemblages	Mgs-Dol-Qtz-Fuchs	Mgs-Qtz-CrSp, ±Chl, Fuchs, Py; trace Ap, Zrn	Mgs-Qtz-CrSp-Fuchs ± Chl, Py, Dol, Hem	Mgs-Qtz-CrSp ± Mag, Chl, Tlc, Ms., Bt, Ab, Tur, Ttn	Mgs-Qtz-CrSp ± Fuchs	Mgs-Qtz-CrSp ± Chl, Tlc, Fuchs, sulfides	Mgs-Qtz ± Dol, Fuchs, Chl, Rt	Cal/Dol-Qtz-Chl-Fuchs, ± CrSp, Py, Rt
Associated carbonated rocks	Mgs-serpentinite; ophiodolomite; carbonated meta-sediments	Serpentinite Tlc-Mgs rock and Tlc-schists	Mgs-Brc-bearing Atg-serpentinite; Atg-Tlc-Mgs rock; Qtz-Tlc-Mgs rock; Mgs-Fuchs rock	soapstone (Tlc-Mgs ± Chl, Mag) Dol-Tr bearing Atg-serpentinite	Qtz-rich listvenites, birbire minor (?) Mgs-Tlc	Tlc-Tr-Anth-Mgs rocks, Mgs-Qtz veins in Tlc-rich rocks	Tlc-Mgs rocks; Fuchs-Chl-Rt veins (decarbonated listvenite?)	carbonate-bearing or carbonatized gabbro; meta-pyroxenite with Carb-Qtz veins
Carbonation temperature	unknown	320–410 °C? (fluid inclusions in Qtz of gold deposit)	> 280 °C, < 420 °C (prograde lizardite to Brc + Atg reaction)	≈275 °C (d ¹⁸ O of Qtz-Mgs)	220–260 °C? (Chl-thermometry)	unkown	250–300 °C (fluid inclusions)	240–350 °C (Chl-thermometry)
Inferred CO₂ source	devolatilization of adjacent meta-sediments (?)	meta-sediment devolatilization due to magmatism (?)	partially subducted meta-sediments (?)	overthrust or host metasediments (?)	devolatilization of accretionary wedge/ subducted sediments?	metamorphic fluid	two magmatic-metamorphic fluids or fluid mixing?	unknown
Main references	Peng et al., 2020	Qiu and Zhu, 2018 Qiu and Zhu, 2015 Robinson et al., 2005	Menzel et al., 2018	Beinlich et al., 2012; Tominaga et al., 2017; Beinlich et al., 2020a	Gahlan et al., 2020 Gahlan et al., 2022 (& references therein)	Boskabadi et al., 2017; Moussa et al., 2021	Schandl and Gorton, 2012 (& references therein)	Grosch et al., 2012

(Mgs: magnesite; Qtz: quartz; Tlc: talc; Dol: dolomite; CrSp: Cr-spinel; FeOx: Fe-oxides; Mag: magnetite; Hem: hematite; Fuchs: Cr-muscovite; Ms.: muscovite; Bt: biotite; Chl: chlorite; Ab: albite; Plag: plagioclase; Tr: tremolite; Anth: anthophyllite; Py: pyrite; Rt: rutile; Zrn: zircon; Ap: apatite; Ttn: titanite; Tur: tourmaline)

silicate-rich listvenites. This is useful if the distinction is based on significantly higher or lower bulk rock M^{2+}/Si —where $M^{2+} = Mg, Fe, Ca, Mn, Ni$ —of listvenite in comparison to the protolith composition (Aftabi and Zarrinkoub, 2013; Boskabadi et al., 2020). We suggest that terms like carbonate-rich or silicate-rich listvenite should not be used to refer to listvenites with similar M^{2+}/Si as the protolith, and certainly not to carbonate-bearing serpentinite or talc-carbonate rocks. We caution further that the common presence of veins and structural heterogeneities in listvenites can cause an apparent chemical bimodality depending on the sample size selected for bulk rock analysis. Some low-temperature listvenites are related to peridotites altered to Cr-spinel and/or fuchsite bearing quartz rocks, which in places have been referred to as birbirites (e.g., Molly, 1959). Birbirite may form by continued or secondary alteration of listvenite (Akbulut et al., 2006; Austrheim et al., 2021; Klein and Garrido, 2011) or, unrelated to carbonation, by direct silicification of serpentinite due to Si-rich fluid infiltration or lateritic Mg leaching (Augustithis, 1967; Lacinska and Styles, 2013).

1.2. Spatial and temporal distribution of listvenite occurrences

Listvenite is a rare rock type, but small occurrences are present in many ophiolites and exhumed metamorphic ultramafic massifs worldwide (Fig. 1). Typically, listvenites crop out as several meter to 10's of meter thick lenses, associated with other variably carbonated and hydrated ultramafic rocks. Table 1 shows a compilation of listvenite occurrences that we selected to showcase comparatively well-studied examples of different ages and settings, with some of their key

characteristics as far as they are known or inferred. Many more reported listvenite occurrences exist (Aydal, 1990; Belogub et al., 2017; Boedo et al., 2015) (and references cited in Halls and Zhao, 1995). The exact timing and tectonic context of listvenite formation is in many cases subject of interpretation or even speculation. Nevertheless, two general observations appear evident: (i) listvenites have formed throughout much of Earth's history, with early examples from Archean greenstone belts possibly as old as 3.23 Ga (Grosch et al., 2012), and others as recent as 16–19 Ma (Hinsken et al., 2017) or even forming at present (Klein et al., 2022); and (ii) listvenites typically occur along tectonic contacts of crustal lithologies with ultramafic rocks in exhumed metamorphic terranes and in ophiolites that delineate major orogenic sutures. Accordingly, most listvenite occurrences are found in mantle rocks exhumed during different phases of orogenesis (Fig. 1). Many of the tectonic contacts comprising listvenites are plate boundary faults characterized by high CO_2 fluxes (Barnes et al., 1978). No listvenites are known from exhumed mantle along active spreading mid-ocean ridges or ocean-continent transitions. Recently discovered talc-magnesite rocks from the St. Paul Atlantic transform fault (Klein et al., 2024) suggest that listvenite formation may also be possible in some oceanic settings but have been missed so far due to comparatively scarce sampling.

Recent studies have proposed that processes similar to listvenite formation may also be active on extra-terrestrial bodies. Alteration of ferromagnesian silicate minerals to talc-carbonate-quartz could explain the CO_2 , methane and silica bearing composition of Enceladus' ocean, as inferred from material emitted from plumes at the moon's south pole (Glein and Waite, 2020; Hsu et al., 2015). On Mars, carbonates of magnesite-siderite composition have been reported in mafic / ultramafic

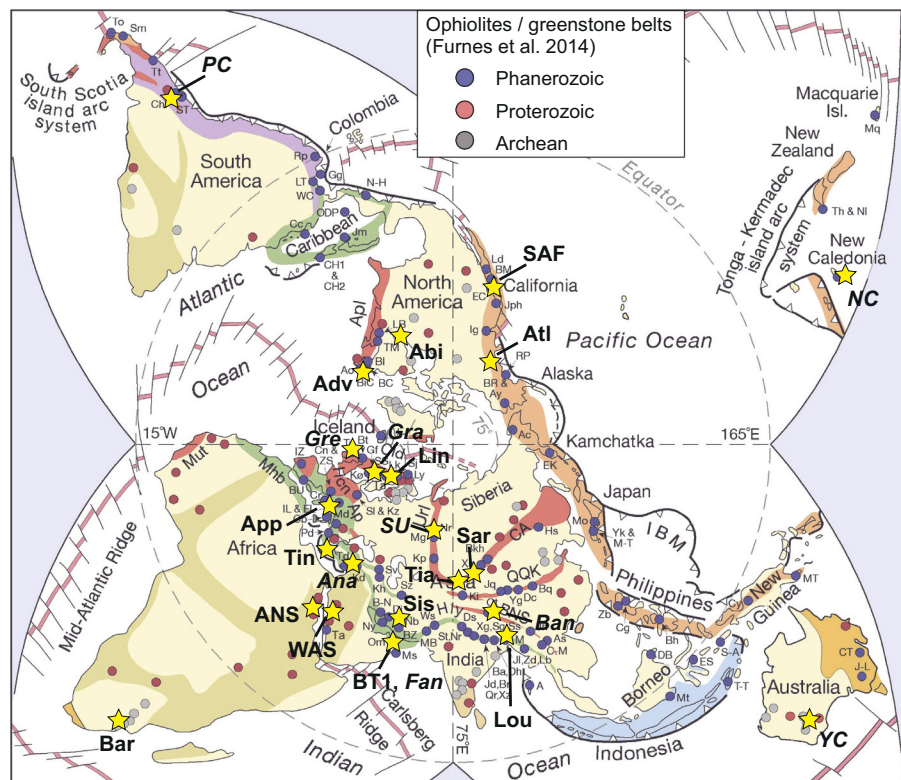


Fig. 1. A non-exhaustive compilation of the global distribution of listvenite occurrences reviewed in this study (yellow stars and abbreviations), in relation to ophiolites and greenstone belts and Proterozoic to Phanerozoic orogenic systems (colored regions) from Furnes et al. (2014) (their Fig. 1; reprinted here without changes). For most occurrences, see Table 1 for details. Listvenites not listed in Table 1 are: **PC**: Argentine Precordillera mafic-ultramafic belt (Boedo et al., 2015); **NC**: New Caledonia magnesite-quartz and talc-carbonate alterations (Spandler et al., 2008; Ulrich et al., 2014); **Gra**: Graberget, Norway (Austrheim et al., 2021); **Gre**: Greggenbaun, Ireland (Halls and Zhao, 1995); **SU**: South Ural, various occurrences (Belogub et al., 2017); **Ana**: Anatolia, Eastern Turkey, various occurrences (Akbulut et al., 2006; Aydal, 1990); **Fan**: Fanjah listvenites, Samail ophiolite, Oman (related to BT1 listvenites) (Decrausaz et al., 2023; Falk and Kelemen, 2015; Nasir et al., 2007; Scharf et al., 2022; Stanger, 1985); **Ban**: Bangong suture, Tibet, China (Ji et al., 2022); **YC**: Yilgarn craton carbonated komatiites, Western Australia (Davis et al., 2001). (For interpretation of the references to colour in this figure legend, the reader is referred to the web version of this article.)

lithologies in Jezero crater (Clavé et al., 2023; Farley et al., 2022) as well as several other locations (see Table 3 in Clavé et al. (2023)) and in Martian meteorites (Steele et al., 2022). Although some of these surface occurrences may rather be analogous to terrestrial magnesite playa deposits (Scheller et al., 2021), they suggest that peridotite carbonation had been active on Mars, possibly including listvenite formation.

1.3. Bulk chemical characteristics of listvenites

The bulk rock chemistry of listvenites reflects that of the ultramafic protolith (e.g., dunite, harzburgite, lherzolite, komatiite; Table 1) combined with the geochemical imprint of volatiles and fluid-mobile elements gained or lost during reactive fluid flow. The reaction sequence forming ophicarbonates, soapstone and listvenite can proceed solely by continued addition of CO₂ (carbonation is isochemical with respect to non-volatile elements), but depending on the conditions some major elements may be added or leached by the percolating fluid. This can lead to divalent metal and Si enrichment or depletion during listvenite formation (non-isochemical carbonation). Although the resulting chemical modifications can be significant, analysis of the bulk major and trace element composition together with the composition of relict Cr-

spinel often allows to infer the protolith of listvenites (e.g., Godard et al., 2021).

Fig. 2 shows a compilation of bulk rock Mg/Si and Ca/Mg versus the CO₂ content of various listvenites and associated carbonated peridotites. While not sufficient to discriminate the protolith prior to carbonation, this illustrates some commonly observed first-order variations. Relative to typical protolith compositions, high-temperature listvenites series often show carbonation at constant Mg/Si with increasing CO₂ (empty symbols in Fig. 2a). In contrast, the formation of low-temperature listvenite (e.g., the Oman Drilling Project (Oman DP) Hole BT1B listvenites and similar carbonation sequences in the Birjand ophiolite of Iran) is commonly non-isochemical at the scale of bulk chemistry samples (Fig. 2a).

Although most listvenites are magnesite-rich and thus have low bulk rock Ca/Mg, some dolomite-rich listvenites show substantial Ca gain, exceeding the contents expected even for a protolith that was locally enriched in clinopyroxene (Fig. 2b). Ca gain may occur during carbonation, e.g. due to aqueous CaHCO₃⁺ in the infiltrating fluid, but may also be the result of secondary overprint of listvenite.

Listvenites can preserve part of the signatures of their inferred ultramafic protoliths for most lithophile trace elements (e.g., Rare Earth

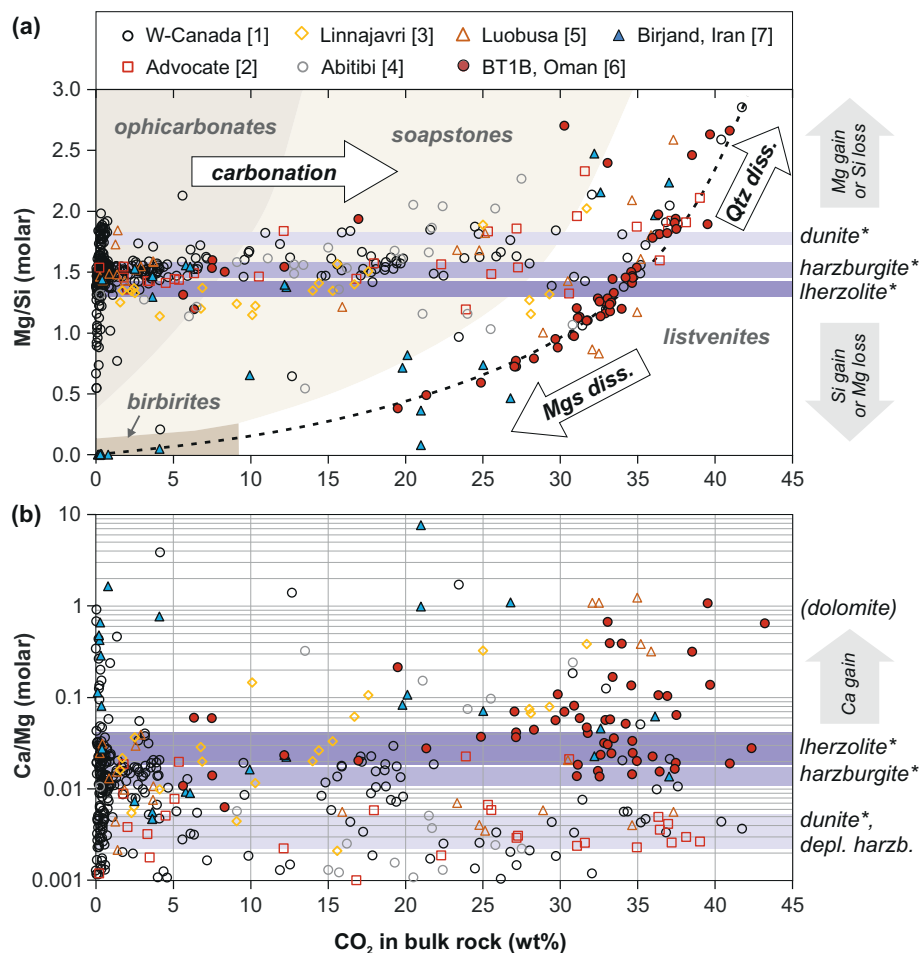


Fig. 2. Molar Mg/Si (a) and Ca/Mg (b) element ratios versus CO₂ content in natural carbonation sequences related to listvenite formation. Data from: [1] various ophiolites in W-Canada (Cutts et al., 2021), [2] Advocate ophiolite, Newfoundland, Canada (Menzel et al., 2018), [3] Linnajavri, Norway (Beinlich et al., 2012), [4] Abitibi belt, Ontario, Canada (Schandl and Gorton, 2012), [5] Luobusa ophiolite, Tibet, China (Zhang et al., 2015), [6] Oman BT1B listvenite (Godard et al., 2021), and [7] Birjand ophiolite, Iran (Aftabi and Zarrinkoub, 2013). While the higher temperature carbonation sequences (empty symbols) are mostly consistent with isochemical carbonation, the low temperature Oman and Birjand listvenites (filled symbols) show significant modification of Mg/Si and Ca/Mg compared to average dunite, harzburgite or lherzolite protoliths (grey bars, after Godard et al. (2000) and Hanghøj et al. (2010); and McDonough (1990) for average continental lithospheric mantle lherzolite). Fields in a) for ophicarbonates, soapstone (both serpentine- and quartz bearing talc-magnesite rocks), listvenites and birbirites are approximate. The dashed line in a) shows the expected theoretical trend if all Mg is hosted in magnesite and all Si in quartz, which may reflect the effects of quartz and magnesite dissolution (Qtz/Mgs diss.).

Table 2
Reactions involved in peridotite carbonation for the simplified (Fe)-Mg-Si-O-H-C chemical system.

<u>Direct carbonation (CO₂-dominated fluid)</u>	
Mg ₂ SiO ₄ + 2 CO _{2, aq} = 2 MgCO ₃ + SiO ₂	R1
olivine + CO _{2, aq} = magnesite + quartz/chalcedony (listvenite)	
2 Mg ₂ SiO ₄ + 2 CO _{2, aq} = 2 MgCO ₃ + Mg ₂ Si ₂ O ₆	R2
olivine + CO _{2, aq} = magnesite + orthopyroxene (sagvandite)	
<u>Stepwise hydration and carbonation reaction sequence (CO₂-bearing aqueous fluid)</u>	
4 Mg ₂ SiO ₄ + Mg ₂ Si ₂ O ₆ + 7 H ₂ O = 3 Mg ₃ Si ₂ O ₅ (OH) ₄ + Mg(OH) ₂	R3
olivine + orthopyroxene + H ₂ O = lizardite/chrysotile + brucite (serpentinization)	
Mg(OH) ₂ + CO _{2, aq} = MgCO ₃ + H ₂ O	R4
brucite + CO _{2, aq} = magnesite + H ₂ O (ophicarbonate)	
17 Mg ₃ Si ₂ O ₅ (OH) ₄ + 3 CO _{2, aq} = 3 MgCO ₃ + Mg ₄₈ Si ₃₄ O ₈₅ (OH) ₆₂ + 3 H ₂ O	R5
lizardite/chrysotile + CO _{2, aq} = magnesite + antigorite + H ₂ O (ophicarbonate)	
2 Mg ₃ Si ₂ O ₅ (OH) ₄ + 3 CO _{2, aq} = 3 MgCO ₃ + Mg ₃ Si ₄ O ₁₀ (OH) ₂ + 3 H ₂ O	R6*
lizardite/chrysotile + CO _{2, aq} = magnesite + talc + H ₂ O (soapstone)	
Mg ₃ Si ₄ O ₁₀ (OH) ₂ + 3 CO _{2, aq} = 3 MgCO ₃ + 4 SiO ₂ + H ₂ O	R7
talc + CO _{2, aq} = magnesite + quartz + H ₂ O (listvenite)	
Mg ₃ Si ₂ O ₅ (OH) ₄ + 3 CO _{2, aq} = 3 MgCO ₃ + 2 SiO ₂ + 2 H ₂ O	R8**
lizardite/chrysotile + CO _{2, aq} = magnesite + quartz/chalcedony + H ₂ O (listvenite)	
$\left\{ \begin{array}{l} 3 \text{CO}_{2, \text{aq}} + 3\text{H}_2\text{O} = 3 \text{HCO}_3^- + 3 \text{H}^+ \\ \text{Mg}_3\text{Si}_2\text{O}_5(\text{OH})_4 + 3\text{H}^+ = 3 \text{Mg}^{2+} + 2 \text{SiO}_{2, \text{aq}} + 3 \text{OH}^- + 2 \text{H}_2\text{O} \\ 3 \text{Mg}^{2+} + 3 \text{HCO}_3^- + 3 \text{OH}^- = 3 \text{MgCO}_3 + 3 \text{H}_2\text{O} \\ 2 \text{SiO}_{2, \text{aq}} = 2 \text{SiO}_2 \end{array} \right.$	
<u>Important redox reactions</u>	
3 FeO (ol, opx) + H ₂ O (+ CO ₂) = Fe ₃ O ₄ + H _{2, aq} (+ C _{org} + CH ₄)	R9
Fe ²⁺ in olivine/pyroxene + water = magnetite + hydrogen	
Fe ₃ O ₄ + CO _{2, aq} = FeCO ₃ + Fe ₂ O ₃	R10
magnetite + CO _{2, aq} = Fe ²⁺ in magnesite + hematite	

(*) with antigorite instead of lizardite/chrysotile the product stoichiometry is approx. 2.65 magnesite +1 talc.

(**) As an example and to illustrate the relation with pH, balanced sub-reactions of dissolution and precipitation are given for reaction R8. Note that the choice of fluid species here is arbitrary, the sub-reactions may also be formulated differently. Similar sub-reactions can be formulated for all other reactions.

Elements). In addition, they are often enriched in fluid mobile trace elements such as potassium —commonly hosted in Cr-bearing muscovites or kaolinite— and Li, Ba, Cs, Sr, Pb, As, and Sb (Boskadi et al., 2020; Godard et al., 2021; Hinsken et al., 2017). Sulfur can be enriched in listvenites containing pyrite and other sulfides, which in turn may or may not host precious metal enrichments such as Ag and Au (Emam and Zoheir, 2013; Escayola et al., 2009; Qiu and Zhu, 2015). Fluid-mobile major and trace element compositions typically show a large variability between different hand specimens of the same listvenite outcrops. Except for Ca and Sr (both enriched in dolomite), systematic correlations characterizing elements of similar affinities (e.g., K, Cs) are rarely observed in listvenites. This may be due in part to the scarcity of representative geochemical datasets on these rocks, which have been analyzed mostly for characterizing ore-potentials (Au, Ag, Cu, Hg, ...) with a focus on mineralized zones of high economical interest. This variability complicates the interpretation of (trace element) geochemical signatures unless clear correlations can be observed, for example with deformation intensity (Qiu and Zhu, 2018).

2. Carbonation reaction sequence

2.1. Main carbonation reactions

Carbonation of ultramafic rocks can proceed via various reactions (Table 2). Which reaction path carbonation follows depends on a variety of factors such as the mineralogy of the precursor rock, P–T (pressure–temperature) conditions, the fluid composition, and the amount of fluid that interacts with a given volume of rock over time (i.e. the time-integrated fluid-rock ratio, f/r). The detailed effect of these factors will be discussed in subsequent parts of this contribution (sections 2.1–3.3). As non-polar fluids like pure supercritical CO₂ have a low relative

permittivity (dielectric constant) that does not favor dissolution of silicates, carbonation progress requires an aqueous fluid consisting of a mixture of H₂O and CO₂. (CO_{2, aq} in Table 2). We therefore refer throughout the manuscript to the CO_{2, aq} concentration when using terms such as CO₂-peridotite interaction or CO₂-bearing fluid.

If the fluid is CO₂-dominated (CO₂ > H₂O), primary silicates like olivine and pyroxenes may directly react to magnesite and quartz (e.g. R1 in Table 2) or magnesite and enstatite (R2 in Table 2). Such CO₂-dominated aqueous fluids can form during metamorphism at elevated temperatures and comparatively low pressures (e.g. > 500 °C, < 1 GPa) (e.g., Groppo et al., 2022). More commonly, carbonation is caused by infiltration of CO₂-bearing aqueous fluid (where H₂O > CO₂). In these cases, the reaction pathway typically follows a stepwise sequence of hydration and carbonation reactions (R3 – R8, Table 2). Low CO₂ input, either due to low CO₂-concentration in the infiltrating fluid or small fluid/rock-ratios, leads to hydration of olivine and pyroxene, forming lizardite/chrysotile and minor brucite (reaction R3). This hydration reaction releases hydrogen due to oxidation of ferrous iron from olivine and orthopyroxene to ferric iron in serpentine-group minerals and magnetite (reaction R9). In presence of CO₂, serpentinization may form magnesite instead of brucite (c.f. R4), and organic carbon compounds or methane in detriment of hydrogen (R9). High CO₂ supply due to elevated CO₂-concentrations and higher fluid-rock ratios causes reactions that form increasingly Si-rich reaction products (antigorite, talc, and quartz/chalcedony) as divalent cations are redistributed into carbonate (R5 – R8). The direct formation of listvenite from serpentine (R8) is common in low-temperature settings where talc precipitation is sluggish (< 130–150 °C). Carbonation experiments (Sieber et al., 2020) have shown that direct replacement of serpentine by quartz-magnesite (R8 instead of R4 – R7; Table 2) may also occur at elevated temperatures in domains of high CO₂ supply. This indicates that departures from a

(rock-buffered) equilibrium reaction sequence with intermediate talc-magnesite formation may also occur in nature where CO_2 concentrations, instantaneous fluid-rock ratios and/or fluid replenishment are high.

At the scale of the mineral-fluid interface, carbonation reactions are commonly described as dissolution – precipitation reactions, as exemplified here on reaction R8 (Table 2). Dissolved $\text{CO}_{2\text{aq}}$ dissociates into bicarbonate (HCO_3^-) and a proton (H^+), which dissolves divalent ions (e.g. Mg^{2+}) and silica ($\text{SiO}_{2\text{aq}}$) from the silicate. Bicarbonate then reacts with Mg^{2+} to precipitate magnesite, and eventually $\text{SiO}_{2\text{aq}}$ precipitates as talc or, as formulated in R8, quartz or chalcedony. Each of the carbonation reactions in Table 2 may thus be viewed as a set of dissociation and precipitation reactions that locally buffer the composition and pH of the infiltrating fluid.

2.2. Changes of phase proportions with progressive carbonation

To illustrate and understand the carbonation reaction sequence in more detail, we calculated thermodynamic models that simulate the interaction of CO_2 -bearing fluid with ultramafic rocks describing the stepwise conversion into listvenite over time as fluid flow continuous. Compared to previous reaction path models of carbonation (Kelemen et al., 2022; Klein and Garrido, 2011; Leong et al., 2023) that mostly simulate batch-reactions (e.g. titration), our new calculations using the infiltration-fractionation mode of the Gibbs energy minimization code *Perple_X* (Connolly and Galvez, 2018) are reminiscent of an idealized flow-through reaction experiment. In these models, in each calculation increment a small amount of fluid (here we chose 1 mol $\text{H}_2\text{O}-\text{CO}_2$ fluid with a molar proportion $X_{\text{CO}_2} = \text{CO}_2/(\text{CO}_2 + \text{H}_2\text{O})$ of 0.029) is added and equilibrated with the rock. As discussed later, the X_{CO_2} of the infiltrating fluid is a major unknown and can vary a lot; the value chosen here is arbitrary but high enough for listvenite formation at the model conditions. Subsequently, the remaining equilibrium fluid (outflow fluid) is removed (fractionated) before addition of another fluid aliquot. Modeling details are described in the Supplementary Material.

Fig. 3 shows the modeling results of progressive carbonation during infiltration of CO_2 -bearing aqueous fluid ($X_{\text{CO}_2} = 0.029$) into initially 1 kg of harzburgite at 300 °C and 0.5 GPa. These conditions are within the range of known common P-T conditions of natural listvenites (Table 1), albeit somewhat arbitrarily chosen here for the purpose of illustration. Because the models do not account for reaction kinetics, they have limited applicability for low-temperature listvenites ($\leq 130\text{--}150$ °C; see further discussion in section 3.2). The evolution of the mineral assemblage (Fig. 3 a) reflects the temporal reaction progress of serpentinization (R3, Table 2) and carbonation (R4 – R7, Table 2) until all divalent cations are eventually incorporated in carbonate. The model predicts initial hydration of orthopyroxene to serpentine and talc followed by hydration of olivine to antigorite and eventually magnetite and brucite, reaching the maximum hydration state after infiltration of 0.15 kg fluid. This hydration reaction sequence of orthopyroxene followed by olivine is consistent with serpentinization experiments at similar temperatures (Allen and Seyfried, 2003). Initially not much carbonate precipitates because only small quantities of CO_2 (~0.03 mol) are added to the system in each fluid aliquot, and because some CO_2 is reduced to graphite and/or CH_4 due to oxidation of FeO in olivine to magnetite (c.f. R9 in Table 2; in Fig. 3 a, graphite is predicted as trace amounts between 0.07 and 0.56 kg fluid infiltration). It is worth to note here that although all iron in the initial rock composition was ferrous and we did not prescribe any oxidation, the model attains already after 0.6 kg fluid infiltration a bulk rock $\text{Fe}^{3+}/\text{Fe}_{\text{total}}$ of 0.43 because the outflow fluids during incipient carbonation contain reduced species (Fig. 3 b).

As the abundance of magnesite in the ophicarbonated assemblage increases, hematite is predicted to replace magnetite (0.6–0.7 kg fluid in Fig. 3 a; corresponding to reaction R10 in Table 2). The breakdown of magnetite to hematite and Fe-rich magnesite at this reaction stage is the main reason for the commonly observed concentric zoning patterns of

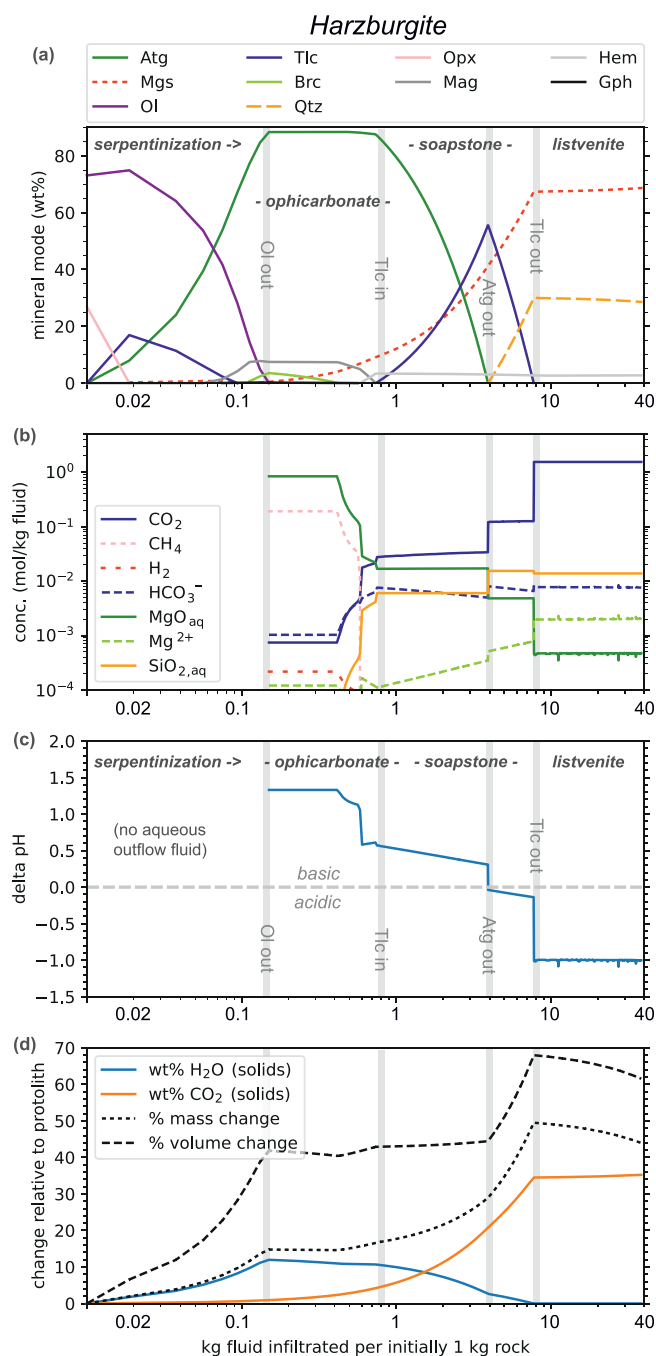


Fig. 3. Evolution of phase proportions (a), outflow fluid composition (selected species) (b), ΔpH (c) and cumulative mass and volume changes (d) with increasing fluid-rock interaction during carbonation of harzburgite from infiltration modeling ($P = 0.5$ GPa, $T = 300$ °C, infiltrating fluid $X_{\text{CO}_2} = 0.029$).

magnesite with respect to Fe contents (Decrausaz et al., 2023; Menzel et al., 2018; Qiu and Zhu, 2018; Tominaga et al., 2017). At >0.8 kg fluid infiltration, serpentine proportions decrease while talc and magnesite become more abundant, forming soapstone (R6). With continuous infiltration of CO_2 -bearing fluid, talc is consumed to form magnesite and quartz (listvenite; R7) once infiltration exceeds 4 kg fluid per initially 1 kg harzburgite (Fig. 3 a). As we will discuss later, the minimum fluid quantity required to form a specific assemblage of this reaction sequence strongly depends on the CO_2 concentration of the infiltrated fluid. Compared to the infiltration models, fluid quantities in nature will be larger because CO_2 and divalent cations are expected to be progressively

depleted from the outflow fluid by the simultaneously progressing carbonation reaction fronts, which further release H₂O due to serpentine and talc dissolution. For example, the reaction of serpentine to talc–magnesite (R6) may be driven by the modified outflow fluid after listvenite formation (R7), which has a lower CO₂ concentration than the externally-derived infiltrating fluid.

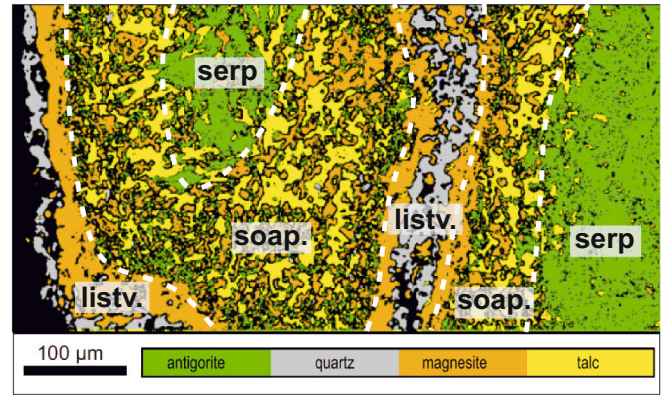
2.3. Evolution of fluid composition

The infiltration models show that the reaction sequence from carbonated serpentine to soapstone and listvenite will strongly alter the equilibrium concentration of Si, Mg and C in the equilibrated outflow fluid (the fluid that is fractionated in each calculation step). SiO_{2,aq}, CO₂ and, to a lesser extent, HCO₃⁻ concentrations increase while

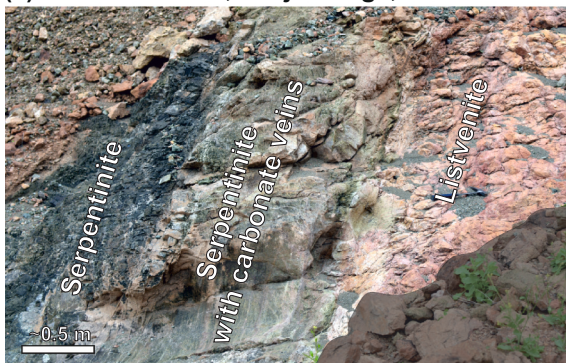
(a) high-T listvenite, Advocate Complex, Newfoundland



(b) experimental μ -Rxn fronts (600°C, 2 GPa, 12h)



(c) low-T listvenite, Fanjah ridge, Oman



(d) low-T listvenite, Hole BT1B, Oman

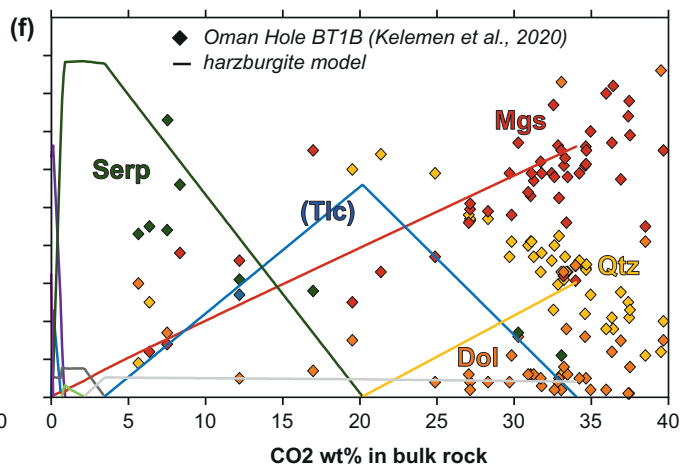
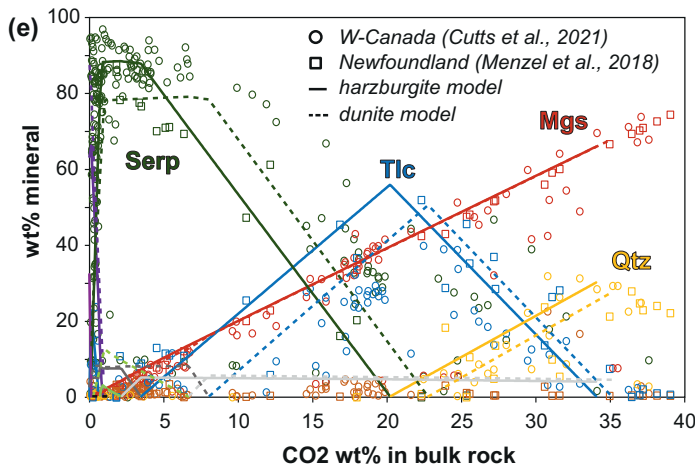
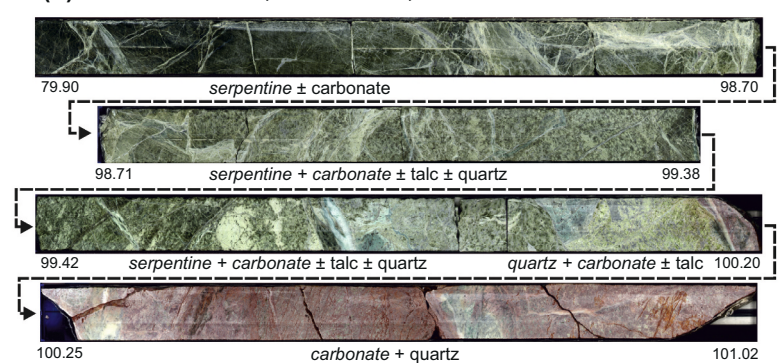


Fig. 4. Reaction fronts related to listvenite formation. (a) High-T (> 280 °C) soapstone and listvenite carbonation fronts in the Advocate Complex, Newfoundland (Menzel et al., 2018). (b) Micro-reaction fronts produced in high-T, high-P carbonation experiments (Sieber et al., 2020). (c) Low-T (< 150 °C) ophicarbonates and listvenite reaction fronts at Fanjah ridge, Samail ophiolite Oman. (d) Transition from serpentinite (green colors) to listvenite (red) in OmanDP Hole BT1B. (e) Comparison of mineral modes versus bulk CO₂ content of natural high T listvenite suites from W-Canada by XRD (Cutts et al., 2021) and Newfoundland by mass-balance (Menzel et al., 2018), and fluid-infiltration modeling (solid and dashed lines respectively: harzburgite and dunite models at 300 °C, 0.5 GPa with infiltrating fluid X_{CO2} = 0.029). (f) Mineral modes in low-T OmanDP Hole BT1B (Kelemen et al., 2020a) show a high discrepancy with models (here shown the same model as in (e), mineral modes are predicted to be similar at lower T). Serpentine: green; talc: blue; magnesite: red; quartz: yellow. The models do not account for dolomite (orange points); while magnetite/hematite (dark and light grey lines) are not reported in the natural datasets. (For interpretation of the references to colour in this figure legend, the reader is referred to the web version of this article.)

MgO_{aq} decreases in response to the changes in phase assemblage with increasing fluid infiltration (Fig. 3 b). This is related to: (i) a progressive acidification of the equilibrated outflow fluid with increasing carbonation, from moderately alkaline pH in presence of brucite and serpentine to mildly acidic in listvenite (Fig. 3 c; see also Fig. 12 in Oelkers et al., 2018); and (ii) a major change in oxygen fugacity ($f\text{O}_2$), from high CH_4 and H_2 concentrations during serpentinization and the interaction with graphite- and magnetite-bearing ophicarbonates (< 0.56 kg fluid infiltration, Fig. 3 c) to increasingly more oxidized compositions with ongoing carbonation. Once all Mg-silicates have reacted to magnesite and quartz (i.e. listvenite), the CO_2 concentration (and thus pH) of the outflow fluid will no longer be controlled by a reaction that consumes CO_2 but by the infiltrated fluid. These pronounced differences in pH, $f\text{O}_2$ and fluid speciation of equilibrated fluid in listvenite compared to serpentinite favor selective entrapment of some fluid mobile trace elements and metals (Godard et al., 2021), which likely is also part of the reason why some listvenites have economic grade gold concentrations (Buisson and Leblanc, 1985; Emam and Zoheir, 2013).

2.4. Mass and volume changes

Serpentinization and carbonation of peridotite are related to significant mass increase unless massive solute transfer occurs on a large scale. Loss of major elements due to Mg, Ca, and Si bearing aqueous complexes in the outflow fluid is predicted to be small at the modelled conditions (Fig. 3 b). Major element loss may even be overestimated here because infiltration of pure $\text{H}_2\text{O}-\text{CO}_2$ is an endmember scenario while in nature some dissolved species are already present in the infiltrating fluid. Thus, unless other factors such as salinity or extremely high fluid flux enhance element transfer relative to our model, hydration during serpentinization and CO_2 gain during listvenite formation need to be balanced by volume expansion. Our exemplary model for a harzburgite protolith indicates a 44% volume increase during the initial serpentinization reaction step (until 0.15 kg fluid infiltration), followed by a nearly constant volume (+ 2–3 vol%) until all serpentine has reacted to talc + magnesite (4 kg fluid infiltration). The nearly constant volume during soapstone formation from serpentinite (reaction R6; see also (Hansen et al., 2005; Sieber et al., 2020)) is due to concomitant water release during this carbonation reaction and the higher density of talc compared to serpentine. With reaction of talc to magnesite and quartz (R7) the volume is predicted to increase by another 18–22%, such that the full reaction sequence to listvenite amounts to a volume expansion of $>62\%$ relative to dry harzburgite (Fig. 3 d). These model predictions are in good agreement with volume expansion of 30–50% for listvenite formation from partially hydrated peridotite (8.0–8.5 wt% H_2O) estimated from isocon mass balance of trace and major element of Oman DP Hole BT1B listvenites (Godard et al., 2021). The inherent mass increase is a major conundrum of listvenites, since reactive volume expansion means that precipitates may easily clog fluid pathways and thus inhibit further fluid infiltration and reaction.

2.5. “Frozen” reaction fronts

Reaction path models are useful tools to understand the chronological evolution of carbonation progress, but bear no direct information on the spatial relationships of fluid flux and reaction products. Time-series experiments designed to capture different reaction extent (Sieber et al., 2020) and reactive percolation (core flow through) experiments (e.g., Andreani et al., 2009; Osselin et al., 2022a; Peuble et al., 2015a, 2015b; Peuble et al., 2019) can provide information on both temporal and spatial evolution, but are limited to observations at the micro- to cm-scales and over relatively short time periods (from a few days to weeks). In natural listvenites and related carbonated ultramafic rocks spatial relationships can be well investigated but the temporal evolution is not directly accessible. In nature, “frozen” reaction fronts in the form of mostly parallel lithological contacts are commonly preserved, for

instance, of the sequence peridotite – serpentinite – ophicarbonates – soapstone – listvenite (Fig. 4). The investigation of meso to micro-scale relationships across these reaction fronts allows inferences about fluid flow and reaction progress at large scale. The formation of growth zoning in magnesite (Decrausaz et al., 2023; Menzel et al., 2018; Qiu and Zhu, 2018; Tominaga et al., 2017) and cross-cutting relationships in the different lithologies can further provide indirect information about the temporal evolution in the natural rock record.

Reaction front contacts between (carbonate-bearing) serpentinite and soapstone and, in case of low-temperature listvenites, ophicarbonates and listvenite are typically very sharp in field outcrops (Fig. 4 a–d; see also e.g. (Beinlich et al., 2020a)). Similarly sharp reaction fronts can be observed at the microscale in time-series experiments that did not attain overall equilibration throughout the experimental capsule (Fig. 4b) (Sieber et al., 2020). In contrast, soapstone – listvenite transitions and particularly serpentinization fronts are commonly more gradual in the field. Reaction fronts may develop bi-symmetrically around a central fluid conduit (as in Fig. 4b), but in natural listvenites they are often asymmetric, with listvenite preferentially present at or close to the contact between peridotites and adjacent rocks (Hansen et al., 2005; Kelemen et al., 2022). In reacted porous cores of reactive percolation experiments, only oxidation fronts are sharp whilst silica and carbonate precipitation appear mainly controlled by local fluid pathways and relative rates of reaction kinetics and fluid flow (e.g., Peuble et al., 2019; see Section 4).

Because magnesite abundance monotonously increases with fluid infiltration (Fig. 3d), the CO_2 content of the solid is a useful indicator of reaction progress that allows comparison between models, experiments and natural rocks. Fig. 4 e shows that the temporal evolution of modal mineral proportions predicted by the fluid infiltration models generally reflects the sequence of reaction fronts observed in nature at moderate to high temperatures. Experiments show a very similar and consistent sequence of assemblages and phase proportions (Sieber et al., 2018). Uncertainties of the estimation of mineral modes by XRD (Cutts et al., 2021) and pressure and temperature differences between the model conditions and the natural case examples are responsible for minor discrepancies but overall the match is remarkably good. This supports the common interpretation of ophicarbonates – soapstone – listvenite associations as the product of a single fluid infiltration event that develops several, simultaneously advancing carbonation fronts. The natural data and model results also underline that pseudo-univariant assemblages such as serpentine-talc-magnesite and magnesite-talc-quartz are commonplace and act as CO_2 and pH buffers in accordance with reactions R6 and R7 (Table 2).

2.6. Synchronous hydration and carbonation?

If the protolith is only partially serpentinized or fresh, carbonation may be related to synchronous hydration (Fig. 3) along an incipient hydration front synchronous to carbonation. In this case, hydration may be caused by the evolved, H_2O -rich fluid after carbonate precipitation happened further upstream, or coeval but faster than carbonation if the CO_2 fluid concentration is not very high. The evolution of water content and density with increasing CO_2 content in natural rock suites related to high-T listvenites (Fig. 5; Cutts et al., 2021) reflects a trend of initial hydration with only scarce CO_2 uptake followed by coupled dehydration and carbonation. Our infiltration models with the arbitrary choice of infiltrated fluid $X_{\text{CO}_2} = 0.029$ are in good accordance with much of the natural data (Fig. 5), indicating that the reaction sequence may include a serpentinization front that advances synchronous to carbonation. Models with very high CO_2 concentrations in the infiltrated fluid (e.g. $X_{\text{CO}_2} = 0.5$; “direct carb.” model path in Fig. 5) predict much less hydration because olivine/pyroxenes are directly replaced by carbonate. Natural carbonated peridotites with densities and volatile content along this reaction path (e.g. 3–10 wt% CO_2 and < 7 wt% H_2O in Fig. 5 a) are very uncommon, and at all reported natural listvenite occurrences

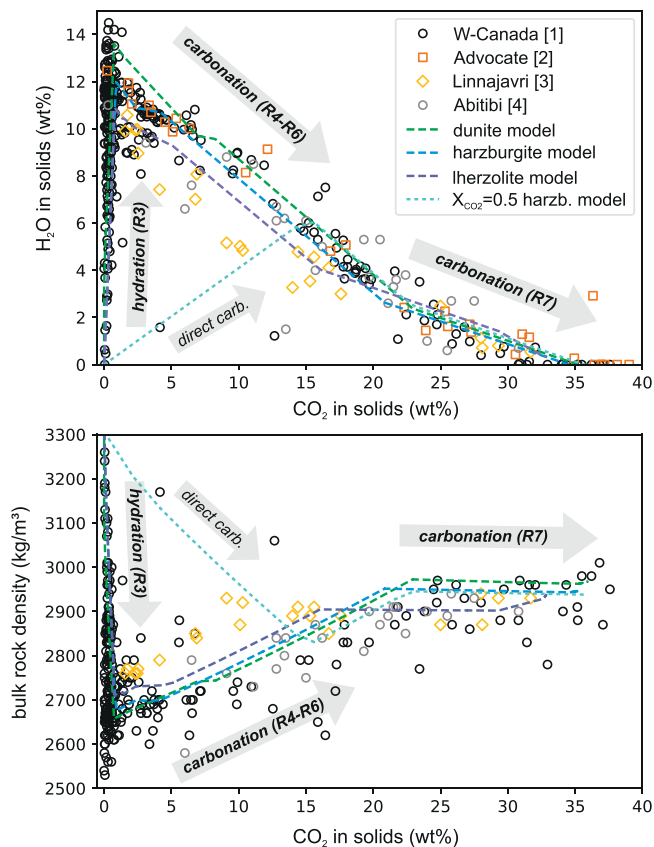


Fig. 5. Hydration and carbonation reaction paths traced by bulk rock H_2O content (calculated from loss on ignition minus CO_2) and density with increasing CO_2 content in solid. For the plots we extended the compiled natural data from W-Canada by [1] Cutts et al. (2021) with data from [2] Advocate ophiolite, Newfoundland, Canada (Menzel et al., 2018), [3] Linnajavri, Norway (Beinlich et al., 2012), and [4] Abitibi belt, Ontario, Canada (Schandl and Gorton, 2012), and compare it with infiltration models. Infiltration model conditions are $300\text{ }^\circ\text{C}$, 0.5 GPa , with infiltrating fluid $X_{\text{CO}_2} = 0.029$. Natural bulk rock densities are slightly lower in nature than predicted by the infiltration models, likely due to the effect of porosity not accounted for by the model. Other discrepancies are due to natural variations in Cr, Al and Fe content of the protolith (particularly in case of Linnajavri), and different pressure and temperature. Direct carbonation trends illustrated by a harzburgite model with infiltrated fluid $X_{\text{CO}_2} = 0.5$ only shows minor hydration, inconsistent with the natural data from high-T listvenite suites.

where the relationship with the ultramafic protolith is preserved, a serpentinization front exists in addition to the carbonation reaction fronts (Table 1; Fig. 5). This suggests that either the protoliths were fully serpentinized in a previous alteration event unrelated to carbonation and at different P–T and fluid conditions (serpentinite protolith; c.f. section 3.1), or that CO_2 concentrations of fluids causing listvenite formation were comparatively rich in H_2O and led to synchronous serpentinization during the incipient reaction steps. Comparatively low CO_2 concentrations of the infiltrated fluid require high time-integrated fluid-rock ratios, which in turn requires that permeability is sustained or repeatedly renewed. Pervasive carbonation of a dry ultramafic protolith without prior or coeval serpentinization possibly only occurs in nature in the case of sagvandites (Bucher and Stober, 2019; Ohnmacht, 1974).

3. Starting conditions and external parameters influencing carbonation

Various factors influence whether carbonation of serpentinite

completes to magnesite-quartz. In the following, we summarize and discuss the influence of external parameters and the “starting” conditions of carbonation, namely the protolith composition, pressure, temperature, fluid composition and far field stress.

3.1. Protolith composition

Any ultramafic lithology composed predominantly of Mg-silicates (\pm Mg–Ca silicates) may react to listvenite when in contact with fluids with high CO_2 concentration (Fig. 3; Fig. 6). Common protoliths inferred in natural examples are partially to fully serpentinized harzburgite (e.g. (Hansen et al., 2005; Menzel et al., 2018)), interlayered harzburgite-dunite and lherzolite (Godard et al., 2021), or metamorphic antigorite-serpentinites (Beinlich et al., 2012; Hinsken et al., 2017). Less commonly described protoliths are komatiites (Grosch et al., 2012; Schandl and Gorton, 2012). The major element composition of the protolith determines how much fluid is required to produce quartz–magnesite and how much CO_2 can theoretically be bound by this process. Infiltration models calculated with the same temperature, pressure and infiltrated fluid composition show that quartz starts to form at the lowest amount of fluid infiltration in komatiite (Supplementary Fig. S1), and increasingly higher fluid-rock interaction in lherzolite, harzburgite and dunite (Fig. 3; Fig. 6). Notably, serpentine is exhausted after infiltration of $\sim 3\text{ kg } X_{\text{CO}_2} = 0.029$ fluid per kg rock at $300\text{ }^\circ\text{C}$ in lherzolite. At the same conditions, it disappears only after $\sim 4.1\text{ kg}$ fluid infiltration in dunite (Fig. 6), but with $< 2\text{ kg}$ fluid infiltration in komatiite (Supplementary Fig. S1). These differences are due to the low Mg/Si and elevated Al contents of komatiite and lherzolite (Supplementary material), which stabilizes abundant chlorite and, once talc reacts out, pyrophyllite. The carbonation capacity of a protolith thus decreases with increasing Al contents because chlorite and clay minerals remain stable in listvenite, making some komatiites and mafic rocks like olivine gabbro and basalt less suitable for carbon sequestration. Our thermodynamic modeling further shows that dunite can store slightly more CO_2 (35.0–35.5 wt%) than harzburgite or lherzolite (~ 32.5 – 33.0 wt%) by transformation of serpentine and talc into quartz and magnesite. Carbonation of clinopyroxene in harzburgite, lherzolite and komatiite will lead to the formation of Ca-bearing magnesite (Sieber et al., 2022) and dolomite (Fig. 6 b), or, at low reaction progress, calcite and tremolite ($< 0.7\text{ kg}$ fluid infiltrated; Fig. 6 b).

Besides the protolith composition, the degree of serpentinization prior to carbonation is an important factor. Because olivine and pyroxene show faster reaction rates with CO_2 than serpentine (Grozeva et al., 2017; Hövelmann et al., 2011; van Noort et al., 2013), comparatively dry or only partially hydrated domains in ultramafic protoliths could be preferential sites of incipient carbonation. However, at the reducing conditions prevalent during serpentinization, olivine and pyroxene may also react initially to serpentine while CO_2 is reduced to CH_4 , formic acid or other organic compounds (McCollom and Seewald, 2007), instead of forming carbonate. The incipient reaction stage of dry or partially hydrated peridotite thus is related to a kinetic competition between serpentinization and carbonation of primary silicates, controlled by the CO_2 concentration in the infiltrated aqueous fluid, the temperature and the presence of catalysers like FeNi-alloys or Cr-spinel (Klein and McCollom, 2013; McCollom and Seewald, 2007). In fully serpentinized ultramafic protoliths, incipient carbonation may be controlled by the distribution of brucite, which has fast reaction rates (Hövelmann et al., 2012b). Most Al and Cr in serpentinized peridotite is typically hosted in Cr-spinel, which commonly persists as rather unreactive relicts in listvenite. In metamorphic antigorite-serpentinite protoliths, antigorite contains significant Al and Cr, which will influence the carbonation reaction as Al is partitioned into newly formed talc and chlorite (Sieber et al., 2020), or – if infiltrated fluids contain dissolved Na or K – albite and mica, respectively (Beinlich et al., 2012). Weathering of peridotite before it reaches the depth and temperature of listvenite formation may also alter the initial carbonation reaction pathway. Brucite dissolution,

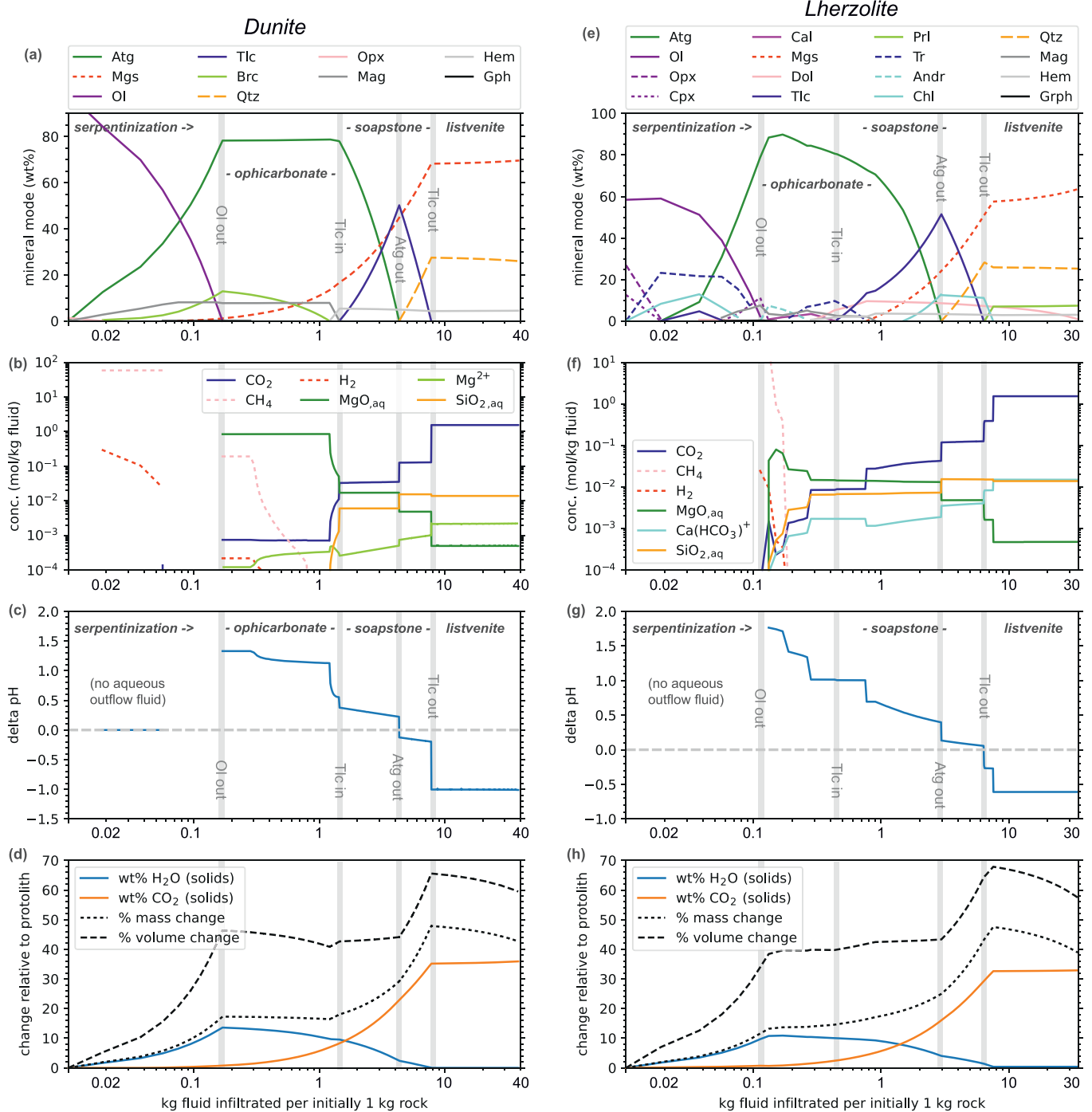


Fig. 6. Evolution of phase proportions, outflow fluid composition (selected species), pH and cumulative mass and volume changes with increasing fluid-rock interaction during carbonation of (a–d) dunite and (e–h) lherzolite from fluid-infiltration modeling ($P = 0.5$ GPa, $T = 300$ °C, infiltrating fluid $X_{\text{CO}_2} = 0.029$).

silicification, and formation of clay and Fe-hydroxides are typical for lateritic weathering of peridotite (Beinlich et al., 2010; Beinlich et al., 2018; Ulrich et al., 2014). While this reduces the carbonation potential, previously weathered protoliths may have higher porosity that favors fluid infiltration.

As illustrated above, a broad variety of protoliths – dunite, harzburgite, lherzolite, komatiite, and possibly also pyroxenites and olivine-rich gabbro, to various degrees serpentinized – can be transformed into listvenite. Hence, the initial bulk rock Mg/Si is not that critical for listvenite formation, provided that olivine, pyroxenes and serpentine-group minerals are abundant in the reacting material. More important

parameters are the CO₂ supply, the infiltrating fluid composition, and a sustained permeability.

3.2. Pressure and temperature

Numerous experimental studies have constrained the subsolidus phase equilibria in the MgO-SiO₂-CO₂-H₂O (\pm CaO \pm FeO \pm Al₂O₃) system in dependence of pressure and temperature (Johannes, 1967, 1969; Koziol and Newton, 1998; Sieber et al., 2018; Wyllie et al., 1983). These experiments show that in a reaction between Mg-silicates and CO_{2, aq} the minimum amount of CO₂ in the fluid required to produce

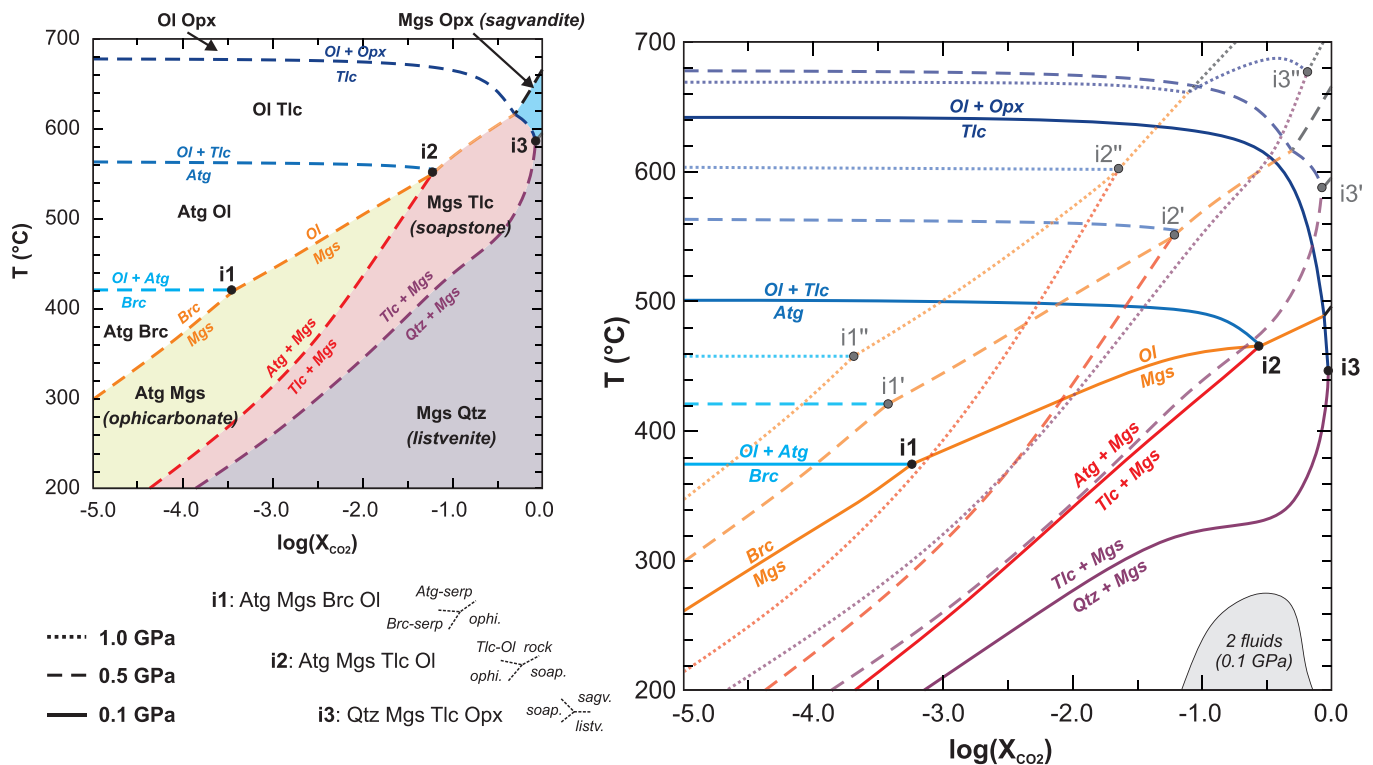


Fig. 7. Fluid-saturated $T\text{-log}(X_{\text{CO}_2})$ pseudosections showing the relationships of pressure, temperature and fluid composition for listvenite and other carbonated peridotite assemblages for a simplified harzburgite composition in the Mg-Fe-Si-CO-H system at (a) 0.5 GPa, and (b) 0.1–1.0 GPa. The colour-coding of boundaries in b) is the same as in a), with boundaries corresponding to dehydration reactions in blue and boundaries of ophicarbonates, soapstone and listvenite assemblages in orange, red and purple. The univariant assemblages at pseudo-invariant points i1 – i3 are shown below a). Fluid immiscibility at $T < 275^\circ\text{C}$ for 0.1 GPa in b) after [Blencoe et al. \(2001\)](#). (For interpretation of the references to colour in this figure legend, the reader is referred to the web version of this article.)

magnesite decreases with pressure and increases with temperature. For a given pressure, higher CO_2 -concentrations in the fluid are required to initiate carbonation as temperature increases. The relationships between pressure, temperature and CO_2 concentration in carbonated peridotites are best illustrated by fluid-saturated $T\text{-log}(X_{\text{CO}_2})$ phase diagrams for different pressures ([Fig. 7](#)), obtained by equilibrium thermodynamic modeling based on the experimental data. Although fluid is considered here as a simplified binary $\text{CO}_2\text{-H}_2\text{O}$ solution and several effects of open-system fluid infiltration are not accounted for, $T\text{-log}(X_{\text{CO}_2})$ phase diagrams are a useful tool to understand listvenite and other carbonated peridotite assemblages like soapstone, ophicarbonates, and sagvandite as they can show: (i) the minimum X_{CO_2} of infiltrating fluid required for listvenite formation at any given P–T condition, (ii) the X_{CO_2} of fluid equilibrated with a carbonated peridotite assemblage, and (iii) phase changes and fluid evolution if listvenite or other carbonated peridotites undergo prograde metamorphism.

Despite being a comparatively rare rock type, listvenites are stable at a wide range of temperatures and pressures ([Fig. 7](#)). The minimum X_{CO_2} of infiltrated fluid required for listvenite formation (purple lines in [Fig. 7](#)) increases with temperature. Higher pressure has the inverse effect, stabilizing listvenite to higher temperatures. The highest temperature at which listvenite may theoretically form at 0.1 GPa is 430°C for CO_2 -dominated fluid ($X_{\text{CO}_2} > 0.8$), or e.g. $\sim 320^\circ\text{C}$ for $X_{\text{CO}_2} \leq 0.1$ (solid lines in [Fig. 7](#) b). At 1.0 GPa, listvenite could theoretically form even at $>650^\circ\text{C}$ for $X_{\text{CO}_2} > 0.5$, and at $>400^\circ\text{C}$ for $X_{\text{CO}_2} > 0.01$ (dotted lines in [Fig. 7](#) b). High-pressure (> 1 GPa) experiments confirm that listvenite can form at such elevated temperatures in forearc conditions of subduction zones, if CO_2 concentrations in the fluid are high enough ([Sieber et al., 2018](#); [Sieber et al., 2022](#)).

It is important to note in [Fig. 7](#) that ophicarbonates, soapstone and listvenite assemblages alone are not suitable to determine pressure or temperature. This is only possible if the univariant assemblages

antigorite-magnesite-brucite-olivine, antigorite-magnesite-talc-olivine or magnesite-talc-quartz-enstatite are observed in equilibrium (pseudo-invariant points i1 – i3, respectively, in [Fig. 7](#)) and one of the essential variables (P or T) is independently determined. Most assemblages related to natural listvenites are divariant and thus do not permit determination of pressure, temperature and fluid X_{CO_2} . Temperature estimates for listvenite formation usually rely on a combination of other thermodynamic relationships in the host peridotite or the related carbonated assemblages and fluid inclusion or clumped isotope thermometry.

At temperatures below $\sim 130\text{--}150^\circ\text{C}$, talc formation (reaction R8) becomes sluggish, thus talc-magnesite assemblages may be absent despite being theoretically stable at $\geq 80^\circ\text{C}$ ([Falk and Kelemen, 2015](#)). Very few of the listvenites from Oman DP Hole BT1B contain talc, while quartz already occurs in serpentinite with comparatively low carbonate content ([Fig. 4](#) c, d, f). Thus, the coexistence of serpentine, quartz and magnesite can be an indicator of low temperatures ([Falk and Kelemen, 2015](#)). Thermodynamic calculations that do not account for kinetic effects cannot fully simulate listvenite formation at low temperatures. Further indications of low temperatures may stem from hematite-graphite intergrowths ([Kelemen et al., 2022](#)) and precipitation of opal and/or chalcedony instead of quartz (below $\sim 90^\circ\text{C}$) (e.g., [Boschi et al., 2009](#); [Cipolli et al., 2004](#); [Ulrich et al., 2014](#)). At temperatures that approach ambient conditions, hydromagnesite, diyingite, or nesquehonite may form instead of magnesite ([Oskierski et al., 2013](#); [Power et al., 2019](#)).

At higher temperatures, the prograde reaction lizardite = antigorite + brucite in serpentinite may serve as a lower bound ($T > 280^\circ\text{C}$) if it can be shown that magnesite replaces lizardite before brucite and that this brucite is metamorphic ([Menzel et al., 2018](#)); the presence of amphibole in listvenite ([Nosouhian et al., 2016](#)) or brucite dehydration to metamorphic olivine in the host serpentinite ($T = 380\text{--}460^\circ\text{C}$) may

further be a hint to elevated temperatures. Because carbonation reactions strongly increase the local equilibrium concentration of aqueous silica in the fluid (Klein and Garrido, 2011), antigorite can be stabilized over lizardite and chrysotile because it has lower Mg/Si. Thus, contrary to the lizardite-antigorite transition of pure serpentinites in a closed system (Schwartz et al., 2013), the occurrence of magnesite-bearing antigorite serpentinite related to listvenite does not indicate elevated temperatures (see also e.g., Falk and Kelemen, 2015).

While estimating the temperature of listvenite formation is challenging but possible, there are currently no independent methods to constrain pressure – and thus, depth – from carbonated peridotite alone. Pressure estimates of listvenite formation rely on the assumption or knowledge of a regional geotherm combined with a temperature constraint, or on deductions from adjacent meta-mafic or meta-sedimentary units containing assemblages or mineral pairs that are sensitive to pressure. In some cases, fluid inclusion barometry may be possible if inclusions are large enough, their composition can be determined and an independent thermometer is available (Roedder and Bodnar, 1980).

3.3. Composition of the infiltrating fluid

3.3.1. CO₂ concentration

Listvenite formation requires that CO₂ in the infiltrating fluid is higher than the equilibrium CO₂ concentration buffered by the magnesite-quartz-talc assemblage (reaction R7 in Table 2; purple lines in Fig. 7) at the relevant temperature and pressure. Thermodynamic modeling (Fig. 7) and experiments (Johannes, 1969) show that, in principle, listvenite formation has no upper X_{CO2} limit. An exception is fluid immiscibility in the CO₂-H₂O system at low temperature and pressure (e.g. < 270 °C at 0.1 GPa; Fig. 7) that limits the possible X_{CO2} of aqueous CO₂-bearing fluid coexisting with (wet) supercritical CO₂ or gas (Blencoe et al., 2001).

The difference in CO₂ concentration of the infiltrated fluid compared to that of the outflow fluid equilibrated with the carbonated peridotite assemblage determines the theoretical minimum quantity of fluid that is necessary to achieve a certain extent of carbonation. Complete conversion of 1 kg harzburgite into listvenite requires addition of about 11.3 mol (nearly 0.5 kg) CO₂. With an X_{CO2} of 0.029 (≈1.55 mol CO₂ / kg fluid) of the infiltrated fluid as chosen in our infiltration models (Fig. 3), this would require 7.3 kg of infiltrated fluid if all CO₂ is fixed in carbonate, or ~ 7.8 kg fluid when accounting for carbon that remains in the outflow fluid (“Tlc out” in Fig. 3). If the infiltrated fluid contains a third of that CO₂ concentration (X_{CO2} ≈ 0.01; i.e. 0.54 mol CO₂ / kg fluid), which is closer to but still higher than the equilibrium X_{CO2} of the magnesite-talc-quartz assemblage at the model conditions (X_{CO2} ≈ 0.0032; c.f. Fig. 7), >24 kg of fluid would be necessary to convert 1 kg harzburgite into listvenite (i.e. a flux-integrated fluid/rock ratio of >24). Likewise, conversion of 1 kg harzburgite into soapstone consisting predominantly of talc and magnesite requires addition of about 6 mol (or 0.24 kg) of CO₂ (“Atg out” in Fig. 3). Listvenites and soapstones are thus indicative of high fluid fluxes.

Inferring the exact CO₂ concentration of the infiltrating fluid from natural listvenites is challenging; usually only the minimum can be estimated with some confidence. Based on the progression distance between the soapstone and listvenite reaction fronts and using the time-integrated flux equation by Ague (1998), Beinlich et al. (2012) estimated that for a temperature of 275 °C the infiltrating fluid causing carbonation at Linnajavri had an X_{CO2} of 0.08–0.01 assuming pressures of 0.1–0.3 GPa, respectively. However, the estimation of X_{CO2} of the infiltrating fluid using the progression distance of reaction fronts builds on the simplifications that infiltrated fluids are composed of pure H₂O and CO₂ and that time-integrated fluid flux was equal and unidirectional across all reaction fronts, while fluid flow may be more complex in nature. A different approach is to estimate the CO₂ fluid concentration that the inferred source rock (e.g. meta-sediments) can potentially attain

at the estimated P–T conditions (Kelemen et al., 2022), but this requires good knowledge about the CO₂ source(s) as well as P and T. Primary fluid inclusions entrapped in growing magnesite or quartz could provide further insights if their composition can be determined (Schandl and Naldrett, 1992). Nonetheless, fluid inclusions have the caveat that they may record not the infiltrated disequilibrium fluid that drives carbonation, but effects of fluid immiscibility or fluid compositions that are partially or fully equilibrated with the reacting assemblage or the host mineral.

3.3.2. Cationic aqueous species and pH

Besides CO_{2,aq}, the infiltrated fluid can contain dissolved carbon in the form of bicarbonate (HCO₃⁻), carbonate (CO₃²⁻), or cation-carbonate complexes like NaHCO_{3,aq} or CaHCO₃⁺. The concentration of such electrolytic carbon-bearing complexes depends on the P–T conditions, pH, dissolved non-volatile element concentrations, and chlorinity. The effects of these variables during listvenite formation are not straightforward. Chlorinity and the presence of solutes in CO₂ bearing aqueous fluids will decrease CO_{2,aq} concentration at any P–T condition (e.g., Duan and Sun, 2003). In turn, dissolved NaCl increases divalent cation concentrations and thus carbonate solubility (Manning et al., 2013). Thus, fluid speciation affects reaction pathways during carbonation. For example, NaHCO_{3,aq} in solution may indirectly promote carbonation because it significantly reduces the amount of Mg²⁺ required to exceed the solubility product of magnesite (Chen et al., 2006). On the other hand, NaHCO_{3,aq} in the infiltrated fluid only contributes directly to carbonation if a coupled process accounts for the released sodium, such as increasing pH of the outflow fluid (formation of NaOH_{aq}) or precipitation of a Na-bearing solid. However, Na-bearing phases such as albite are rather rare in listvenites (Beinlich et al., 2012). Preliminary calculations suggest that Na⁺ in the outflow fluid is commonly accommodated by HCO₃⁻ to attain charge balance, thus the direct role of charged carbonate species during carbonation is likely limited.

Bicarbonate and carbonate concentrations are higher at more basic pH, however, dissolution rates of olivine and serpentine strongly decrease with increasing pH (Cipolli et al., 2004; Daval et al., 2013; Oelkers et al., 2018). Infiltration or mixing of Mg- or Ca-bearing bicarbonate fluids with elevated pH may indeed form carbonates in ultramafic rocks, as inferred for example for vein formation in weathering horizons (Mervine et al., 2014; Ternieten et al., 2021a) and oceanic ophalcites (Grozeva et al., 2017), but is unlikely to cause effective dissolution and pervasive replacement of olivine and serpentine by magnesite and quartz. On the other hand, dissolution of olivine and serpentine is much more effective in moderately acidic, CO_{2,aq}-bearing aqueous fluid, causing the release of Mg²⁺ and SiO_{2,aq} (Daval et al., 2013). This locally buffers pH to more basic conditions such that CO_{2,aq} transforms to bicarbonate and/or carbonate ions, which in turn enables carbonate precipitation while SiO_{2,aq} may precipitate as talc or quartz (R8* in Table 2).

Selective enrichments in fluid mobile elements and metals, specifically in alkali and alkali-earth elements, compared to their protoliths are typically observed in listvenites, indicating that infiltrating reacting fluids were solute-bearing non ideal solutions (e.g. Godard et al., 2021). While less common than magnesite-dominated listvenite, formation of dolomite-rich and sometimes calcite-bearing listvenites in various places indicates that Ca-bearing aqueous fluids can play a role in some carbonation settings (Amarbayar et al., 2023; Austrheim and Andersen, 2023; Falk and Kelemen, 2015). In carbonation experiments of natural weathered peridotite performed in a Na-Ca-Cl-CO₂ aqueous solution, Hövelmann et al. (2011) observed that Mg was leached into the solution because magnesite was undersaturated and dolomite formation was kinetically inhibited compared to calcite. In contrast, Na-Cl-CO₂ fluids led to magnesite precipitation. These observations suggest that the formation of dolomite- or calcite-dominated listvenites may be due to the presence of CaCl₂ in the infiltrating fluid, suppressing magnesite precipitation due to the formation of MgCl₂ in the fluid. Alternatively,

secondary infiltration of CaCl_2 bearing fluids may cause dolomite or calcite to replace previous magnesite in listvenite (Amarbayar et al., 2023). Because knowledge about the composition and speciation of the infiltrating fluid causing carbonation is usually lacking, the influence of chlorine-bearing complexes on natural listvenite formation is not yet fully understood.

3.3.3. Oxygen fugacity ($f\text{O}_2$)

Methane or hydrogen in the infiltrating fluid, derived from serpentinization of adjacent peridotites or from organic-carbon bearing source rocks, may cause a bulk rock reduction during listvenite formation. Because carbonation is related to partitioning of Fe into magnesite and, typically, hematite (R10 in Table 2; Fig. 3), the internally buffered $f\text{O}_2$ drastically increases, in some cases potentially reaching the sulfide-sulfate buffer (Frost, 1985). Thus, any reduced species in the infiltrating fluid are likely to become oxidized, with a coupled reduction of Fe^{3+} in magnetite, hematite or serpentine to Fe^{2+} in magnesite. This process may explain decreasing bulk $\text{Fe}^{3+}/\text{Fe}_{\text{total}}$ ratios with carbonation and the formation of hematite-absent listvenites, as observed in some places (e.g. Decrausaz et al., 2023; Menzel et al., 2018) and in piston-cylinder experiments (Sieber et al., 2020). Oxidation of methane in response to the reaction of CO_2 with Fe-oxides and Mg-silicates may thus present another carbon input, although subordinate to $\text{CO}_{2,\text{aq}}$.

3.4. Far-field stress & deformation

Tectonic stress and deformation may alter the microstructure and permeability of the ultramafic protolith in a way that favors CO_2 -influx and carbonation. In particular shear zones are sites of enhanced fluid flow and reactivity, because deformation can create connected pore

networks and increase reactive surface areas due to pulverization or dynamic recrystallization. Fresh peridotites deform by brittle fracturing at $T < 600$ °C, which allows percolation of aqueous fluid along the fractures, causing serpentinization. In major shear zones, this can lead to locally complete serpentinization and a related change in deformation style to brittle-ductile mechanisms controlled by the comparatively weak serpentine-group minerals. The higher permeability along serpentinized shear zones compared to partially serpentinized or fresh peridotite may enhance infiltration of CO_2 -bearing fluids. Serpentine fault zones (e.g., Angiboust et al., 2014; Quesnel et al., 2016; Tarling et al., 2019) or pre-conditioned peridotites damaged by brittle deformation are thus likely the most favorable sites for listvenite formation.

4. Feedback processes influencing reactivity, porosity and permeability

For the carbonation to continue over time, fluid flow and CO_2 concentration must remain high enough, and reaction zones must be permeable. Carbonation progress may be limited by reaction (i.e. dissolution, nucleation and/or crystal growth rates) or transport processes (the continued supply of reactants, most importantly CO_2 , with the aqueous fluid). Chemical (reaction) and hydrological (transport) processes are coupled to thermal and mechanical (deformation) processes during carbonation, leading to non-trivial feedback mechanisms that depend also on the externally controlled “starting” conditions (Fig. 8 a & b). Part of the complexity of these feedbacks during listvenite formation is due to the mineralogy changing with reaction progress and due to their spatial and time scale dependency, resulting in micro-environments. Thus, a multitude of simultaneous, coupled thermo-hydro-mechanical-chemical (THMC) processes (e.g., Steefel et al.,

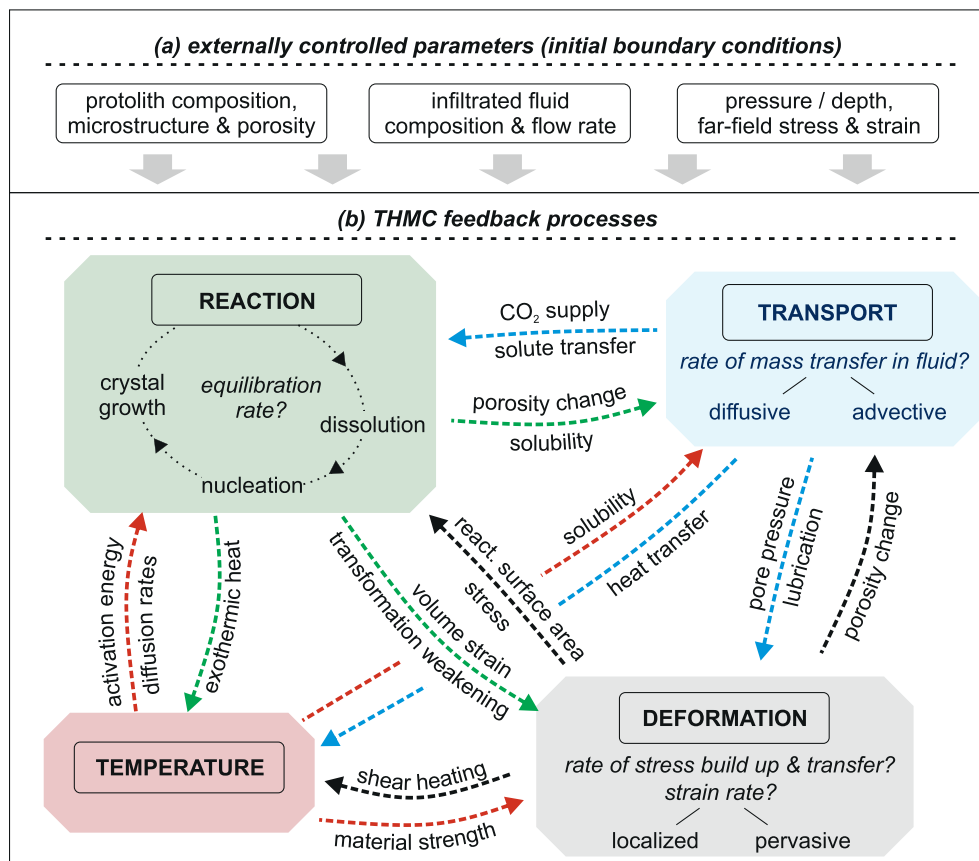


Fig. 8. Schematic overview of (a) external parameters (i.e. initial boundary conditions) and (b) thermo-hydro-mechanical-chemical (THMC) feedback processes. All processes are subject to spatio-temporal variability, including the initial boundary conditions (e.g., P, T may decrease upon exhumation; protolith microstructure and composition may vary as reaction fronts move into the ultramafic rock units, infiltrated fluid composition may change).

2005) is causally related to listvenite formation, and strongly influences effective reaction rates, fluid flow paths and the final carbonation assemblages and microstructures (Fig. 8 showing only of selection of possible feedbacks). We propose that the interplay of these processes and their spatio-temporal evolution is the key to why in some cases carbonation stagnates (because reactive volume expansion clogs porosity, *c.f.* section 2.4), while in other cases the protolith completely transforms into carbonate-quartz (because porosity and fluid flow are maintained or renewed). In the following, we discuss the effect of different processes and feedback mechanisms with a focus on whether they may enhance or inhibit carbonation reaction progress.

4.1. Dissolution, nucleation and crystal growth

Carbonation reactions can be described as the dissolution of the parental Mg-silicate, and the nucleation and growth of the reaction products through precipitation (“reaction” in Fig. 8 b). The progress of dissolution and precipitation reaction then primarily depends on the saturation state of each phase, as the degree of oversaturation controls the nucleation rate as well as type and rate of crystal growth. Besides temperature and further external parameters, the saturation state strongly depends on fluid composition, particularly pH, which in turn is a function of the CO₂ concentration that drives reaction progress (section 2.3). However, as CO₂ fluid concentration decreases with precipitation of carbonate and dehydration of serpentine or talc, dissolution, nucleation and crystal growth all depend on continued CO₂ supply and thus on fluid transport processes (Fig. 8 b). Experimental investigations that aim to determine carbonation reaction kinetics (e.g., Daval et al., 2013; Lacinska et al., 2016; Oelkers et al., 2018; Saldi et al., 2013) are usually designed to avoid rate limitations due to transport processes, using powdered samples suspended and mixed in a large fluid reservoir. These experiments show that dissolution kinetics influenced by temperature, pH (or CO₂ concentration), surface area, and grain morphology, but that they depend also on the mineralogy: they are the highest for oxides (MgO) and hydroxides (brucite) and decrease with increasing silica content from forsterite, to serpentine and pyroxene (Kelemen et al., 2011; Matter and Kelemen, 2009). Precipitation of magnesite is controlled by similar parameters, and may be enhanced if Fe-bearing magnesite forms instead of pure MgCO₃ (Saldi et al., 2013) and through catalytic effects of minor and accessory phases like chromite or Ni-sulfides. Compositional heterogeneities as well as the distribution of minerals with high carbonation affinity (e.g., brucite) and of minor phases with catalytic effects thus influence where carbonation in a natural rock commences.

Depending on the respective saturation states and kinetics of the different minerals, dissolution and precipitation can occur in-situ via interface-coupled replacement, or spatially decoupled, meaning that one or several reaction products precipitate in sites different from where dissolution of the Mg-silicate occurred. Spatial decoupling of dissolution and precipitation of the reaction products is typically observed during core flow-through experiments, revealing that different mechanisms control dissolution and precipitation in reactive domains (e.g., Andreani et al., 2009; Peuble et al., 2015a, 2015b). The crystallographic orientation of minerals, often anisotropic (olivine, serpentine), predominantly influences dissolution kinetics, whilst the fluid composition and thus the interplay between reaction kinetics and solute transport control precipitation (Peuble et al., 2015a).

Spatial decoupling of precipitation of the reaction products can—similar to incongruent dissolution—lead to the precipitation of monomineralic layers of amorphous silica, sheet-silicates, or Fe-hydroxides. Such often nano-scale coatings are a major concern in many carbonation experiments because they can be impermeable and shield the reacting Mg-silicate from further contact with CO₂ and thereby inhibit reaction (e.g., Andreani et al., 2009; King et al., 2010). However, if such layers hamper mineral dissolution is not conclusive as in some experiments Si-rich layers remained fluid permeable (Hövelmann et al.,

2012a), and the field record preserves no clear evidence that passivating layers are a major barrier for listvenite formation in nature.

Deformation can influence carbonation reaction mechanisms because strain-induced grain size reduction—e.g. by cataclasis or dynamic recrystallization—changes the reactive surface area of the dissolving Mg-silicate. Deviatoric stress causes local pressure perturbations in multi-phase assemblages with heterogeneous mineral strength, and leads to variations in surface energies depending on the surface orientation relative to the stress field. Stress related to deformation therefore has a direct impact on dissolution processes (known as pressure-solution or dissolution-precipitation creep; e.g., Malvoisin and Baumgartner (2021)) and favors spatial decoupling of dissolution and precipitation during reaction (Putnis, 2021) because it contributes to heterogeneous dissolution, nucleation and growth rates in different microstructural sites. Stress may further significantly alter nucleation and growth mechanisms during reactions (Gilgannon et al., 2023). The details of these effects are not yet well understood for carbonation.

Determining which parameters controlled dissolution, nucleation and precipitation mechanisms in fossil and heterogeneous natural systems is challenging. Detailed microstructural and textural analysis of listvenite and associated carbonated rocks shed some light onto these processes, although usually not quantitatively. For instance, different consecutive stages of crystal growth recorded by variable crystal habits in zoned magnesite and quartz may indicate systematic variations in saturation state. This process is for example documented in the Oman DP BT1B listvenites (Beinlich et al., 2020b; Menzel et al., 2022b), where zoned magnesite grains with euhedral crystal habit in the core have dendritic growth structures at their rims, suggesting a change from predominantly equilibrium to disequilibrium growth (Fig. 9 a). In other samples, rims with euhedral crystal facets overgrow “cauliflower”-textured and porous magnesite cores (Beinlich et al., 2020b). As illustrated well by cathode-luminescence microscopy, quartz in the BT1B listvenites also commonly shows different crystallization habits in dependence of saturation states, ranging from dendritic growth, faceted growth (Fig. 9 b), radial chalcedony aggregates to globular aggregates (Menzel et al., 2022a; Menzel et al., 2022b). The latter may represent recrystallization of initially amorphous silica precipitation. Similar variations in crystal habit between different growth stages are common in listvenites elsewhere (Menzel et al., 2018; Qiu and Zhu, 2018; Tominaga et al., 2017). Such changes between equilibrium and disequilibrium growth stages, in some cases possibly also with intermittent partial carbonate dissolution, indicate changes in fluid composition, fluid flow rate, or both. We speculate that local, possibly oscillatory fluctuations between under- and oversaturated states due to dynamically changing pore pressure, fluid flow paths and pH may enhance growth rates of dolomite and magnesite, particularly during low temperature carbonation. Such oscillations may have a large impact on carbonate growth, as evidenced experimentally for dolomite precipitation at ambient conditions (Kim et al., 2023).

4.2. CO₂ transport and fluid flow – general considerations

Listvenite formation in nature is strongly controlled by transport processes because reaction progress requires continued CO₂ supply. Transport of CO₂, H₂O and other dissolved components in aqueous fluid occurs by diffusion and advection, with the main driving forces being chemical and hydrological (pore-fluid pressure) gradients, respectively. To allow efficient mass transfer, both diffusion and advection require an interconnected porosity that is sustained or renewed despite the volume expansion by precipitation of the carbonation reaction products. Because reactions of brucite, serpentine and talc with CO₂ release water (Table 2), carbonation reaction progress would stagnate if the equilibrated fluid is not removed and replaced by new CO₂-bearing fluid. While serpentinization consumes the fluid and can proceed to completion at comparatively low fluid/rock ratios if fluids are H₂O-rich (Fig. 3), listvenite formation requires much higher fluid/rock ratios and

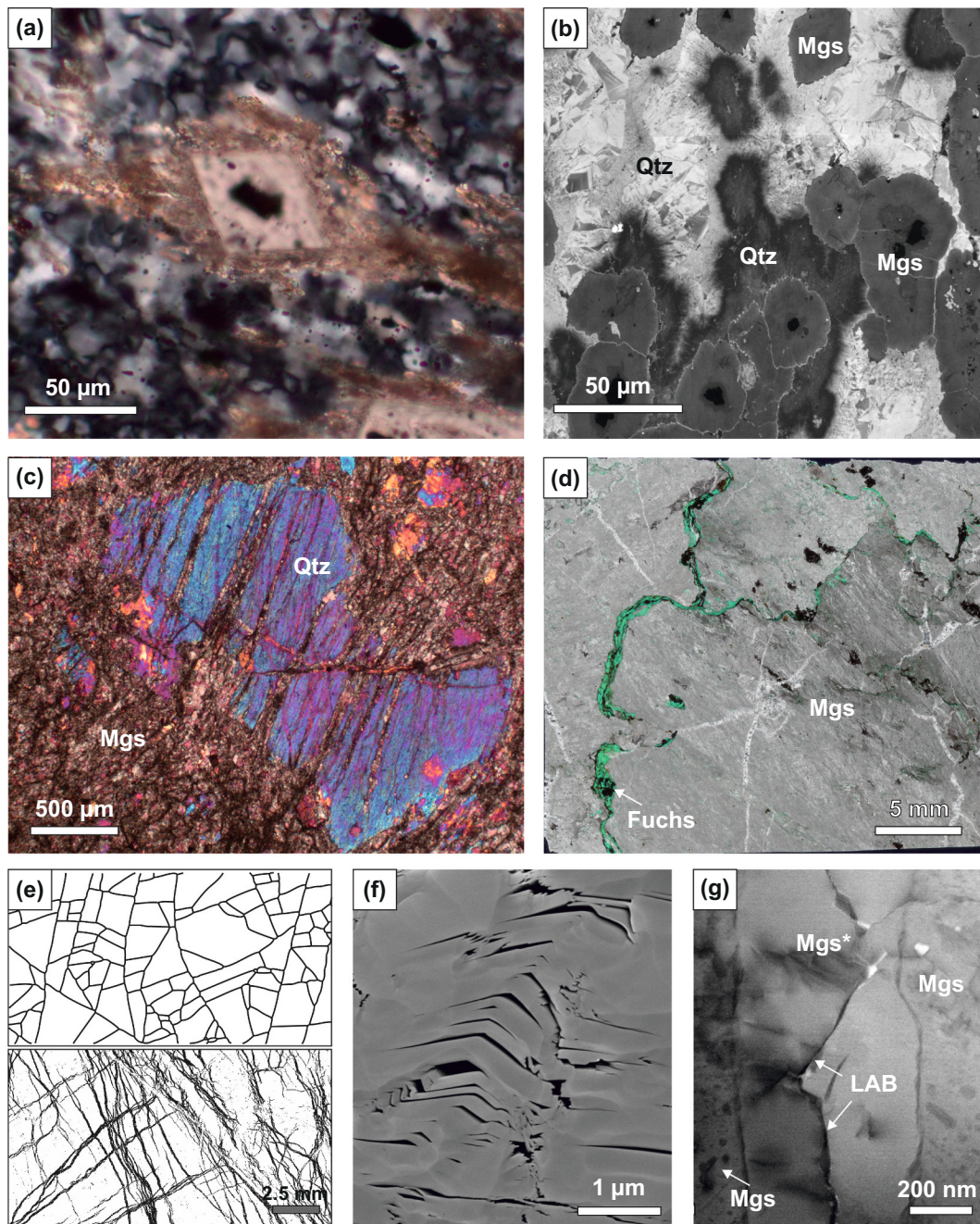


Fig. 9. Examples of microstructures indicative of THMC processes during carbonation, including (a + b) crystal growth, (c + d) solute transfer and (e-g) porosity renewal by deformation. (a) Change from euhedral equilibrium to dendritic disequilibrium growth of magnesite; cross-polarized micrograph of Oman BT1B listvenite 16–3:28–31 from Menzel et al. (2022b). (b) SEM-cathodoluminescence image showing radial disequilibrium quartz precipitation (dark) followed by faceted growth (bright); after Menzel et al. (2022a). (c) Pseudomorphic quartz aggregate after bastite/orthopyroxene, showing local Mg redistribution; Oman BT1B listvenite 56–4:17–21. (d) Magnesite-rich listvenite with fuchsite vein resembling a stylolite, showing Si leaching; cross-polarized thin section scan of Advocate listvenite Adv-09 in Menzel et al. (2018). (e) Digitized hierarchical vein pattern of olivine serpentinization (after Iyer et al., 2008) in comparison to conjugate/anastomosing magnesite vein patterns in Oman BT1B listvenite (Menzel et al., 2022a). (f) Nano-porosity formation by creep cavitation through top-to-right shear and bending of serpentine grains; broad-ion-beam polished SEM image, OmanDP serpentinite Hole BA1B, 81–2:76–81. (g) TEM bright-field image of inclusion-free magnesite re-precipitation (Mgs*) along a nano-crack related to a low-angle boundary (LAB), showing porosity renewal by nano-fracturing; Oman BT1B listvenite 14–3:65–66 from Menzel et al. (2022b).

sustained permeability.

4.2.1. CO₂ transport vectors and fluid flow

To understand reaction progress and the related development of parallel advancing reaction fronts during peridotite carbonation, it is useful to consider first the macroscale fluid flow geometry, i.e. how CO₂ is supplied to the reaction fronts. As idealized endmembers, carbonation

reaction may be driven by CO₂ diffusion in the aqueous fluid phase (scenario A in Fig. 10) or by advective fluid flow (B & C in Fig. 10). Advective flow can be separated into two principal vectors, normal and lateral with respect to the orientation of the advancing reaction fronts (B and C, respectively, in Fig. 10).

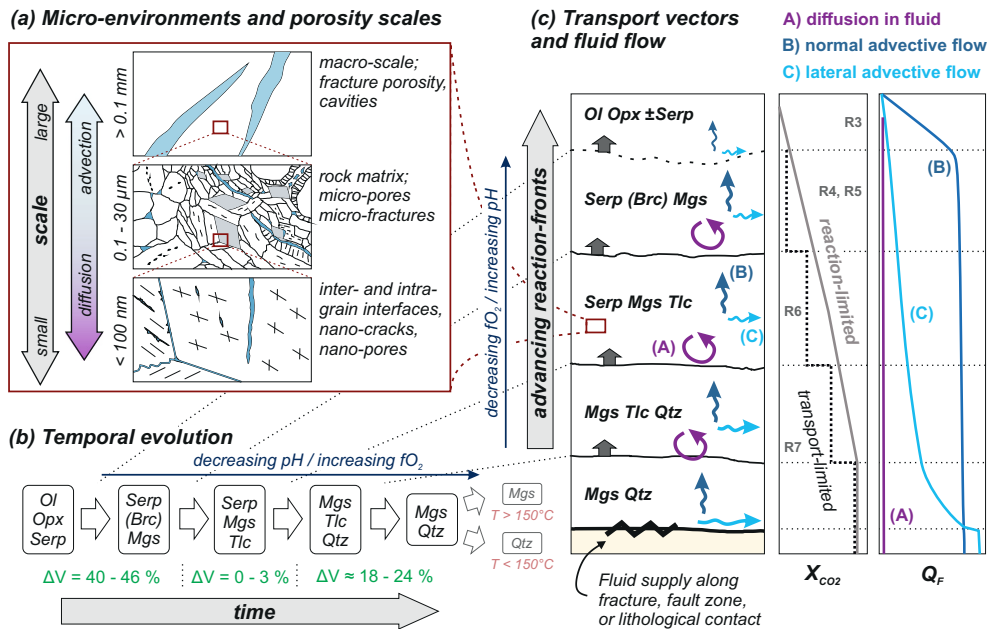


Fig. 10. Schematic illustration of the scale dependence and spatial configuration of micro-environments (a), fluid transport and CO₂ supply during the coupled temporal (b) and spatial (c) evolution of peridotite carbonation across simultaneously advancing reaction fronts. Details about the temporal evolution and related volume changes (ΔV): see Figs. 3 & 6. The idealized plots in (c) show the X_{CO_2} for reaction and transport limited carbonation progress across the reaction fronts, with the stepwise profile corresponding to the equilibrium X_{CO_2} of reactions R3 - R7 (Table 2); and the integrated flux (Q_F) corresponding to the endmember scenarios of (A) purely diffusive CO₂ and mass transfer, (B) advective fluid flow normal to reaction fronts, and (C) lateral advective fluid flow when assuming a hydrological gradient that is mainly oriented sub-parallel to the reaction fronts. The latter may be due to lateral fluid flow along the fracture, fault zone or lithological contact that supplies CO₂ to the ultramafic rock. The schematically illustrated fluxes assume that fluid is H₂O-rich, thus for B) fluid flow only decreases significantly at the serpentinization front. Compared to the total fluid flux shown here, integrated fluxes of CO₂ are expected to decrease monotonously, reflected by the CO₂ content in the different reaction products (Fig. 4).

(A) In principle, the formation of listvenites and related carbonation reaction fronts does not require advective fluid flow but could result from CO₂ diffusion in the aqueous pore fluid along a chemical gradient between peridotite and an adjacent country rock with high CO₂ chemical potential (scenario A in Fig. 10). As long as there is interconnected porosity filled with an aqueous fluid film, diffusion can supply CO₂ also in the absence of a hydrological gradient (i.e. in a stagnant fluid) or with very low fluid fluxes (Q_F in Fig. 10). This process might play an important role during the development of micro-reaction fronts in carbonation batch experiments where diffusional distances are short, although some advective fluid flow may also occur (Sieber et al., 2020). Provided there is enough time and that the interconnected porosity does not become clogged, diffusive mass transfer might also form carbonation reaction fronts at a large scale. A similar process has been suggested for the formation of metasomatic zones in metamorphic rocks, such as blackwalls (Brady, 1977).

(B) In the end-member case of advective fluid flow normal to reaction fronts (scenario B in Fig. 10), and assuming that fluid is comparatively water-rich (CO₂ < H₂O), time-integrated fluid flux would be similar in all reaction zones apart from where serpentinization consumes fluid.

A consequence of this simplified advective fluid flow geometry is that —unless the fluid is extremely CO₂-rich— the zone of fully serpentinized peridotite should be much wider than that of listvenite. For instance, with a fluid X_{CO_2} of ~ 0.03 as used in our models (Fig. 3), each kg peridotite transformed to listvenite would be related to full serpentinization of about 70 kg of dry peridotite. This would mean that a 40 m wide listvenite layer should be accompanied by a ~ 3 km wide zone of completely serpentinized peridotite if all fluid was consumed by the fluid-rock interaction (using densities of 2700 and 2940 kg/m³ for serpentinite and listvenite, respectively). Such a setting may be a

feasible explanation for some natural occurrences (Beinlich et al., 2012), but unlikely in cases where comparatively fresh peridotite is preserved not far from listvenite (Falk and Kelemen, 2015).

(C) Part or much of the advective fluid flow may be lateral, parallel to the orientation of the reaction fronts (scenario C in Fig. 10). Thus, the different reaction zones would record different time-integrated flux, with decreasing flow rates further away from the main fluid conduit. This flow geometry is likely important in listvenites that form preferentially in vicinity to high-permeability fluid conduits like lithological contacts, fractures, or fault or shear zones, because lateral fluid flow is enhanced along-strike of such structures. Possibly lateral flow is also enhanced along the reaction fronts themselves, in particular where the lithological change implies a rheological contrast. The occurrence of parallel veins and localized, fluid-induced deformation at the reaction fronts may indicate an important lateral flow component.

In some cases, simplified models (e.g. diffusion-only) may be justified as first-order estimates. However, natural systems are structurally heterogeneous while fluid flow is inherently transient. Fluid flow and CO₂ transfer in these reactive domains are likely best described by a combination of these endmember scenarios, with a substantial temporal and spatial variability.

4.2.2. Transport and porosity in heterogeneous microstructures

On the macro-scale, advective fluid flow along high-permeability zones such as fractures or lithological contacts likely predominantly controls the CO₂ supply. Fluid flow along a fracture may repeatedly vary between stagnant phases and advective flux in response to cyclic pore pressure variations typical for fault zones (Garofalo et al., 2023). Pervasive carbonation on the other hand depends on the micro-scale porosity of the rock matrix (Fig. 10). There, permeability is lower and

carbonation may become increasingly controlled by diffusion-driven CO₂ transfer within interconnected but comparatively stagnant pore fluid. Advective fluid flow is expected to be minimal in stagnant “dead-ends” and isolated pores, and along nano-scale interfaces like grain boundaries and nano-cracks, where CO₂ supply to the reactive surfaces is entirely controlled by diffusion (Fig. 10 a). At the nano-scale, boundary layer and nano-confinement effects become important, which change the electric permittivity (and in turn the mineral saturation states) and hydrodynamic properties of aqueous fluid in comparison to a non-confined bulk fluid at otherwise the same conditions (e.g., Cole and Striolo, 2019; Emmanuel and Ague, 2009; Escario et al., 2018). In particular serpentines show a large range of grain shapes, ranging from platy to fibrous and tubular habits. Nanopores are ubiquitous in serpentinites (Beinlich et al., 2020b; Malvoisin et al., 2021; Tutolo et al., 2016), with pore shapes depending on the crystal form of the different serpentine polytypes and brucite (Chogani and Plümpfer, 2023).

These different structures from multiscale fractures to nano-porosity control fluid renewal in pores and at the mineral interfaces, and thus in turn reaction pathways and effective carbonation rates that depend on the linkages between transport and reaction kinetics. This leads to the development of different spatially, hydrodynamically and chemically distinct micro-environments (Steeffel et al., 2005) in which fluid flow and reactivity may vary significantly within a single sample as a function of grain size, grain shape anisotropy, and crystal habit of olivine/pyroxene, serpentine-group minerals or talc, as well as the corresponding size, shape and connectivity of pores. The different serpentine micro-structures like serpentine-magnetite (\pm brucite) mesh veins around serpentine or relict olivine in mesh cores, bastite serpentine pseudomorphs after orthopyroxene, and commonly various serpentine vein generations, thus represent different micro-environments with heterogeneous porosity structure, hydrodynamic properties, and carbonation affinity. The details of these effects are not yet fully understood for carbonation reactions as these complex reactive systems are difficult to investigate from the natural rock record and challenging to model.

Reactive percolation experiments (Andreani et al., 2009; Osselin et al., 2022a; Peuble et al., 2018; Peuble et al., 2019) can provide insights to better understand the complex coupling between fluid flow rates, flow paths, fluid chemistry and reaction kinetics. These experiments approach hydrologically realistic conditions of the carbonation process, where over time large volumes of fluid with comparatively constant composition infiltrates and percolates the core sample (high time-integrated but comparatively low instantaneous fluid/rock ratios; reminiscent of scenario B in Fig. 10 c). However, none so far was able to reproduce complete carbonation to listvenite, likely primarily due to time limitations. Nonetheless, these experiments show the influence of fluid flux properties on incipient carbonation. Most importantly, these experiments show that carbonation processes and rates vary strongly depending on the flow rate in different texture and porosity domains of the reactive rock (Andreani et al., 2009; Peuble et al., 2018) (c.f. Fig. 10) and the development of micro-environments within a single core sample (Peuble et al., 2015a, 2015b). The highest flow rates and supply of CO₂ occur along macro-scale fractures and veins. However, in these domains high experimental flow rates may easily inhibit local chemical equilibrium if fluid velocity is faster than dissolution and precipitation kinetics. In interconnected micro-scale fractures and pores, flow rates are lower than the experimentally controlled overall flux. There, transport becomes predominantly diffusive, and dissolution and precipitation may take place at the same place, but the carbonation rates are accordingly lower. Consequently, differences in fluid flow rate at different scales affect the local solution chemistry, which in turn affects precipitation of secondary phases that may or may not clog porosity in different textural domains.

In natural systems, the incipient fluid flow and carbonation reaction rates are also scale dependent and vary as a function of the pre-existing porosity structure inherited from serpentinization. With consumption of serpentine and precipitation of the reaction products, the nano- to micro

porosity evolves dynamically, influenced by various thermo-hydro-mechanical-chemical (THMC) feedback processes that control the resulting grain and pore structure of soapstone and listvenite.

4.3. Porosity renewal by dissolution and solute transfer

Theoretically, listvenite formation could proceed isochemically with respect to non-volatile elements. However, as time-integrated fluid-rock ratios can be very high, changes in major element composition of the solid due to solute transfer need to be taken into account. Such changes are controlled by different dissolution kinetics of different minerals, differences in nucleation and growth kinetics, and by the fluid composition and its speciation as a function of pressure, temperature and fluid flux (Fig. 8). Removal of mass through dissolution and transfer into passing fluids may locally produce the porosity required for continued fluid flux and prevent clogging of permeability by volume expansion as some reaction products precipitate further downstream. This may occur if dissolution rates of the parental phase and fluid flow rates are higher than nucleation and/or growth rates of the products (Putnis, 2015), or when two product phases that are expected to form by carbonation — e.g. magnesite and quartz — have significantly different solubility in the present fluid. For example, Mg²⁺ released by dissolution of Mg-silicate may under certain conditions precipitate in-situ as magnesite whereas SiO_{2,aq} is transported away from the reaction interface and deposited elsewhere, as observed in some carbonation experiments (Grozeva et al., 2017; Lacinska et al., 2017; Peuble et al., 2015a; Sieber et al., 2022). If during the direct replacement of serpentine by quartz and magnesite (R8 in Table 2) >50 mol% of SiO_{2,aq} dissolved from serpentine is transported away with the fluid (< 50% precipitating as quartz), the volume change of reaction becomes negative and porosity is created. In the extreme case for R8 of no in-situ precipitation of quartz, leaching of SiO_{2,aq} may theoretically create up to 22% porosity. Thus, dissolution and precipitation can become spatially decoupled, with porosity created at the interface due to mass removal by the percolating fluid. Porosity renewal by solute transfer appears to be more common at lower temperatures because equilibration between the different minerals and fluid is more sluggish, which favors decoupling of dissolution and precipitation. Other factors that may substantially enhance porosity renewal by dissolution and solute transfer are chlorinity and *f*O₂ of the percolating fluid (Manning et al., 2013; Tiraboschi et al., 2017).

The effect of solute transfer on carbonation reaction progress may be explored through the predicted solubility of different major elements in the different carbonated assemblages leading to listvenite. For example, at the conditions of our infiltration models (Fig. 3 b, Fig. 6 b), Mg loss into the outflow fluid leads to intermittent volume decrease during incipient carbonation of dunite to ophicalcarbonate (Fig. 6 b & d). Thus, brucite dissolution may create porosity during this reaction stage. In soapstone and listvenite assemblages, instead Si loss may produce some transient porosity because equilibrium SiO_{2,aq} concentrations increase with carbonation progress (Fig. 3 b, Fig. 6 b). However, for Si removal to significantly accommodate some of the volume expansion of the reaction from talc to magnesite-quartz, lower CO₂ concentrations in the infiltrated fluid and accordingly much larger integrated fluid/rock ratios than in our models would be necessary. Besides the integrated *f*/*r*, the influence of solute transfer in each specific case strongly depends on pressure, temperature, and infiltrated fluid composition (see also section 3.3; and Klein and Garrido (2011) for low-P conditions).

Flow-through percolation experiments that use olivine powder or dunite as a starting material have shown that direct carbonation of olivine or orthopyroxene grains can proceed to some extent through porosity formation by dissolution (e.g. etch pits) and the development of reactive boundary layers at grain boundaries and along micro-fractures (Hövelmann et al., 2012a; Peuble et al., 2018), a process typical of pseudomorphic replacement by interface-coupled dissolution-precipitation (Putnis, 2015). However, in these experiments carbonation easily stagnates because porosity along fractures and grain boundaries clogs by

precipitation of serpentine, carbonate, or amorphous silica (Hövelmann et al., 2012a), due to the large solid volume increase of >44% of olivine carbonation to magnesite and quartz (R1, Table 2; Kelemen et al., 2011). Prior serpentinization reduces the volume increase related to listvenite formation to 18–20% (Figs. 3 & 6). Thus, porosity may be more easily maintained during carbonation of serpentine in comparison to fresh olivine.

In natural samples, investigating the length scales of chemical heterogeneities in listvenites and related rock types relative to the inferred protolith composition can provide insights into the effect of solute transfer (e.g., Fig. 2; Fig. 9 c). For example, while the average Mg/Si of the Oman DP BT1B listvenites is similar to that of the harzburgite and lherzolite protoliths (Godard et al., 2021; Okazaki et al., 2021), there is significant variability of Mg/Si at the scale of bulk rock chemistry samples (Fig. 2 a). In particular, rocks with intermediate CO₂ bulk rock contents (e.g. 20–30 wt%) have a substantially lower Mg/Si compared to the protolith compositions. This decrease in Mg/Si for listvenites with moderate CO₂ content may be due to local silicification (replacement of serpentine and talc by quartz, with porosity renewal due to leaching of Mg) during the final stage of carbonation, or the result of preferential magnesite dissolution during secondary alteration. In the Oman DP BT1B listvenites, much of the leached Mg likely precipitated again in veins, forming carbonate-rich listvenite domains with high Mg/Si (data points with Mg/Si > 1.8 in Fig. 2 a).

On the hand specimen and thin section scale, mono-mineralic patches and veins are clear indicators of local solute transfer through selective dissolution and/or precipitation. Pseudomorphic replacement structures – a common feature of peridotite carbonation (Andreani et al., 2009; Hövelmann et al., 2011; Sieber et al., 2022) – are ideal to constrain the length scales and controlling factors of solute transfer because they are signs of interface coupled dissolution precipitation processes (Altree-Williams et al., 2015; Putnis and Putnis, 2007), in contrast to secondary precipitation unrelated to listvenite formation. Spectacular pseudomorphic patches of quartz intergrown with minor Cr-bearing muscovite and/or kaolinite after orthopyroxene/bastite in the Oman DP BT1B listvenites (Fig. 9 c) are evidence for local removal of Mg and preferential precipitation of quartz. This kind of chemical heterogeneity cannot be explained solely by the lower Mg/Si of orthopyroxene and bastite in comparison to olivine and mesh serpentine, nor by solid-state diffusion, but requires locally pervasive solute transfer during the final stage of listvenite formation. Similar signs of porosity creation by solute transfer are evident in early antitaxial magnesite veins in Hole BT1B, which represent the incipient reaction stage of carbonation (i.e. formation of carbonate-bearing serpentinite prior to listvenite formation). Much of these veins passively overgrow oxides in the matrix without signs of further dilatant opening, forming micro-reaction fronts from an initially dilatant fracture through replacement of serpentine by magnesite and leaching of SiO_{2,aq} by the fluid (Menzel et al., 2022a). Thus, in spite of carbonate precipitation, reactive fluid flow is sustained because selective dissolution locally causes solid volume decrease. A similar process has also been inferred as an important mechanism promoting porosity renewal and carbonation at the plate-interface of subduction zones (Okamoto et al., 2021).

Because carbonation progress depends on CO₂ reaching the respective reaction fronts, an important question is to which extent listvenite, once formed, remains permeable. He-porosities in ophicarbonates, soapstone and listvenite from Linnajavri, Norway, vary between 0.5 and 3.8%, without obvious correlation with the degree of carbonation (Beinlich et al., 2012). In Oman DP Hole BT1B, porosity in 2 cm³ sample cubes ranges from 0.3 to 6.8% (mean: 2.8%) in listvenite compared to 6.7–13.5% (mean: 10.0%) in carbonate-bearing serpentinite (Kelemen et al., 2020a). Post-mortem micro-tomography of samples from high P-T carbonation experiments also showed significant porosity within the reaction products (Sieber et al., 2020; Sieber et al., 2022). Although measured porosities at ambient conditions may not be equal to the fluid-filled porosity during reaction and the exact relationships between

porosity and permeability are uncertain, it appears evident that pervasive fluid percolation from the fluid source to the reaction fronts may proceed to some extent through listvenite. Our thermodynamic fluid infiltration models (Fig. 3; Fig. 6) predict that continued reactive fluid flux after complete carbonation to quartz–magnesite may lead to a slight solid mass and volume decrease, suggesting that solute transfer can sustain or newly create porosity in listvenite. Thermodynamic modeling indicates that fluid equilibrated with listvenite has a molar Mg/Si > 1.5 at temperatures <150–180 °C (Supplementary Fig. S2), meaning that magnesite is predicted to be more soluble than quartz, in comparison to higher temperatures where fluid Mg/Si < 1, i.e. quartz is more soluble. Thus, porosity renewal in listvenite could proceed by selective dissolution of either magnesite or quartz. In the extreme case, this may produce magnesite-rich listvenite at high temperatures (Fig. 9 d) (Menzel et al., 2018) and quartz-rich assemblages –birbirite – at low temperatures (Aftabi and Zarrinkoub, 2013; Akbulut et al., 2006; Austrheim et al., 2021; Okazaki et al., 2021; Stanger, 1985). This systematic difference between low and high-temperature carbonation is independent of pressure (Supplementary Fig. S2), and in good agreement with carbonation reaction-path models at lower pressure (10–100 MPa; Klein and Garrido, 2011).

4.4. Porosity renewal by deformation

Deformation is a key process renewing porosity during peridotite carbonation through various localized –e.g., fracturing and vein formation– and distributed mechanisms, such as creep cavitation, dilatant granular flow and transformation weakening. We group the latter processes here under the term “reaction assisted ductile deformation”. Because deformation is only rarely accounted for in carbonation models and experiments (Lisabeth et al., 2017), our understanding of the influence of stress and strain on the evolution of reactive porosity during listvenite formation largely relies on interpretation of the microstructural record of natural listvenites. To obtain a well-supported interpretation from natural listvenite, it is imperative to identify those structures that formed during carbonation reaction (e.g., Menzel et al., 2022b), while filtering out structures formed later by overprinting processes (e.g., Menzel et al., 2020b). Furthermore, it is useful to consider that deviatoric stresses are not directly visible in the microstructural record, and that small amounts of strain (e.g. 5–10%) may leave little trace in rocks but nonetheless have a substantial impact on the hydrodynamic evolution during carbonation.

4.4.1. Fracturing and vein formation

The most obvious record of deformation-induced porosity renewal during listvenite formation is precipitation of the reaction products along veins formed by fracturing. Vein formation during carbonation can be caused by reaction-induced fracturing, externally imposed tectonic far-field stresses and deformation, or a combination of both. Reaction-induced fracturing can occur during reactions with major volume expansion, where the crystallization pressure (i.e. the volume strain caused by crystal growth) results in local gradients in deviatoric stress (Røyne and Jamtveit, 2015). Experimental, field and modeling studies indicate that this process can create hierarchical fracture networks that allow sustained fluid flux despite volume expansion during hydration of periclase to brucite (Plümper et al., 2022; Uno et al., 2022; Zheng et al., 2018) and serpentinization of olivine (Farough et al., 2016; Macdonald and Fyfe, 1985; Rudge et al., 2010). Similarly, reaction-induced fracturing has been suggested to enhance carbonation of olivine (Kelemen and Hirth, 2012; Zhu et al., 2016). Reaction-induced fracturing is however inhibited if mean stresses are too high (Guren et al., 2021; Zheng et al., 2018).

Veins, often of multiple generations, are commonplace in listvenites (Beinlich et al., 2012; Kelemen et al., 2020a; Menzel et al., 2018), but their characteristics and formation mechanisms are rarely investigated in detail. In listvenite of Hole BT1B, Oman, several vein generations

formed coeval to carbonation reaction progress (Menzel et al., 2022a). With the exception of pseudomorphic vein networks after serpentine mesh, the patterns of these veins are not hierarchical but parallel or conjugate (Fig. 9 e). This indicates an important influence of tectonic stresses, in combination with pore pressure variations, on fracturing and vein formation (Menzel et al., 2022a), consistent with the observation that the listvenites occur along a major shear zone, similar to many listvenites elsewhere (Table 1). Deviatoric stress from volume expansion possibly contributed to fracturing, but that is masked by the effects of far field stresses. Once formed, veins are compositional and rheological heterogeneities with a different response to deviatoric stress compared to the rock matrix. This may cause dilatant deformation and fluid flux to localize along vein–wall rock interfaces, forming micro-scale reaction fronts and pathways to supply the serpentinite matrix with the CO₂ necessary for pervasive replacement (Menzel et al., 2022a).

4.4.2. Reaction assisted ductile deformation

Dilatant granular flow and creep cavitation are ductile (i.e., distributed) deformation mechanisms that are known to form porosity and enhance fluid flow in natural shear zones (Fusseis et al., 2009). In particular creep cavitation during grain boundary sliding and in the strain shadow of porphyroclasts may thus act as a fluid pump (Fusseis et al., 2023; Fusseis et al., 2009). In serpentinite, ophicarbonates and soapstone, bending and kinking of sheet silicates like brucite, lizardite, antigorite and talc can be viewed as a form of creep cavitation that creates nano-porosity channels within the nano- to micro-scale hinges (Fig. 9 f). Creep cavitation by bending is more likely to occur where relatively harder secondary phases (e.g. Fe-oxides, Cr-spinel, magnesite, quartz) phases impede basal sliding of the sheet silicate, and if elevated pore pressures facilitate locally dilatant rather than compressive shear. These conditions are to be expected during carbonation influenced by external stress within a shear zone, representing a mechanism of porosity renewal that may sustain or enhance carbonation reaction progress. Similar to mylonitic shear zones (Fusseis et al., 2023), micro-porosity may further open preferentially in strain shadows of Fe-oxide and Cr-spinel porphyroclasts as well as of newly formed magnesite, if listvenite formation is synkinematic. Pervasively foliated listvenites of Hole BT1B in the Samail ophiolite contain clear microstructural evidence of synchronous carbonation and ductile deformation (Menzel et al., 2022b). In addition to the discussed mechanisms of dynamic porosity renewal, these listvenites show porosity formation by inter-granular nano-cracking within single magnesite grains, which is manifested in inclusion-free magnesite re-precipitation along crystallographic low-angle boundaries (Fig. 9 g) (Menzel et al., 2022b). Although a localized deformation mechanism at the small scale, electron backscatter diffraction mapping showed that such low-angle boundaries are widespread in magnesite grains of these listvenites, suggesting that on a larger scale nano-cracking may be considered a ductile phenomenon in this situation.

Crystal plastic deformation and dissolution-precipitation creep in serpentinite, soapstone and listvenite can also anneal porosity, thus inhibiting pervasive infiltration of CO₂-bearing fluid. Although critical for fluid-rock interactions and carbonation, the structure and evolution of micro- to nanoscale porosity in variously carbonated serpentinite during deformation is not well understood.

Carbonation reaction progress in turn directly affects the rheology and deformation style. Natural examples and experiments suggest that rocks can become substantially weaker while undergoing reaction, compared to both the protolith and the reaction products (Stünitz et al., 2020; Urai and Feenstra, 2001). This transient process is known as transformation weakening and could also be active during peridotite carbonation (Fig. 8). Similarly, the intermittent formation of talc-rich assemblages during listvenite formation (Fig. 3; Fig. 6) is anticipated to enhance ductile deformation during this reaction stage. The reaction-assisted ductile deformation observed in Hole BT1B listvenites indicates that deformation microstructures typically attributed to comparatively

high-temperature processes such as dislocation creep (shape and crystallographic preferred orientations as well as low-angle boundaries) can be formed at very low temperature due to oriented crystal growth and dissolution-precipitation under deviatoric stress and anisotropic fluid flow in foliated serpentinite (Menzel et al., 2022b). These results also underline that the conversion into listvenite is related to a change in rheology, which cause a change from apparent ductile deformation during pervasive fluid flux and transformation, to likely more brittle deformation behavior once serpentinite is fully carbonated to magnesite and quartz. Deformation microstructures in listvenites are therefore not suitable to directly infer temperature variations or different phases of fluid flow based on classical interpretations of deformation mechanisms, as proposed in some studies (e.g. Gahlan et al., 2022), unless a very detailed microstructure and texture analysis combined with thermometry is done.

4.5. Effective carbonation rates

A critical question about listvenite formation is the time scale of CO₂-fluid-rock interaction, which is intimately linked to the dissolution, nucleation and precipitation kinetics as well as to fluid flow rates. The overall rate of carbonation progress can be determined experimentally through the amount of reaction products forming over different time intervals, or by monitoring changes in the reacting fluid composition. The carbonation rate is controlled by the slowest, rate-limiting process. In simplified terms, carbonation progress may be either reaction-limited or transport-limited. This competition is commonly expressed in terms of the first Damköhler number (Da), which is a measure of the residence time of fluid at the reaction interface versus the kinetic equilibration timescale. In case of reaction-limited carbonation (Da → 0), dissolution, nucleation, and/or precipitation rates are slower than CO₂ (and solute) transfer. Thus, the infiltrated pore fluid that drives the reaction could have significantly higher X_{CO2} than the expected equilibrium value (Fig. 10 c). If carbonation is transport-limited (Da → ∞), the CO₂ transfer in fluid is the limiting factor (Fig. 8 b) and the CO₂ concentration in fluid in each reaction zone will tend to approach the equilibrium X_{CO2} of the respective assemblage (Fig. 10 c). In this case, the width of reaction zones should be rather narrow unless flux has a strong lateral component or infiltrated CO₂ concentration varied.

The overall rate of mineral carbonation is influenced by a multitude of factors, most importantly processes that enhance or reduce porosity and supply of CO₂ to the reaction interface and their respective rates (sections 4.2 & 4.3), the mineralogy, CO₂ concentration in the fluid, temperature, pH, and grain size. Therefore, the rate limiting process will vary throughout the temporal and spatial evolution of single systems. Different simultaneously progressing carbonation reactions may have different rate-limiting processes because dissolution-precipitation kinetics and transport properties differ between the various minerals involved. For instance, the common scarcity or complete lack of talc-magnesite rocks (soapstones) in low-temperature listvenites (Table 1; Fig. 4 d, e) suggests that at ≤ 150 °C carbonation of serpentinite to magnesite-talc is kinetically inhibited, i.e. reaction-limited. In such cases, listvenite formation can proceed through the direct replacement of serpentinite by magnesite and quartz/chalcedony (R8 in Table 2). This carbonation pathway is best explained by reaction overstepping due to high CO₂-concentrations sustained by fast fluid replenishment. Dendritic growth microstructures of magnesite, chalcedony precipitation instead of quartz and the occurrence of quartz–magnesite replacement veins in partially carbonated serpentinite (Beinlich et al., 2020b; Menzel et al., 2022a; Menzel et al., 2022b) can be indicators of high oversaturation during dominantly transport-limited, direct carbonation of serpentinite to listvenite at low temperatures.

There is a large body of experimental studies reporting carbonation reaction rates, at a wide range of P–T conditions, starting materials and fluid compositions and using different experimental approaches (e.g. see literature compilations of olivine carbonation rates in Miller et al., 2019,

and Sendula et al., 2021). However, many carbonation experiments designed to estimate reaction rates are often not representative of natural listvenite formation because they commonly use powdered samples, which additionally may be suspended and stirred in solution. Such experiments avoid or minimize transport-limitation of reaction progress due to clogging of porosity because the volume of sample + initial fluid is similar or larger than the volume of the solid reaction products + reacted fluid. Accordingly, carbonation rates in experiments using cores (natural and/or rock analogues) as starting material are at least 20–100 times slower than similar experiments with powders (Andreani et al., 2009; Osselin et al., 2022a; Peuble et al., 2015a, 2015b, 2018, 2019; Sieber et al., 2018; Sieber et al., 2020; Sieber et al., 2022). Experiments at elevated P–T conditions (550–650 °C, 1–2 GPa) and high CO₂ concentrations show fast effective carbonation rates of peridotites and serpentinites also in non-powdered starting material, with full replacement in ~0.1 to 1.1 mm wide magnesite–talc reaction zones within <1 to 8 days (Fig. 4 b) (Sieber et al., 2020; Sieber et al., 2022). An experiment at 375 °C of the same authors showed substantially lower carbonation rates. Experimental studies at lower temperatures (70–200 °C) achieved carbonate bearing reaction zones in sample cores on the order of several μm to ~100 μm in width, even after one to eight months run time (Hövelmann et al., 2012a; Lacinska et al., 2017). Reaction rates obtained from in-situ monitoring magnesite formation by Raman spectroscopy on synthetic CO₂-rich fluid inclusions (i.e. batch micro-reactors) in olivine are even slower (Sendula et al., 2021). Thus, based on these experiments, carbonation reaction fronts may propagate with velocities in the order of ~0.001 m/yr or less at low temperatures (< 200 °C) to 0.05–0.8 m/yr at high P–T (550–650 °C). As experiments have ideal conditions for carbonation with respect to CO₂ concentration and fluid quantity, effective carbonation rates in nature are likely lower. Deducing carbonation rates in natural rocks is much more challenging. By adjusting the timescales of diffusion–reactive transport models to fit the observed sharpness of the serpentinite to soapstone reaction front at Linnajavri, Beinlich et al. (2020a) inferred that the studied 2.6 m wide talc–magnesite zone had formed in a timescale as short as 20 to 130 years. This corresponds to a propagation velocity of the reaction front of 0.02 to 0.13 m/yr, several orders of magnitude faster than in low

temperature (< 200 °C) experiments (Hövelmann et al., 2012a), and similarly fast as in experiments at >550 °C (Sieber et al., 2020). However, soapstone at Linnajavri formed at ~300 °C and likely significantly lower CO₂ fluid concentration (Beinlich et al., 2012) compared to experiments. Both soapstone formation at Linnajavri and the discussed high-P carbonation experiments mainly regard the transformation of serpentinite to talc–magnesite, a reaction step that is not related to any major volume expansion (Fig. 3 d; Fig. 6 d). Effective rates of listvenite formation may therefore be significantly different, and more strongly influenced by other factors such as advective fluid flux, strain rate and the related rates of porosity renewal.

5. CO₂ fluid sources and geodynamic settings

The provenance of the CO₂-bearing aqueous fluid causing listvenite formation and the geodynamic context are often unclear and subject to interpretation. As outlined before, the fluid needs to meet two principle requirements to potentially form listvenite: (i) a CO₂ concentration higher than that corresponding to the X_{CO₂} of the talc–magnesite–quartz equilibrium, and (ii) a sufficiently high time-integrated fluid flux (or sufficiently high length and time scales of CO₂ diffusion). While modern seawater and groundwater is abundant close to the surface and can indeed lead to carbonate precipitation in peridotite (e.g., Bach et al., 2011; Terniuten et al., 2021a), they have too low CO₂ concentrations to drive the reaction of talc–magnesite to magnesite–quartz. Therefore, such fluids will not form listvenite even when heated to temperature favorable for magnesite precipitation – unless there is a process that enriches them in CO₂. In line with this consideration, most natural case studies of listvenites infer based on field, isotopic and geochemical indications that carbonation was caused by interaction with metamorphic or magmatic–metamorphic fluids (Table 1). In some cases, listvenite formation is thought to have occurred due to mixing of deep CO₂ with shallower aqueous fluids (Table 1). We thus discuss here three idealized settings where the required CO₂ concentration and quantity of fluid to form listvenite may be achieved in nature: (a) release of CO₂-bearing-fluid due to devolatilization of source rocks adjacent to peridotite, implying that fluid production and carbonation occurred at similar P–T

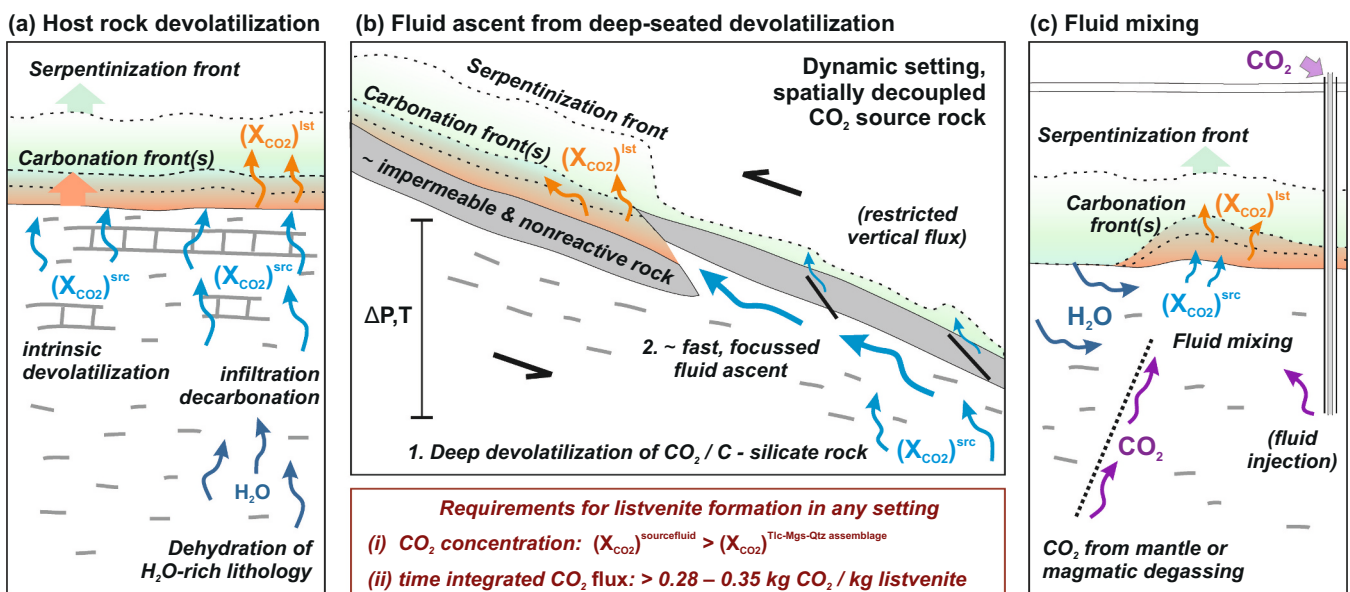
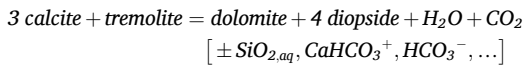


Fig. 11. Schematic sketches of source-to-sink relationships of listvenite formation settings. (a) Host rock devolatilization (either intrinsic or triggered by infiltration) in nearby CO₂ / C bearing silicate rocks: source devolatilization and carbonation occur at similar P–T conditions. (b) Large scale CO₂-bearing fluid transfer of deeper sourced devolatilization fluid without or only partial CO₂ loss by re-equilibration, due to fast advective ascent. (c) CO₂-bearing carbonation fluid produced by mixing of differently sourced CO₂-rich fluid and H₂O-fluid; e.g., comparatively non-reactive CO₂ from mantle or magmatic degassing may ascend along faults until mixed with and dissolved into aqueous fluid. This setting is similar to deep CO₂ injection for carbon sequestration where CO₂ gas with time dissolves into the formation water.

conditions (Fig. 11 a; section 5.1); (b) ascent of CO₂-bearing-fluid from deep-seated devolatilization, rising over substantial length scales such that fluid production and peridotite carbonation are spatially decoupled and may have occurred at different P–T conditions (Fig. 11 b; section 5.2); and (c) mixing of comparatively shallow H₂O-rich fluid with ascending, deeper-sourced CO₂-rich fluid (Fig. 11 c; section 5.3).

5.1. CO₂-bearing fluid from host-rock devolatilization

Metamorphic devolatilization and infiltration-driven devolatilization of carbonate ± organic carbon bearing meta-sediments are commonly considered as the CO₂ source (Table 1). Metamorphic devolatilization refers to the fluid release by dehydration and decarbonation reactions upon heating, such as illustrated for example by the reaction typical for impure marbles:



Instead of a prograde temperature increase, decarbonation reactions are also triggered by infiltration of H₂O-rich aqueous fluid (e.g. fluid released from a carbonate-free lithology). This process is commonly referred to as infiltration-driven decarbonation. In both cases, the released fluid will contain electrolytic solute components (formed by

aqueous dissociation, i.e. dissolution) besides molecular volatile species. The relative proportions of H₂O and CO₂ (i.e. X_{CO2}) and solutes in the fluid depend on P, T, the composition of the rock's equilibration volume, and, in case of an externally derived fluid, the infiltrated fluid composition. Devolatilization fluids vary strongly (e.g. X_{CO2} may range from 10⁻⁶ up to 0.7), with a general trend of low X_{CO2} at high P and low T (e.g. blueschist-facies conditions) and increasingly higher X_{CO2} towards low P and high T (Connolly and Cesare, 1993; Kerrick and Connolly, 2001). At high pressure conditions (> 1 GPa), dissolved carbon in the form of charge electrolytic complexes become increasingly important because the relative permittivity of water decreases with increasing T but increases with P (Galvez et al., 2015; Sverjensky et al., 2014). The heat necessary to trigger the metamorphic or infiltration-driven release of water and CO₂ from the source rock may originate from burial/thrusting (and thermal re-equilibration of the thus perturbed geotherm), subduction, orogenic metamorphism, or magmatic intrusion.

Thermodynamic modeling helps to understand which lithologies are suitable CO₂ sources and which tectono-metamorphic settings are favorable for listvenite formation. Our new modeling as well as previous work indicate that mixed carbonate-silicate meta-sediments like calcschists can produce CO₂-rich fluids during metamorphism (Groppo et al., 2022; Kelemen et al., 2022; Leong et al., 2023) and therefore are ideal CO₂ sources. Such rocks can produce particularly CO₂-rich fluid if they

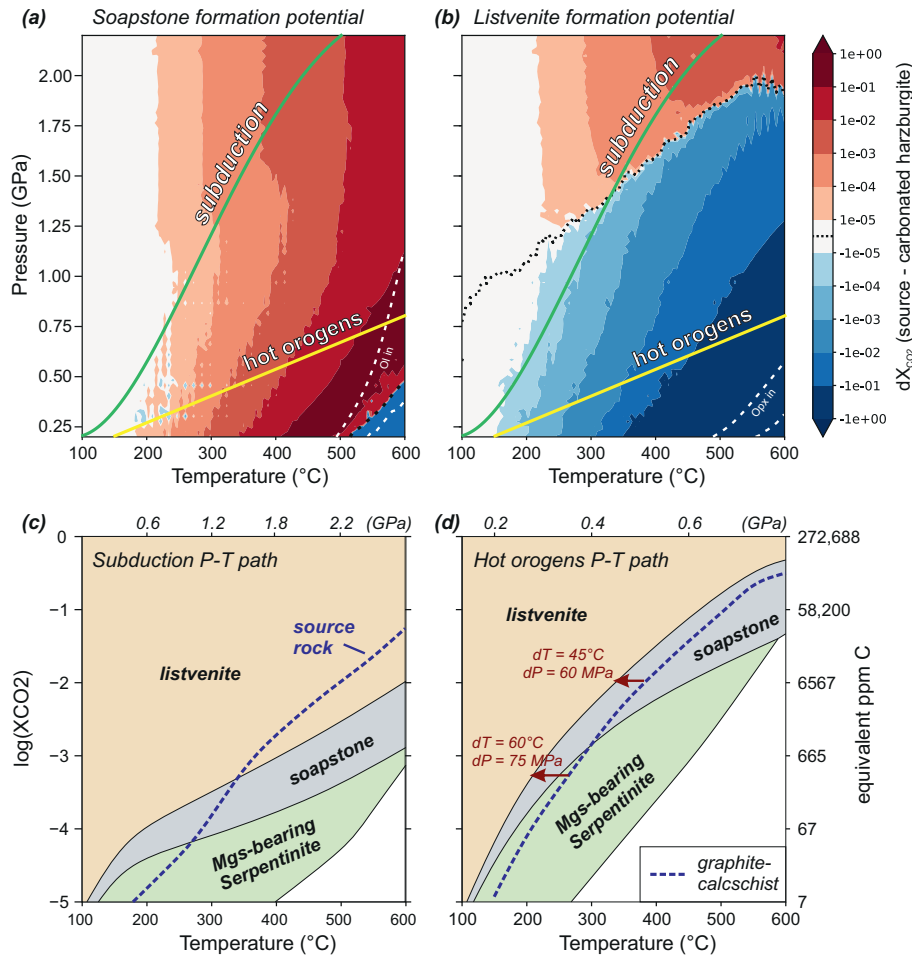


Fig. 12. Thermodynamic modeling insights on CO₂ sources and favorable geodynamic contexts. **(a) and (b):** Potentials to form soapstone (a) and listvenite (b) from the CO₂-bearing fluid produced by a graphite-calcschist in dependence of P and T, expressed as contour plots of the difference of X_{CO2} between source rock and carbonated harzburgite (dX_{CO2}). Red colors indicate conditions where X_{CO2} of the sedimentary source fluid is higher than that required for the soapstone (Atg-Tlc-Mgs) or listvenite (Qtz-Tlc-Mgs) equilibria at the same P–T. **(c) and (d):** X_{CO2} of the graphite-calcschist fluid (dashed line) in comparison to X_{CO2} required for different carbonated assemblages in harzburgite, along the subduction and hot orogenic P–T paths shown in (a) and (b). Subduction path: intermediate-type slab top PT-path of Colombia-Ecuador from van Keken and Wilson (2023); hot orogenic P–T path after Groppo et al. (2022). See text for further discussion and supplementary material for modeling details. (For interpretation of the references to colour in this figure legend, the reader is referred to the web version of this article.)

additionally contain organic carbon or graphite, which may also be mobilized by oxidative dissolution (Tumiati et al., 2020). X_{CO_2} of fluids in equilibrium with graphite-calcschist is low at blueschist-facies conditions and increases strongly towards upper greenschist and amphibolite-facies conditions where various metamorphic reactions occur (c.f. Supplementary Figs. S3 and S4). This trend is typical of meta-sediments in general (Kerrick and Connolly, 2001). In contrast, fluid equilibrated with pure calcite or limestone/marble has too low CO_2 concentrations that are predominantly controlled by dissolution, and will not form soapstone or listvenite when interacting with peridotite (Leong et al., 2023). Fig. 12 shows P–T diagrams of the fluid X_{CO_2} produced by devolatilization of a graphite and carbonate bearing calcschist relative to that required to form soapstone (Fig. 12 a) and listvenite (Fig. 12 b) (see supplementary material for modeling details). The X_{CO_2} of calcschist fluid is higher than that corresponding to the antigorite-talc-magnesite equilibrium in peridotite for most metamorphic conditions (red colors in Fig. 12 a), whether along subduction or orogenic collision P–T paths (Fig. 12 c & d). Thus, soapstone formation can be explained by CO_2 release from adjacent rock units at the same P–T conditions as peridotite (c.f. Fig. 11 a). Soapstone can form rather independent of depth and becomes more feasible at higher temperatures (higher dX_{CO_2} in Fig. 12 a means less fluid is needed). Somewhat counter-intuitively, based on our models, listvenite formation through CO_2 release from adjacent meta-sediments — without fluid cooling and large scale transport — appears not feasible at greenschist to amphibolite facies conditions despite the rather high X_{CO_2} of graphite-calcschist fluids. This is because fluid equilibrated with the magnesite-quartz-talc assemblage has even higher X_{CO_2} , thus other processes are required to permit listvenite formation at these metamorphic conditions. On the other hand, CO_2 -concentrations of fluid produced by equilibrium devolatilization of adjacent graphite-calcschists are high enough to permit listvenite formation during subduction metamorphism (Fig. 12 b & c). While proposed for some listvenite occurrences (Table 1), definite proof of listvenite formation in subduction zones is lacking so far in the natural rock record due to the difficulty to constrain pressure and depth of carbonation. However, evidence from soapstones and ophicarbonates in exhumed subduction melanges and high-pressure metamorphic complexes (Herviou and Bonnet, 2023; Peng et al., 2020; Scambelluri et al., 2016; Spandler et al., 2008), experiments (Sieber et al., 2018; Sieber et al., 2022) and thermodynamic models (e.g., Fig. 12) clearly show that carbonation of forearc mantle wedge peridotites is not only possible but to be expected.

5.1.1. A case example of an inferred local CO_2 source: Linnajavri, Norway

The soapstones and listvenites of Linnajavri, Norway, are a comparatively well studied case example of serpentinite carbonation where the CO_2 -bearing fluid is inferred to have derived from adjacent meta-sediments (Beinlich et al., 2020a; Beinlich et al., 2012; Tominaga et al., 2017). This interpretation is based on the observations that the Linnajavri soapstone and, in places, listvenite lenses crop out at the contact between variably carbonated serpentinite lenses and the surrounding carbonate-micaschist, and that carbonate-quartz veins in the latter rocks have similar ^{18}O and ^{13}C as magnesite and quartz in the carbonated serpentinite (Beinlich et al., 2012). More definite evidence is, however, still lacking, and the CO_2 concentration and fluid quantity that carbonate-micaschist might have produced at the estimated P–T conditions of carbonation (275–300 °C, 0.3 GPa) are unclear. Assuming that the CO_2 concentration of fluid equilibrated with carbonate-micaschist at these conditions is similar to that of our modelled graphite-calcschist ($X_{\text{CO}_2} = 0.003$, Supplementary Fig. S4), host rock devolatilization can explain soapstone formation at Linnajavri, but not listvenite formation (Fig. 12 a, b). This modelled CO_2 concentration of graphite-calcschist fluid at the conditions of carbonation at Linnajavri is significantly lower than the minimum required for listvenite at these conditions ($X_{\text{CO}_2} > 0.010$; Beinlich et al. (2012)). Besides CO_2 concentrations, it is further important to consider the carbon mass balance. The

soapstones at Linnajavri are estimated to a total mass of at least 100 Mt. (Lindhahl and Nilsson, 2008), corresponding to 0.034 km^3 soapstone or $> 16 \text{ Mt.}$ sequestered CO_2 for an average CO_2 content of 16 wt% (c.f. Fig. 5 b). With an X_{CO_2} of 0.003 of infiltrated fluid ($\approx 7.3 \text{ g CO}_2/\text{kg}$ fluid), this would require $>22 \text{ kg}$ fluid for each kg soapstone, or overall $>2200 \text{ Mt.}$ fluid. Even when assuming a high fluid production of 5 wt% from devolatilization of graphite-calcschist, fluid from $>16.24 \text{ km}^3$ of metasediment would need to interact with serpentinite to form the outcropping volume of soapstone (assuming densities of 2.95 and 2.70 g/cm^3 for listvenite and meta-sediment, respectively). In other words, formation of a 10 m thick soapstone layer would require devolatilization of a 4.7 km meta-sediment column for these boundary conditions (1.4 km meta-sediment when assuming $X_{\text{CO}_2} = 0.01$ of the infiltrating fluid), and about the double for the same thickness of listvenite. It appears thus unlikely that simple settings of advective fluid infiltration due to devolatilization of adjacent meta-sediments during sub-greenschist facies metamorphism (as illustrated in Fig. 11 a) can lead to massive, 10s to 100 s of meter thick soapstone and listvenite deposits. Rather, some CO_2 transfer may occur by diffusion in an interconnected stagnant pore fluid over comparatively long time-scales, or externally sourced water-rich fluids infiltrate the host meta-sediments, where they cause infiltration-driven decarbonation. Nonetheless, the modeling suggests that neither diffusional transfer nor infiltration-driven decarbonation will result in carbonation fluids with sufficiently high CO_2 concentrations for listvenite formation, other than in subduction settings (Fig. 12).

5.2. Fluid ascent from deep-seated devolatilization

Many studies of natural listvenites infer P–T conditions corresponding to regional or warm orogenic metamorphism (Table 1), indicating that processes other than simple metamorphic devolatilization of adjacent rocks are required. Our first-order models indicate that in a setting with a geotherm similar to that of hot orogens, listvenite formation is possible if devolatilization fluids released from a lithology like graphite-bearing calcschist ascent and cool by at least 45–60 °C without much loss of CO_2 before infiltrating into ultramafic rocks (Fig. 12 d). If the fluid pathway follows a cooling trajectory equivalent to the geothermal gradient, this would require fluid transport without CO_2 loss over a vertical distance in the order of 1.8–2.8 km, depending on the rock density in this depth interval. This translates to a minimum transport distance of about 2.0–3.2 km in case of a steeply (60°) oriented fluid conduit, or 3.2–5.6 km if fluid ascends along a 30° dipping thrust fault. Partial CO_2 loss during fluid ascent due to partial equilibration with the host rocks may not necessarily prevent listvenite formation but would require accordingly longer fluid transport distances. Although this thermodynamically-informed back-on-the-envelope calculation neglects many of the complexities — for example, here we considered only CO_2 as the main driver of carbonation — it shows that fast fluid ascent from a deeper CO_2 source is a reasonable explanation for listvenite formation (Fig. 11 b). This scenario is particularly relevant for cases where carbonation occurred along km-scale fault zones such as basal thrusts of ophiolites (de Obeso et al., 2022), shear zones accommodating the exhumation of high-P metamorphic complexes (Peng et al., 2020) or deeply rooted transform faults like the San Andreas fault (Klein et al., 2022). High rates of CO_2 degassing observed in springs along plate boundary faults (Barnes et al., 1978) underline that this is a favorable setting for carbonation of ultramafic rock. A similar mode of listvenite formation due to slab-parallel fluid ascent and cooling might lead to extensive carbonation of the cold nose of the mantle wedge of subduction zones, as explored with thermodynamic modeling by Leong et al. (2023).

5.2.1. A case example of fluid ascent from deep-seated devolatilization: BT1B listvenites, Oman

The listvenites of Oman Drilling Project site BT1B in the Samail ophiolite are a good example of a setting where CO_2 -fluid was produced

from a deeper source rock, channelized along a major fault zone and transported over likely rather long distance before reacting with peridotite. Evidence supporting this comes from a combination of field and (micro)structural observations, isotope geochemistry data and thermodynamic considerations. The listvenites occur as several decameter wide and several hundreds of meter long continuous layers in the lowermost mantle section of the ophiolite, commonly in close proximity to the underlying metamorphic sole (Kelemen et al., 2022; Nasir et al., 2007). The metamorphic sole is a meta-igneous – metasedimentary unit that records subduction initiation, exhumation and accretion to the ophiolite base (e.g., Soret et al., 2017), thus demarcating the previous subduction plate interface that evolved into the basal thrust during ophiolite emplacement. The substantially higher metamorphic grade and widely distinct $\delta^{13}\text{C}$ and $^{87}\text{Sr}/^{86}\text{Sr}$ isotopic signature of the metamorphic sole compared to listvenite clearly show that it was not the CO_2 -source for peridotite carbonation (de Obeso et al., 2022; Kelemen et al., 2022). The isotope geochemical data instead indicates that the CO_2 -bearing fluid derived from structurally underlying meta-sediments similar to those of the “Hawasina” formation (de Obeso et al., 2022). The latter is a weakly metamorphosed rock unit derived from distal passive margin sediments that were thrust onto the continental margin together with the ophiolite. Thermodynamic modeling suggests that meta-sediments composed of carbonate-silicate mixtures are the most suitable fluid source, but also that the CO_2 concentration of fluid in equilibrium with such rocks is not high enough to drive the reaction to quartz-magnesite at the P–T conditions at which listvenites formed (90–150 °C, and likely ≥ 0.3 GPa) (Beinlich et al., 2020b; Falk and Kelemen, 2015; Kelemen et al., 2022). Combined, the data and models point to a deep-seated source rock that released CO_2 -bearing fluids at higher temperatures than those recorded by listvenite (Fig. 11 c). This fluid was likely focussed and channelled upwards along the basal fault, restricted from vertical ascent by the rather impermeable and comparatively non-reactive metamorphic sole. The microstructural evidence that listvenite formation at site BT1B was coeval to deformation (Menzel et al., 2022b) further supports a dynamic setting, where deep-sourced CO_2 -bearing fluid could rise along the high-permeability fluid conduit of the basal fault without much loss of CO_2 before infiltrating the peridotite.

5.3. Fluid mixing

High CO_2 -concentrations of fluid, in disequilibrium with both ultramafic rocks and their host rocks, are possible when ascending, deep-sourced CO_2 -rich fluid mixes with comparatively shallow H_2O -rich fluid (Fig. 11 c). In this case, the composition of the carbonation fluid depends less on mineral-fluid equilibria in the host rock but on the relative fluid flow rates of shallow H_2O -rich and deep CO_2 -rich fluid, and the CO_2 concentration of the latter. Deep CO_2 may ascent in the form of immiscible fluid, supercritical CO_2 or exsolved gas bubbles, with limited re-equilibration with the host rocks, and only produce reactive aqueous carbonation fluids once mixing with H_2O . Thus, carbonation fluids may in principle have very high CO_2 concentrations, with a maximum set by the CO_2 solubility in water and the miscibility gap at low pressure (Fig. 7) (Blencoe et al., 2001). Such a setting is similar to carbonation triggered by deep injection of CO_2 gas (Fig. 11 c) and some mineral carbonation experiments (Sanna et al., 2014), where the dissolved inorganic carbon concentration is a function of the partial gas pressure of CO_2 . In natural systems, the CO_2 may for instance originate from degassing of the mantle (Rielli et al., 2022; see below) or of magmatic intrusions (Bénézech et al., 2013; Schandl and Gorton, 2012). Hydrothermal advection around magmatic intrusions favors fluid mixing that may lead to carbonation. Soapstone in the St. Paul transform fault in the Atlantic represents an end-member of peridotite carbonation by mixing of magmatic CO_2 with seawater (Klein et al., 2024), where contact-metamorphic CO_2 sources can be excluded.

5.3.1. A possible case example of fluid mixing

A good example of natural carbonation by fluid mixing may be the carbonated serpentinites in the Ligurian ophiolite of central Tuscany, Italy (Rielli et al., 2022). At these sites, dolomite and magnesite veins and domains of magnesite cemented by chalcedony occur along transfer faults crosscutting serpentinite. These likely formed at $T < 90$ °C, as indicated by the presence of opal. Based on C and O stable isotope compositions of carbonates and the structural context, CO_2 is inferred to originate from degassing of mantle or mantle-derived magmatism, rising along crustal-scale extensional faults before mixing with shallow meteoric waters and reacting with serpentinite (Rielli et al., 2022). Fluid mixing likely leads to high fluctuations of CO_2 concentration of the reactive fluid and thus highly variable precipitation assemblages and structures, which may explain why carbonated serpentinites such as those from the Ligurian ophiolite (Boschi et al., 2009; Rielli et al., 2022) have the appearance of hydrothermal stockwork or vein deposits in contrast to well-developed reaction fronts of classical listvenite outcrops elsewhere (Table 1).

5.4. Indications from dating, structural relationships and geochemistry of listvenite

Constraining the tectonic and geodynamic context of listvenite formation requires a multidisciplinary approach combining insights about the timing and P–T conditions of carbonation, the likely CO_2 source and the structural context. The uncertainties related to all of these parameters are usually substantial (see also section 3.2). While the broad timing may be estimated reasonably well from the regional context (Table 1), obtaining precise knowledge of the age of carbonation is challenging but critical to determine the specific geodynamic setting. Direct timing of carbonation may be obtained by internal Rb–Sr isochron dating of Cr-muscovite bearing listvenite whole rock and mineral separates (Falk and Kelemen, 2015; Hinsken et al., 2017), $^{40}\text{Ar}/^{39}\text{Ar}$ dating of Cr-muscovite mineral separates (Schandl and Gorton, 2012), in-situ U–Pb dating of carbonate (Scharf et al., 2022), or, in rare cases, zircon U–Pb dating (Qiu and Zhu, 2018). As with any dating method, a key issue besides analytical uncertainty is the attribution of which process has been dated. Cr-bearing muscovites may reliably date the actual carbonation process, because they are the product of Cr-spinel breakdown in the moderately acidic conditions of the final listvenite formation stage, with a stability that is likely equivalent to that of pyrophyllite in our infiltration models (Fig. 6 b). They further typically occur in textural equilibrium with carbonate and quartz, and are commonly the only host of Rb. However, this method may be subject to large uncertainties because of potential addition or loss of Rb and/or Sr (Falk and Kelemen, 2015). In-situ U–Pb dating of magnesite is a promising method, but highly challenging due to commonly extremely low U and Pb contents of magnesite formed by carbonation of peridotite, unknown closure temperatures, and the possibility of secondary isotopic resetting by magnesite dissolution-reprecipitation. Dolomite or calcite veins cutting listvenite are more likely to contain sufficient U and Pb compared to magnesite and may in some cases provide rather precise dates for veining (Scharf et al., 2022). However, millions of years may pass between initial listvenite formation and secondary fracturing with dolomite/calcite vein precipitation, thus these may provide only a minimum age. Post-listvenite influx of Ca-bearing fluid can deposit mobile Sr, U and Pb in dolomite/calcite, and dissolution of magnesite during secondary or supergene weathering of listvenite can be accompanied by Pb enrichment (Austrheim et al., 2021). Therefore, detailed microstructural analysis is necessary to identify whether the analyzed carbonate corresponds to syn-carbonation aggregates and veins (Menzel et al., 2022a), or to veins and whole rock domains that were overprinted and chemically modified in a later stage unrelated to listvenite formation (Menzel et al., 2020b). Without such analysis it remains unclear which process the obtained ages actually date.

Many of the case examples listed in Table 1 provide evidence or

suggest that carbonation occurred in active tectonic settings. Various listvenite occurrences are situated along the basal thrust of the respective ophiolite, indicating that carbonation likely took place during a stage of ophiolite emplacement. We consider plate-scale thrust faults as particularly favorable settings for listvenite formation, because this situation provides both the heat needed for metamorphic devolatilization in lower-plate lithologies and a preferential conduit for channelized fluid ascent (Fig. 11 b). Careful structural analysis of cross-cutting relationships and shear sense indicators may help to infer whether carbonation occurred in a compressional or extensional tectonic regime, but this task is challenging as structures in listvenites can be extremely complex due to various stages of fluid-rock interaction in addition to secondary overprints unrelated to listvenite formation.

Sediments that produce particularly CO₂-rich fluids during metamorphic devolatilization — ideally consisting of mixtures of silicates, carbonates and organic carbon — are more commonly found at or proximal to continental margins rather than in deep-sea environments. Thus, mantle rocks of the upper plate forearc wedge of continental subduction zones transitioning into continental collision likely have a higher potential to form listvenites than those of typical ocean-ocean or ocean-continent subduction zones. The common enrichment of K in Cr-bearing muscovite in listvenite may further suggest a certain continental affinity of the fluid sources but more source-to-sink studies using isotope and trace element geochemistry (e.g., de Obeso et al., 2022; Godard et al., 2021) are necessary to validate this hypothesis. High-P experiments have shown that carbonation of peridotites and serpentinite sequesters, to some extent, fluid mobile elements such as Ca²⁺, Sr²⁺, Pb²⁺ and Ba²⁺ from reactive COH-fluids into newly formed carbonates (Sieber et al., 2018). Thus, combined with knowledge of the source rocks and their devolatilization behavior regarding trace elements, the chemical (and isotopic) signature of listvenite may have the potential to provide further insights into the depth and geodynamic context of carbonation.

6. Preservation or carbon remobilization?

The extent of peridotite carbonation and prevalence of listvenites throughout the geological record may be substantially underestimated because weathering and metamorphism can obliterate recognizable carbonation assemblages. This is particularly relevant for the Archean, when carbonation of ultramafic rocks (including komatiites) was likely more widespread than at present due to higher CO₂ concentrations in the atmosphere, seawater and meteoric-influenced hydrothermal fluids (Catling and Zahnle, 2020; Ueda et al., 2017).

6.1. Fuchsite-bearing quartzites and dolomite-quartz rocks – Cryptic listvenites?

Enigmatic Cr-enriched fuchsite-bearing quartzites occur in many Archean cratons, in places associated with (meta-)mafic-ultramafic rock sequences (e.g., Martyn and Johnson, 1986; Wang and Santosh, 2019). These rocks bear many resemblances with more recent examples of fuchsite-bearing quartzite formed by supergene magnesite dissolution from listvenite (Austrheim et al., 2021) and silicified serpentinites (birbirite) (Augustithis, 1967; Lacinska and Styles, 2013; Molly, 1959). They may thus represent the alteration product of listvenites from which carbonate was dissolved or has been replaced by quartz, with Cr-spinel replaced by Cr-bearing muscovite. This may occur (i) coeval with carbonation by continued, massive fluid flux, if temperatures are <150 °C where magnesite solubility in CO₂-bearing fluid is higher than that of quartz (Supplementary Fig. S2) (Klein and Garrido, 2011), (ii) during a secondary hydrothermal alteration event unrelated to carbonation, or (iii) as a result of surface weathering (Beinlich et al., 2018). Tectonic activity post-dating carbonation can enhance magnesite dissolution from listvenite (Menzel et al., 2020b). While carbonation of serpentine to quartz-magnesite commonly does not substantially increase the SiO₂

content relative to MgO (Fig. 3), listvenite formation followed by secondary carbonate dissolution is indeed a viable pathway to form silica-rich lithologies from ultramafic rock. Thus carbonation of ultramafic rocks followed by secondary overprint — leaving a quartzite residue while Mg is lost to rivers and oceans — may add Si-rich lithologies to continental crust over time (Austrheim et al., 2021). Accordingly, many chromite or fuchsite-bearing quartzites may in fact be former listvenites. However, distinguishing if Cr-enriched quartzite formed by alteration of listvenite, as described above, through silicification of serpentinite without prior carbonation, or mixing of detrital chromite in quartz-rich sediment is not straightforward.

Besides selective carbonate weathering, secondary hydrothermal fluids different from those responsible for carbonation may also overprint listvenite. If these secondary fluids are enriched in Ca, they may lead to replacement of magnesite by Ca-carbonates (Amarbayer et al., 2023). Ultimately this process can form Cr-bearing dolomite-quartz or even calcite-quartz rocks, which after metamorphism or deformation may be difficult to distinguish from (detrital chromite-bearing) impure marble.

6.2. Regional and subduction metamorphism of listvenite

The hypothesis that abundant listvenite may form in subduction zones along the slab-mantle interface and within the cold part of the mantle wedge (Kelemen and Manning, 2015) raises the question how likely it is that these rocks “survive” and are exhumed with their carbonation textures preserved, and under which conditions CO₂ uptake is reversed by metamorphism. Fig. 13 shows the main metamorphic phase relations of listvenite and soapstone as a function of P and T. The listvenite assemblage Mgs-Qtz-Tlc-Hem has a very large stability field that widens with increasing pressure, indicating that — unless there is external infiltration of H₂O-rich fluid — most low- to medium-grade metamorphic conditions do not cause any carbon remobilization. Mantle wedge listvenites that are detached and dragged down with the subducted slab will not undergo closed-system decarbonation until heated to >750 °C, when talc and magnesite start to react to orthopyroxene and CO₂-H₂O fluid. How much CO₂ is released by prograde devolatilization depends on the amount of talc initially present and the subduction P-T path, but even in case of talc-magnesite rocks with higher water and lower carbonate content than listvenite, much of the carbonate remains stable (Fig. 13 b; see also Menzel et al., 2020a). With a bulk rock density of >2.9 g/cm³, listvenites are less buoyant than serpentinite and many meta-sediments. If incorporated into the slab and not modified by external fluid infiltration, listvenites are thus prone to transport highly carbon-enriched and oxidized rock volumes to great depth in subduction zones.

For regional metamorphism, the models predict that at upper amphibolite facies conditions listvenites react to magnesite-orthopyroxene rocks (sagvandite), while releasing CO₂-dominated fluid (X_{CO2} > 0.6; Fig. 13 a). Similarly, soapstone is predicted to form olivine-bearing sagvandite at >630 °C (Fig. 13 b). Sagvandites are usually interpreted to form by interaction of peridotite with CO₂ at temperatures >550 °C (Bucher and Stober, 2019; Ohnmacht, 1974; Sieber et al., 2022), calling for a re-evaluation whether some of these may instead be metamorphosed listvenite and soapstone. At granulite facies conditions and during contact metamorphism, listvenite and soapstone undergo complete decarbonation to olivine-orthopyroxene rocks, releasing very CO₂ rich fluid (Fig. 13).

Massive infiltration of H₂O-rich fluid into listvenite can reverse carbonation through carbonate dissolution at any metamorphic grade, as evidenced for example by spectacular pseudomorphic microstructures of serpentine replacing former carbonate (Dunkel et al., 2019). Reversal of listvenite formation by hydration to talc- or serpentine-bearing assemblages is endothermic and requires pervasive fluid flow, but may occur in fluid-rich settings undergoing prograde metamorphism such as shear zones in subduction zones. Likewise, carbonate from

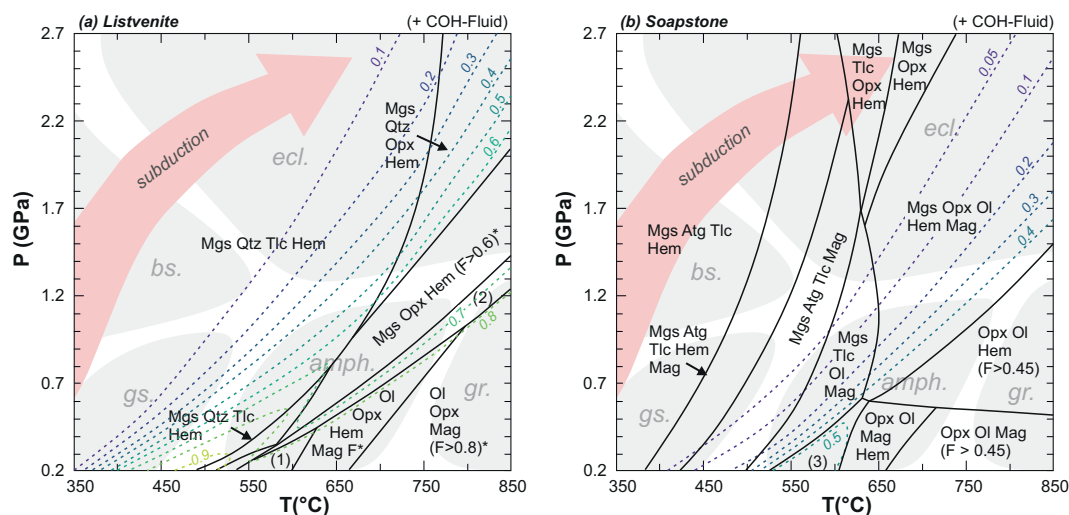


Fig. 13. Metamorphic phase relations and devolatilization of listvenite and soapstone. P–T pseudosections of (a) talc-bearing listvenite and (b) antigorite-talc-magnesite rock (soapstone) with excess water to obtain fluid compositions at all conditions. Fluid X_{CO_2} is indicated by dashed contour lines and values in brackets (F), the latter being minimum values; devolatilization devoid of excess water results in nearly pure CO_2 fluid in fields indicated by (*). Model rock compositions as obtained from the harzburgite infiltration model; see supplementary material for modeling methods. Numbered assemblages (1): Ol Opx Hem; (2): Mgs Opx \pm Hem/Mag; (3) Tlc Ol Mag Hem. Superposed metamorphic facies fields after Bucher and Grapes (2011).

magnesite-talc rocks in subduction zones can be lost and released into fluid due to infiltration-driven decarbonation, for example triggered by dehydration of antigorite in the host serpentinites (Menzel et al., 2020a). To be effective, infiltration-driven decarbonation of talc-magnesite rocks or listvenite in subduction zones requires pervasive infiltration (and drainage) of significant amounts of H_2O -rich fluid ($f/r > 2$).

7. Listvenite formation and engineered CO_2 sequestration

Injection of CO_2 into subsurface basaltic and ultramafic rock formations to induce mineral carbonation (“subsurface CO_2 mineralization” in the following) is a method to permanently store captured CO_2 (e.g., Kelemen et al., 2019; Oelkers et al., 2023; Snæbjörnsdóttir et al., 2020; and references therein). Here we briefly discuss some lessons learned from studies on listvenite formation and how projects of subsurface CO_2 mineralization in ultramafic rocks can in turn improve our understanding of carbonation in natural systems.

Theoretically, triggering listvenite formation from ultramafic rocks by injection of CO_2 is an ideal strategy for safe long-term storage of CO_2 from industrial sources or direct air capture (Matter and Kelemen, 2009; Power et al., 2013), because high amounts of carbon can be stored in comparatively small rock volumes (up to ~ 35 wt% CO_2 ; or 290 Mt. C / km^3 listvenite rock). Natural listvenite occurrences show that complete, pervasive replacement of large rock volumes is possible: for instance, listvenites in the Fanjah region of the Samail ophiolite, Oman, can be estimated to 1–2 km^3 based on field mapping (e.g., Decrausaz et al., 2023; Kelemen et al., 2022). Moreover, carbon remains safely bound in weathering-resistant magnesite-quartz rock over long geological time spans ($> > 1000$ years; Table 1). Accordingly, the global CO_2 storage potential of exhumed mantle rocks is substantial, with a good long-term integrity of the storage reservoirs. However, industrial scale implementation faces various scientific, practical, societal and economic challenges. Concentrating here on the scientific challenges and gaps in knowledge, these are in particular: (i) obtaining the optimal P–T–X conditions, (ii) sustaining permeability, and (iii) monitoring and modeling of reactive systems at the mesoscale (volumes of 1–1000 m^3 ; timespans of years to hundreds of years).

At optimal P–T–X conditions for engineered systems (< 5 km depth, 170–200 $^\circ\text{C}$, and CO_2 -rich fluid — CO_2 -saturated water or wet supercritical CO_2), laboratory batch experiments have shown that a considerable extent of peridotite carbonation is possible within comparatively

short time (days to weeks) (Kelemen and Matter, 2008; Kelemen et al., 2011; Miller et al., 2019; Sanna et al., 2014). Carbonation is also observed in porous core samples for flow-through experiments mimicking the hydrodynamic conditions of subsurface CO_2 mineralization, although carbonation rates appear hampered by hydrodynamic conditions (e.g., Andreani et al., 2009; Peuble et al., 2019). The temperature, necessity of mining and grinding of the feedstock material and difficulties to remove the reaction products from reactor vessels make industrial reactors and other ex-situ applications energy, environmental and economic cost intensive. Many of these issues can be avoided during subsurface CO_2 mineralization. Injection of CO_2 -bearing fluid into basalts at ~ 750 m depth and temperatures up to 260 $^\circ\text{C}$ successfully led to CO_2 mineralization at the hydrothermally active site of the CarbFix2 Project on Iceland (Clark et al., 2020; Oelkers et al., 2023). With normal geothermal gradients (25–30 $^\circ\text{C}/\text{km}$) in ultramafic rocks, significantly deeper boreholes would be required to attain temperatures of 170–200 $^\circ\text{C}$. The natural rock record shows that listvenites can form already at 90 $^\circ\text{C}$ (Table 1), with slower predicted carbonation rates but still significantly faster than at ambient conditions (Paukert et al., 2012). This temperature corresponds to 3–4 km depth, conditions that are attainable in enhanced (or “stimulated”) deep geothermal energy systems (e.g., Kumari and Ranjith, 2019).

A major challenge for subsurface CO_2 mineralization is permeability, which is notoriously low in partially serpentinitized peridotites. In the OmanDP drill cores of the Samail ophiolite, the measured mean permeability ranged from 10^{-17} to 10^{-19} m^2 for dunite and 10^{-20} to 10^{-21} m^2 for harzburgite sections (Katayama et al., 2020), but is much higher in fractures. Natural samples indicate that fracturing and vein formation are very common in serpentinites and listvenites (e.g., Menzel et al., 2022a). Hence, permeability in any given rock volume is highly heterogeneous, and its evolution during carbonation is challenging to predict. In nature, an interplay of deformation and solute transfer processes renew porosity and thus sustain permeability (c.f. sections 4.4 & 4.5). CO_2 -serpentinite interaction in some sections of the San Andreas fault system suggest that in actively deforming settings, talc formation due to carbonation may additionally have the positive side effect of favoring aseismic creep over seismic rupture because water-saturated talc has low friction coefficients and is velocity-strengthening (Klein et al., 2022; Moore and Rymer, 2007). However, the interplays between different hydration and carbonation reactions, fluid pore pressures, stress and changing rheology are far from being understood well enough

to risk subsurface injection of CO₂-bearing fluids into a seismically active fault zone. For engineered subsurface CO₂ mineralization, the challenges of low initial permeability and porosity reduction by clogging may partially be addressed by (i) targeting fossil serpentinite fault zones that are highly fractured, with accordingly higher permeability and reactive surface area, (ii) modifying the injected fluid composition to favor incipient dissolution over precipitation, and (iii) induced hydro-fracturing. Induced hydro-fracturing — a common method to create permeability applied in enhanced geothermal systems (e.g., Kumari and Ranjith, 2019, and references therein) — could be used to create initial fluid pathways in subsurface peridotites in settings that are presently not tectonically active (Power et al., 2013), provided that the inherent (micro-)seismicity is controlled to acceptable risk levels. Nonetheless, the conditions (e.g. CO₂ concentration, pH and flux of fluid) that may prevent or at least minimize clogging of porosity and/or fractures by carbonate precipitation are still unclear and require further study. Likewise, there is a wealth of experimental studies investigating the effects of pH, chlorinity and a variety of chemical additives on carbonation reactions rates. In comparison, little is known to date about the detailed composition of fluids causing listvenite formation in nature, calling for more research on fluid inclusions and mobile element geochemistry.

Subsurface CO₂ mineralization has the benefit of comparatively limited surface land-use conflicts, but comes at the high cost required for deep drilling operations in crystalline rock (Kelemen et al., 2020b). Coupling subsurface mineral carbonation with geothermal energy and possibly natural H₂ production (Osselin et al., 2022b; Templeton et al., 2024) may potentially alleviate some of these costs. Although many questions remain about compatibility and practicality, such combined approaches may present a promising way forward. Further research exploring possible synergies between CO₂ storage, geothermal energy, and natural H₂ is warranted, among other aspects: (i) to find methods to maintain or renew fracture permeability while also causing carbonation, (ii) to prevent the possible, undesired formation of CH₄ instead of H₂ (c. f. Fig. 3; Fig. 6), and (iii) to evaluate if leakage of CO₂, CH₄ and H₂ can be inhibited by self-healing of fractures through carbonate precipitation.

The timescales of listvenite formation are difficult to constrain from natural rocks (see section 4.5). Careful monitoring of the carbonation extents, ideally obtained from pilot sites of subsurface CO₂ mineralization, in combination with more laboratory experiments and field data, will allow to better quantify carbonation efficiency and rates under natural conditions, thus guiding to a deeper understanding of listvenite formation. In turn, experiments and research on natural listvenites provide the necessary scientific knowledge for developing field scale subsurface CO₂ mineralization projects in ultramafic rocks, in particular with respect to the optimal P–T–X conditions and the modeling and quantification of coupled thermo-hydro-mechanical-chemical processes at the meso-scale. We posit that integrating knowledge from natural geological processes will further help to design monitoring and verification protocols for safe CO₂ storage by mineral carbonation.

Summary and outlook

- I. Listvenites and similar extensively carbonated ultramafic rocks are — although volumetrically sparse — common in many ophiolites and exhumed metamorphic massifs throughout most of Earth's geological history. For many natural occurrences, critical data on pressure/depth, temperature, age, or tectonic/structural context of carbonation is however uncertain, subject to interpretation, or missing (Table 1). As some of these parameters are inherently difficult to estimate from serpentinite, soapstone and listvenite, future studies would ideally adopt a holistic and multifaceted approach combining insights from petrology, geochemistry and structural geology, also of neighboring rocks and the non-reacted ultramafic protolith(s). Such efforts are warranted because listvenites, due to their reactive origin, bear substantial indirect information about otherwise cryptic processes, such as CO₂-bearing fluid release from meta-mafic and meta-sedimentary rocks or the development of large-scale focused fluid flow paths at depth and their interplay with deformation in major shear zones.
- II. The carbonation reaction sequence leading to listvenite and related reaction fronts is well understood and goes along with drastic changes with respect to equilibrium fluid composition, pH, oxygen fugacity, as well as a substantial increase in mass and volume. We show that this evolution with reaction progress — including serpentinization — can be simulated with great detail and consistency by thermodynamic infiltration models. Less clear are the consequences these changes, particularly of pH and *f*O₂, have for the mobility of metals, fluid-mobile trace elements, minor volatiles and halogens.
- III. The main requirements for listvenite formation are (i) an ultramafic protolith, (ii) infiltration of aqueous fluid with sufficiently high CO₂ concentration (depending on the P–T conditions), and (iii) high time-integrated fluid/rock ratios and processes that allow continued fluid flow despite nominal volume expansion of reaction. Major open questions remain about the impact of cationic aqueous species, reduced volatiles, carbon bearing solute complexes and halogens in the infiltrated fluids.
- IV. The rate-limiting process of listvenite formation in nature is likely mass transport (specifically, CO₂ supply) in settings with temperatures higher than 150 °C. A multitude of thermo-hydro-mechanical-chemical (THMC) feedbacks influence precipitation of reaction products, fluid flow, and in turn, effective carbonation rates. These feedbacks change dynamically as mineralogy, microstructure and pore properties change with reaction progress, and have variable impact at different scales. We infer that the most important mechanisms of porosity renewal allowing continued reaction progress are (i) solute transfer, (ii) fracturing and veining, and (iii) reaction assisted ductile deformation. Detailed microstructural investigation can provide a qualitative assessment of these mechanisms and their impact on porosity-permeability evolution and reaction progress. However, given the complexity of THMC feedback processes, many open questions remain. Important issues are to better estimate the natural time scales of listvenite formation at different conditions, and understand the effect of nano-confinement on dissolution-precipitation and mass transfer across different porosity scales and morphologies. Further needed are better constraints of the relative importance of diffusional versus advective mass transfer in different micro-environments and how they are affected by different THMC processes and external parameters.
- V. The CO₂ source for listvenite formation is inferred to be, in most natural cases, metamorphic devolatilization and/or dissolution of carbonate ± organic carbon bearing meta-mafic or meta-sedimentary lithologies. This does not exclude other CO₂ sources, in particular magmatic degassing can be important in places. However, some settings, such as simple meteoric alteration or dissolution of pure limestone, are clearly not viable. First-order thermodynamic modeling suggests that while soapstone can form in many metamorphic settings, listvenite formation mostly requires rapid, large scale ascent and cooling of deeper sourced fluids. As the overwhelming majority of listvenite occurrences are spatially related to major fault or shear zones, deformation is likely the key factor that facilitates such large scale channeling and ascent of CO₂-bearing fluid. Besides their role as a carbon sink, listvenites may thus also be viewed as fossil archives of massive fluid flux along deforming plate interfaces. Improving our knowledge of age, depth and structural context of natural listvenites and surrounding rocks, more source-to-sink investigations based on isotope and/or trace element geochemistry,

as well as thermodynamic transport models are needed to establish the geodynamic settings of listvenite occurrences.

- VI. There is likely a large number of cases where lithologies that had been listvenites are not recognized as such because of secondary alteration or metamorphism. In particular fuchsite or Cr-spinel bearing quartzites that have not received much attention due to their enigmatic origin may shed more light onto possible secular variations of the impact of listvenite formation on the deep carbon cycle throughout Earth's history.
- VII. Although natural listvenite formation commonly appears to occur in geological contexts that are impossible or not feasible to induce artificially — especially where listvenite forms at >5 km depth or is synkinematic to shear zone deformation — many of the involved processes and feedback mechanisms are also relevant for subsurface carbon sequestration by mineral carbonation. The naturally exposed record of fossil listvenites and their related carbonation reaction fronts provide invaluable insights for developing strategies of artificial subsurface mineral carbonation, because mid to large scale subsurface field experiments in ultramafic rocks are still lacking and would always remain inaccessible to direct observation.

Funding

M.D.M. acknowledges a postdoctoral fellowship (Postdoc_21_00791) funded by the Junta de Andalucía (Consejería de Conocimiento y Universidades), Spain, and cofunded by “EFRD a way making Europe” and the ESF program “FSE invierte en tu futuro”. For this research, MG was supported by the Agence Nationale de la Recherche, France (grant no. ANR-18-CE01-0014-01 LISZT).

Author contributions

Manuel D. Menzel: Conceptualization, Formal analysis, Investigation, Thermodynamic Modeling, Methodology, Validation, Visualisation, Writing – original draft, Writing – review & editing. **Melanie J. Sieber:** Conceptualization, Validation, Writing – review & editing. **Marguerite Godard:** Conceptualization, Validation, Writing – review & editing.

Declaration of competing interest

The authors declare that they have no known competing financial interests or personal relationships that could have appeared to influence the work reported in this paper.

Data availability

Thermodynamic modeling was done using the open-access Fortran programs of *Perple_X* (available at: <https://www.perplex.ethz.ch/>) by James Connolly. All setup variables and modeling compositions necessary to reproduce the models are described and included in the Supplementary material of this study.

Acknowledgments

Discussions with many colleagues throughout the past years have helped to develop and shape the content presented in this study. In particular, we would like to acknowledge here Thierry Decrausaz, Juan Carlos de Obeso and the participants of the Oman Drilling project. We further thank Carlos Garrido and Lisa Eberhard for their feedback on an early draft of the manuscript, Frieder Klein and anonymous for their peer-review comments, and Yildirim Dilek for editorial handling. M.D.M. is deeply grateful to the late Janos L. Urai, for proposing and encouraging this study, for all the discussions about THMC feedback mechanisms, and having been a great mentor.

Appendix A. Supplementary data

Supplementary data to this article can be found online at <https://doi.org/10.1016/j.earscirev.2024.104828>.

References

- Aftabi, A., Zarrinkoub, M.H., 2013. Petrogeochemistry of listvenite association in metaophiolites of Sahlabad region, eastern Iran: Implications for possible epigenetic Cu–Au ore exploration in metaophiolites. *Lithos* 156–159, 186–203.
- Ague, J.J., 1998. Simple models of coupled fluid infiltration and redox reactions in the crust. *Contrib. Mineral. Petrol.* 132, 180–197.
- Akbulut, M., Piskin, O., Karayigit, A.I., 2006. The genesis of the carbonatized and silicified ultramafics known as listvenites: a case study from the Mihalicik region (Eskisehir), NW Turkey. *Geol. J.* 41, 557–580.
- Allen, D.E., Seyfried, W.E., 2003. Compositional controls on vent fluids from ultramafic-hosted hydrothermal systems at mid-ocean ridges: an experimental study at 400°C, 500 bars. *Geochim. Cosmochim. Acta* 67, 1531–1542.
- Altire-Williams, A., Pring, A., Ngathai, Y., Brugger, J., 2015. Textural and compositional complexities resulting from coupled dissolution-reprecipitation reactions in geomaterials. *Earth Sci. Rev.* 150, 628–651.
- Amarbayar, N., Dandar, O., Wang, J., Okamoto, A., Uno, M., Batsaikhan, U., Takayanagi, H., Iryu, Y., Tsuchiya, N., 2023. Progressive carbonation and Ca-metasomatism of serpentinized ultramafic rocks: insights from natural occurrences and hydrothermal experiments. *Contrib. Mineral. Petrol.* 178, 38.
- Andreani, M., Luquot, L., Gouze, P., Godard, M., Hoisé, E., Gibert, B., 2009. Experimental study of carbon sequestration reactions controlled by the percolation of CO₂-rich brine through peridotites. *Environ. Sci. Technol.* 43, 1226–1231.
- Angiboust, S., Pettke, T., De Hoog, J.C.M., Caron, B., Oncken, O., 2014. Channelized fluid flow and eclogite-facies metasomatism along the subduction shear zone. *J. Petrol.* 55, 883–916.
- Agustithis, S.S., 1967. On the phenomenology and geochemistry of differential leaching and element agglutination processes. *Chem. Geol.* 2, 311–329.
- Austrheim, H., Andersen, T.B., 2023. Extreme enrichment of arsenic and antimony during alteration of serpentinized peridotites to form listvenite-like dolomite–quartz rocks and Ni–Cr-rich jasper and quartzites in the Highland Border Complex of Scotland. *J. Geol. Soc. Lond.* 180 jgs2023-2054.
- Austrheim, H., Corfu, F., Renggli, C.J., 2021. From peridotite to fuchsite bearing quartzite via carbonation and weathering: with implications for the Pb budget of continental crust. *Contrib. Mineral. Petrol.* 176, 94.
- Aydal, D., 1990. Gold-bearing listwaenites in the Araç Massif, Kastamonu, Turkey. *Terra Nova* 2, 43–52.
- Bach, W., Rosner, M., Jöns, N., Rausch, S., Robinson, L.F., Paulick, H., Erzinger, J., 2011. Carbonate veins trace seawater circulation during exhumation and uplift of mantle rock: results from ODP Leg 209. *Earth Planet. Sci. Lett.* 311, 242–252.
- Barnes, I., O'Neill, J.R., Rapp, J.B., White, D.E., 1973. Silica-carbonate alteration of serpentine; wall rock alteration in Mercury Deposits of the California Coast Ranges. *Econ. Geol.* 68, 388–398.
- Barnes, I., Irwin, W.P., White, D.E., 1978. Global distribution of carbon dioxide discharges, and major zones of seismicity. *Water-Resources Investigations Report* 78-39, 17.
- Barry, P.H., de Moor, J.M., Giovannelli, D., Schrenk, M., Hummer, D.R., Lopez, T., Pratt, C.A., Segura, Y.A., Battaglia, A., Beaudry, P., Bini, G., Cascante, M., d'Errico, G., di Carlo, M., Fattorini, D., Fullerton, K., Gazel, E., González, G., Halldórsson, S.A., Iacovino, K., Kulongoski, J.T., Manini, E., Martfnez, M., Miller, H., Nakagawa, M., Ono, S., Patwardhan, S., Ramírez, C.J., Regoli, F., Smedile, F., Turner, S., Vetriani, C., Yücel, M., Ballentine, C.J., Fischer, T.P., Hilton, D.R., Lloyd, K.G., 2019. Forearc carbon sink reduces long-term volatile recycling into the mantle. *Nature* 568, 487–492.
- Beinlich, A., Austrheim, H., Glodny, J., Erambert, M., Andersen, T.B., 2010. CO₂ sequestration and extreme Mg depletion in serpentinized peridotite clasts from the Devonian Solund basin, SW-Norway. *Geochim. Cosmochim. Acta* 74, 6935–6964.
- Beinlich, A., Plümper, O., Hövelmann, J., Austrheim, H., Jamtveit, B., 2012. Massive serpentinite carbonation at Linnajavri, N-Norway. *Terra Nova* 24, 446–455.
- Beinlich, A., Austrheim, H., Mavromatis, V., Grguric, B., Putnis, C.V., Putnis, A., 2018. Peridotite weathering is the missing ingredient of Earth's continental crust composition. *Nat. Commun.* 9, 634.
- Beinlich, A., John, T., Vrijmoed, J.C., Tominaga, M., Magna, T., Podladchikov, Y.Y., 2020a. Instantaneous rock transformations in the deep crust driven by reactive fluid flow. *Nat. Geosci.* 13, 307–311.
- Beinlich, A., Plümper, O., Boter, E., Muller, I.A., Kourim, F., Ziegler, M., Harigane, Y., Lafay, R., Kelemen, P.B., Oman Drilling Project Science Team, 2020b. Ultramafic rock carbonation: constraints from Listvenite Core BT1B, Oman Drilling Project. *J. Geophys. Res. Solid Earth* 125 e2019JB019060.
- Belogub, E.V., Melekestseva, I.Y., Novoselov, K.A., Zabolina, M.V., Tret'yakov, G.A., Zaykov, V.V., Yuminov, A.M., 2017. Listvenite-related gold deposits of the South Urals (Russia): a review. *Ore Geol. Rev.* 85, 247–270.
- Bénézech, P., Stefánsson, A., Gautier, Q., Schott, J., 2013. Mineral solubility and aqueous speciation under hydrothermal conditions to 300 °C – the carbonate system as an example. *Rev. Mineral. Geochem.* 76, 81–133.
- Blencoe, J.G., Naney, M.T., Anovitz, L.M., 2001. The CO₂-H₂O system: III. A new experimental method for determining liquid-vapor equilibria at high subcritical temperatures. *Am. Mineral.* 86, 1100–1111.

- Boedo, F.L., Escayola, M.P., Perez Lujan, S.B., Vujovich, G., Ariza, J.P., Naipauer, M., 2015. Geochemistry of Precordillera serpentinites, western Argentina: evidence for multistage hydrothermal alteration and tectonic implications for the Neoproterozoic-early Paleozoic. *Geol. Acta* 0263–0278.
- Boschi, C., Dini, A., Dallai, L., Ruggieri, G., Gianelli, G., 2009. Enhanced CO₂-mineral sequestration by cyclic hydraulic fracturing and Si-rich fluid infiltration into serpentinites at Malenrata (Tuscany, Italy). *Chem. Geol.* 265, 209–226.
- Boskabadi, A., Pitcairn, I.K., Broman, C., Boyce, A., Teagle, D.A.H., Cooper, M.J., Azer, M.K., Stern, R.J., Mohamed, F.H., Majka, J., 2017. Carbonate alteration of ophiolitic rocks in the Arabian–Nubian Shield of Egypt: sources and compositions of the carbonating fluid and implications for the formation of Au deposits. *Int. Geol. Rev.* 59, 391–419.
- Boskabadi, A., Pitcairn, I.K., Leybourne, M.L., Teagle, D.A.H., Cooper, M.J., Hadzizadeh, H., Nasiri Bezenjani, R., Monazzami Bagherzadeh, R., 2020. Carbonation of ophiolitic ultramafic rocks: Listvenite formation in the Late Cretaceous ophiolites of eastern Iran. *Lithos* 352–353, 105307.
- Brady, J.B., 1977. Metasomatic zones in metamorphic rocks. *Geochim. Cosmochim. Acta* 41, 113–125.
- Bucher, K., Grapes, R., 2011. *Petrogenesis of Metamorphic Rocks*, 8th ed. Springer, Springer Heidelberg Dordrecht London New York.
- Bucher, K., Stober, I., 2019. Interaction of Mantle Rocks with crustal fluids: sagvandites of the Scandinavian Caledonides. *J. Earth Sci.* 30, 1084–1094.
- Buisson, G., Leblanc, M., 1985. Gold in carbonatized ultramafic rocks from ophiolite complexes. *Econ. Geol.* 80, 2028–2029.
- Catling, D.C., Zahnle, K.J., 2020. The Archean atmosphere. *Sci. Adv.* 6, eaax1420.
- Chavagnac, V., Monnin, C., Ceuleneer, G., Boulart, C., Hoareau, G., 2013. Characterization of hyperalkaline fluids produced by low-temperature serpentinization of mantle peridotites in the Oman and Ligurian ophiolites. *Geochem. Geophys. Geosyst.* 14, 2496–2522.
- Chen, Z.-Y., O'Connor, W.K., Gerdemann, S.J., 2006. Chemistry of aqueous mineral carbonation for carbon sequestration and explanation of experimental results. *Environ. Prog.* 25, 161–166.
- Chogani, A., Plümper, O., 2023. Decoding the nanoscale porosity in serpentinites from multidimensional electron microscopy and discrete element modelling. *Contrib. Mineral. Petrol.* 178, 78.
- Cipolli, F., Gambardella, B., Marini, L., Ottonello, G., Vetuschci Zuccolini, M., 2004. Geochemistry of high-pH waters from serpentinites of the Gruppo di Voltri (Genova, Italy) and reaction path modeling of CO₂ sequestration in serpentinite aquifers. *Appl. Geochem.* 19, 787–802.
- Clark, D.E., Oelkers, E.H., Gunnarsson, I., Sigfússon, B., Snæbjörnsdóttir, S.Ó., Aradóttir, E.S., Gíslason, S.R., 2020. CarbFix2: CO₂ and H₂S mineralization during 3.5 years of continuous injection into basaltic rocks at more than 250 °C. *Geochim. Cosmochim. Acta* 279, 45–66.
- Clavé, E., Benzerara, K., Meslin, P.Y., Forni, O., Royer, C., Mandon, L., Beck, P., Quantin-Nataf, C., Beyssac, O., Cousin, A., Bousquet, B., Wiens, R.C., Maurice, S., Dehouck, E., Schröder, S., Gasnault, O., Mangold, N., Dromart, G., Bosak, T., Bernard, S., Udry, A., Anderson, R.B., Arana, G., Brown, A.J., Castro, K., Clegg, S.M., Cloutis, E., Fairén, A.G., Flannery, D.T., Gasda, P.J., Johnson, J.R., Lasue, J., Lopez-Reyes, G., Madariaga, J.M., Manrique, J.A., Le Mouélic, S., Núñez, J.I., Ollila, A.M., Pilleri, P., Pilorget, C., Pinet, P., Poulet, F., Veneranda, M., Wolf, Z.U., the SuperCam, t, 2023. Carbonate detection with SuperCam in igneous rocks on the floor of Jezero Crater, Mars. *J. Geophys. Res. Planets* 128 e2022JE007463.
- Cole, D., Striolo, A., 2019. The influence of nanoporosity on the behavior of carbon-bearing fluids. In: Orcutt, B.N., Daniel, I., Dasgupta, R. (Eds.), *Deep Carbon: Past to Present*. Cambridge University Press, Cambridge, pp. 358–387.
- Connolly, J.A.D., Cesare, B., 1993. C-O-H-S fluid composition and oxygen fugacity in graphitic metapelites. *J. Metamorph. Geol.* 11, 379–388.
- Connolly, J.A.D., Galvez, M.E., 2018. Electrolytic fluid speciation by Gibbs energy minimization and implications for subduction zone mass transfer. *Earth Planet. Sci. Lett.* 501, 90–102.
- Cutts, J.A., Steinhorsdottir, K., Turvey, C., Dipple, G.M., Enkin, R.J., Peacock, S.M., 2021. Deducing mineralogy of serpentinized and carbonated ultramafic rocks using physical properties with implications for carbon sequestration and subduction zone dynamics. *Geochem. Geophys. Geosyst.* 22 e2021GC009989.
- Dasgupta, R., 2013. Ingassing, storage, and outgassing of terrestrial carbon through geologic time. *Rev. Mineral. Geochem.* 75, 183–229.
- Daval, D., Hellmann, R., Martinez, I., Gangloff, S., Guyot, F., 2013. Lizardite serpentine dissolution kinetics as a function of pH and temperature, including effects of elevated pCO₂. *Chem. Geol.* 351, 245–256.
- Davis, B.K., Hickey, K.A., Rose, S., 2001. Superposition of gold mineralisation on pre-existing carbonate alteration: structural evidence from the Mulgarrrie gold deposit, Yilgarn Craton. *Aust. J. Earth Sci.* 48, 131–149.
- de Obeso, J.C., Kelemen, P.B., Leong, J.M., Menzel, M.D., Manning, C.E., Godard, M., Cai, Y., Bolge, L., Oman Drilling Project Phase 1 Science, P., 2022. Deep sourced fluids for peridotite carbonation in the Shallow Mantle Wedge of a Fossil Subduction Zone: Sr and C Isotope Profiles of OmanDP Hole BT1B. *J. Geophys. Res. Solid Earth* 127 e2021JB022704.
- Decrausaz, T., Godard, M., Menzel, M.D., Parat, F., Oliot, E., Lafay, R., Barou, F., 2023. Pervasive carbonation of peridotite to listvenite (Semail Ophiolite, Sultanate of Oman): clues from iron partitioning and chemical zoning. *Eur. J. Mineral.* 35, 171–187.
- Duan, Z., Sun, R., 2003. An improved model calculating CO₂ solubility in pure water and aqueous NaCl solutions from 273 to 533 K and from 0 to 2000 bar. *Chem. Geol.* 193, 257–271.
- Dunkel, K., Jamtveit, B., Austrheim, H., 2019. Ophicarbonates of the Feragen Ultramafic Body, central Norway. *Nor. J. Geol.* 99, 1–18.
- Emam, A., Zoheir, B., 2013. Au and Cr mobilization through metasomatism: microchemical evidence from ore-bearing listvenite, South Eastern Desert of Egypt. *J. Geochem. Explor.* 125, 34–45.
- Emmanuel, S., Ague, J.J., 2009. Modeling the impact of nano-pores on mineralization in sedimentary rocks. *Water Resour. Res.* 45.
- Epstein, G.S., Bebout, G.E., Angiboust, S., 2021. Fluid and mass transfer along transient subduction interfaces in a deep paleo-accretionary wedge (Western Alps). *Chem. Geol.* 559, 119920.
- Escario, S., Godard, M., Gouze, P., Leprovost, R., 2018. Experimental study of the effects of solute transport on reaction paths during incipient serpentinization. *Lithos* 323, 191–207.
- Escayola, M., Proenza, J., van Staal, C., Rogers, N., Skulski, T., 2009. The Point Rouse Listvenites, Baie Verte, Newfoundland: altered ultramafic rocks with potential for gold mineralization. *Current Research Geological Survey Report* 09-1, 1–12.
- Falk, E.S., Kelemen, P.B., 2015. Geochemistry and petrology of listvenite in the Semail ophiolite, Sultanate of Oman: complete carbonation of peridotite during ophiolite emplacement. *Geochim. Cosmochim. Acta* 160, 70–90.
- Farley, K.A., Stack, K.M., Shuster, D.L., Horgan, B.H.N., Hurowitz, J.A., Tarnas, J.D., Simon, J.I., Sun, V.Z., Scheller, E.L., Moore, K.R., McLennan, S.M., Vasconcelos, P. M., Wiens, R.C., Treiman, A.H., Mayhew, L.E., Beyssac, O., Kizovski, T.V., Tosca, N. J., Williford, K.H., Crumpler, L.S., Beegle, L.W., Bell 3rd, J.F., Ehlmann, B.L., Liu, Y., Maki, J.N., Schmidt, M.E., Allwood, A.C., Amundsen, H.E.F., Bhartiya, R., Bosak, T., Brown, A.J., Clark, B.C., Cousin, A., Forni, O., Gabriel, T.S.J., Goreva, Y., Gupta, S., Hamran, S.E., Herd, C.D.K., Hickman-Lewis, K., Johnson, J.R., Kah, L.C., Kelemen, P. B., Kinch, K.B., Mandon, L., Mangold, N., Quantin-Nataf, C., Rice, M.S., Russell, P.S., Sharma, S., Siljestrom, S., Steele, A., Sullivan, R., Wadhwa, M., Weiss, B.P., Williams, A.J., Woglsland, B.V., Willis, P.A., Acosta-Maeda, T.A., Beck, P., Benzerara, K., Bernard, S., Burton, A.S., Cardarelli, E.L., Chide, B., Clave, E., Cloutis, E.A., Cohen, B.A., Czaja, A.D., Debaille, V., Dehouck, E., Fairén, A.G., Flannery, D.T., Fleron, S.Z., Fouchet, T., Frydenvang, J., Garczynski, B.J., Gibbons, E.F., Hausrath, E.M., Hayes, A.G., Henneke, J., Jorgensen, J.L., Kelly, E.M., Lasue, J., Le Mouélic, S., Madariaga, J.M., Maurice, S., Merusi, M., Meslin, P.Y., Milkovich, S.M., Million, C.C., Moeller, R.C., Nunez, J.I., Ollila, A.M., Paar, G., Paige, D.A., Pedersen, D.A.K., Pilleri, P., Pilorget, C., Pinet, P.C., Rice Jr., J.W., Royer, C., Sautter, V., Schulte, M., Sephton, M.A., Sharma, S.K., Sholes, S.F., Spanovich, N., St Clair, M., Tate, C.D., Ueckert, K., VanBommel, S.J., Yanchilina, A.G., Zorzano, M.P., 2022. Aqueously altered igneous rocks sampled on the floor of Jezero crater, Mars. *Science* 377 eabo2196.
- Farough, A., Moore, D.E., Lockner, D.A., Lowell, R.P., 2016. Evolution of fracture permeability of ultramafic rocks undergoing serpentinization at hydrothermal conditions: an experimental study. *Geochem. Geophys. Geosyst.* 17, 44–55.
- Frost, B.R., 1985. On the stability of sulfides, oxides, and native metals in serpentinite. *J. Petrol.* 26, 31–63.
- Furnes, H., de Wit, M., Dilek, Y., 2014. Four billion years of ophiolites reveal secular trends in oceanic crust formation. *Geosci. Front.* 5, 571–603.
- Fussei, F., Regenauer-Lieb, K., Liu, J., Hough, R.M., De Carlo, F., 2009. Creep cavitation can establish a dynamic granular fluid pump in ductile shear zones. *Nature* 459, 974–977.
- Fussei, F., Allsop, C., Gilgannon, J., Schrank, C., Harley, S., Schlepütz, C.M., 2023. Strain shadow “megapores” in mid-crustal ultramylonites. *Geology* 51, 748–752.
- Gahlan, H.A., Azer, M.K., Asimow, P.D., Al-Kahtany, K.M., 2020. Petrogenesis of gold-bearing listvenites from the carbonatized mantle section of the Neoproterozoic Ess ophiolite, Western Arabian Shield, Saudi Arabia. *Lithos* 372–373, 105679.
- Gahlan, H.A., Azer, M.K., Asimow, P.D., Al-Kahtany, K.M., 2022. Formation of gold-bearing listvenite in the mantle section of the Neoproterozoic Bir Umq ophiolite, Western Arabian Shield, Saudi Arabia. *J. Afr. Earth Sci.* 190, 104517.
- Galvez, M.E., Pubellier, M., 2019. How do subduction zones regulate the carbon cycle? In: Orcutt, B.N., Daniel, I., Dasgupta, R. (Eds.), *Deep Carbon: Past to Present*. Cambridge University Press, Cambridge, pp. 276–312.
- Galvez, M.E., Manning, C.E., Connolly, J.A.D., Rumble, D., 2015. The solubility of rocks in metamorphic fluids: a model for rock-dominated conditions to upper mantle pressure and temperature. *Earth Planet. Sci. Lett.* 430, 486–498.
- Garofalo, P.S., Scarsi, M., Gundlach-Graham, A., Schwarz, G., Günther, D., 2023. Feedbacks between fast brittle faulting, hydrothermal fluid flow, and metal transport within carbonated ultramafics (Ligurian Western Alps, Italy). *Mineral. Deposita* 58, 833–852.
- Giampouras, M., Garrido, C.J., Zwicker, J., Vadillo, I., Smrzka, D., Bach, W., Peckmann, J., Jiménez, P., Benavente, J., García-Ruiz, J.M., 2019. Geochemistry and mineralogy of serpentinization-driven hyperalkaline springs in the Ronda peridotites. *Lithos* 350–351, 105215.
- Gilgannon, J., Freitas, D., Rizzo, R.E., Wheeler, J., Butler, I.B., Seth, S., Marone, F., Schlepütz, C.M., McGill, G., Watt, I., Plümper, O., Eberhard, L., Amiri, H., Chogani, A., Fussei, F., 2023. Elastic stresses can form metamorphic fabrics. *Geology* 52, 166–170.
- Glein, C.R., Waite, J.H., 2020. The Carbonate Geochemistry of Enceladus’ Ocean. *Geophys. Res. Lett.* 47.
- Godard, M., Jousselin, D., Bodinier, J.-L., 2000. Relationships between geochemistry and structure beneath a palaeo-spreading centre: a study of the mantle section in the Oman ophiolite. *Earth Planet. Sci. Lett.* 180, 133–148.
- Godard, M., Carter, E.J., Decrausaz, T., Lafay, R., Bennett, E., Kourim, F., de Obeso, J.C., Michibayashi, K., Harris, M., Coggon, J.A., Teagle, D.A.H., Kelemen, P.B., the Oman Drilling Project Phase 1 Science, P., 2021. Geochemical profiles across the listvenite-metamorphic transition in the basal megathrust of the semail ophiolite: results from drilling at OmanDP Hole BT1B. *J. Geophys. Res. Solid Earth* 126 e2021JB022733.
- Goff, F., Lackner, K.S., 1998. Carbon dioxide sequestering using ultramafic rocks. *Environ. Geosci.* 5, 89–101.

- Gropo, C., Rolfo, F., Frezzotti, M.L., 2022. CO₂ outgassing during collisional orogeny is facilitated by the generation of immiscible fluids. *Commun. Earth Environ.* 3, 13.
- Grosch, E.G., Vidal, O., Abu-Alam, T., McLoughlin, N., 2012. P-T constraints on the metamorphic evolution of the Paleoproterozoic Kromberg type-section, Barberton Greenstone Belt, South Africa. *J. Petrol.* 53, 513–545.
- Grozeva, N.G., Klein, F., Seewald, J.S., Sylva, S.P., 2017. Experimental study of carbonate formation in oceanic peridotite. *Geochim. Cosmochim. Acta* 199, 264–286.
- Guren, M.G., Sveinsson, H.A., Hafreager, A., Jamtveit, B., Malthe-Sørenssen, A., Renard, F., 2021. Molecular dynamics study of confined water in the periclase-brucite system under conditions of reaction-induced fracturing. *Geochim. Cosmochim. Acta* 294, 13–27.
- Halls, C., Zhao, R., 1995. Listvenite and related rocks: perspectives on terminology and mineralogy with reference to an occurrence at Cregganbaun, Co. Mayo, Republic of Ireland. *Mineral. Deposita* 30, 303–313.
- Hanghøj, K., Kelemen, P.B., Hassler, D., Godard, M., 2010. Composition and Genesis of Depleted Mantle Peridotites from the Wadi Tayin Massif, Oman Ophiolite; Major and Trace Element Geochemistry, and Os Isotope and PGE Systematics. *J. Petrol.* 51, 201–227.
- Hansen, L.D., Dipple, G.M., Gordon, T.M., Kellett, D.A., 2005. Carbonated serpentinite (listwanite) at Atlin, British Columbia: a geological analogue to carbon dioxide sequestration. *Can. Mineral.* 43, 225–239.
- Herviu, C., Bonnet, G., 2023. Paleocene-eocene high-pressure carbonation of Western Alps serpentinites: positive feedback between deformation and CO₂-CH₄ fluid ingress responsible for slab slicing? *Geochim. Geophys. Geosyst.* 24 e2022GC010557.
- Hinsken, T., Bröcker, M., Strauss, H., Bulle, F., 2017. Geochemical, isotopic and geochronological characterization of listvenite from the Upper Unit on Tinos, Cyclades, Greece. *Lithos* 282–283, 281–297.
- Hövelmann, J., Austrheim, H., Beinlich, A., Anne Munz, I., 2011. Experimental study of the carbonation of partially serpentinized and weathered peridotites. *Geochim. Cosmochim. Acta* 75, 6760–6779.
- Hövelmann, J., Austrheim, H., Jamtveit, B., 2012a. Microstructure and porosity evolution during experimental carbonation of a natural peridotite. *Chem. Geol.* 334, 254–265.
- Hövelmann, J., Putnis, C.V., Ruiz-Agudo, E., Austrheim, H., 2012b. Direct nanoscale observations of CO₂ sequestration during brucite [Mg(OH)₂] dissolution. *Environ. Sci. Technol.* 46, 5253–5260.
- Hsu, H.-W., Postberg, F., Sekine, Y., Shibuya, T., Kempf, S., Horányi, M., Juhász, A., Altobelli, N., Suzuki, K., Masaki, Y., Kuwatani, T., Tachibana, S., Sirono, S.-I., Moragas-Klostermeyer, G., Srama, R., 2015. Ongoing hydrothermal activities within Enceladus. *Nature* 519, 207–210.
- IPCC, 2021. Climate Change 2021: The Physical Science Basis. Contribution of Working Group I to the Sixth Assessment Report of the Intergovernmental Panel on Climate Change. In: Masson-Delmotte, V., Zhai, P., Pirani, A., Connors, S.L., Péan, C., Berger, S., Caud, N., Chen, Y., Goldfarb, L., Gomis, M.I., Huang, M., Leitzell, K., Lonnoy, E., Matthews, J.B.R., Maycock, T.K., Waterfield, T., Yelekçi, O., Yu, R., Zhou, B. (Eds.), Sixth Assessment Report of the Intergovernmental Panel on Climate Change. Cambridge University Press, Cambridge, United Kingdom and New York, NY, USA.
- IPCC, 2023. Climate Change 2023: Synthesis Report. Contribution of Working Groups I, II and III to the Sixth Assessment Report of the Intergovernmental Panel on Climate Change. In: Core Writing Team, Lee, H., Romero, J. (Eds.), Sixth Assessment Report of the Intergovernmental Panel on Climate Change, IPCC, Geneva, Switzerland, pp. 35–115.
- Iyer, K., Jamtveit, B., Mathiesen, J., Malthe-Sørenssen, A., Feder, J., 2008. Reaction-assisted hierarchical fracturing during serpentinization. *Earth Planet. Sci. Lett.* 267, 503–516.
- Ji, C., Zhang, K.-J., Yan, L.-L., 2022. Hydrothermal metasomatism and solid-phase transfer in petrogenesis of listvenite: the Meso-Tethyan ophiolite, Central Tibet, China. *Contrib. Mineral. Petrol.* 178, 4.
- Johannes, W., 1967. Zur Bildung und Stabilität von Forsterit, Talk, Serpentin, Quarz und Magnesit im System MgO-SiO₂-H₂O-CO₂. *Contrib. Mineral. Petrol.* 15, 233–250.
- Johannes, W., 1969. An experimental investigation of the system MgO-SiO₂-H₂O-CO₂. *Am. J. Sci.* 267, 1083–1104.
- Katayama, I., Abe, N., Hatakeyama, K., Akamatsu, Y., Okazaki, K., Ulven, O.I., Hong, G., Zhu, W., Cordonnier, B., Michibayashi, K., Godard, M., Kelemen, P., the Oman Drilling Project Phase 2 Science, P., 2020. Permeability profiles across the crust-mantle sections in the Oman drilling project inferred from dry and wet resistivity data. *J. Geophys. Res. Solid Earth* 125, e2019JB018698.
- Kelemen, P.B., Hirth, G., 2012. Reaction-driven cracking during retrograde metamorphism: Olivine hydration and carbonation. *Earth Planet. Sci. Lett.* 345–348, 81–89.
- Kelemen, P.B., Manning, C.E., 2015. Reevaluating carbon fluxes in subduction zones, what goes down, mostly comes up. *Proc. Natl. Acad. Sci.* 112, E3997–E4006.
- Kelemen, P.B., Matter, J., 2008. In situ carbonation of peridotite for CO₂ storage. *Proc. Natl. Acad. Sci.* 105, 17295–17300.
- Kelemen, P.B., Matter, J., Streit, E.E., Rudge, J.F., Curry, W.B., Blusztajn, J., 2011. Rates and mechanisms of mineral carbonation in peridotite: natural processes and recipes for enhanced, in situ CO₂ capture and storage. In: Jeanloz, R., Freeman, K.H. (Eds.), Annual Review of Earth and Planetary Sciences, vol. 39, pp. 545–576.
- Kelemen, P., Benson, S.M., Pilorgé, H., Psarras, P., Wilcox, J., 2019. An overview of the status and challenges of CO₂ storage in minerals and geological formations. *Front. Climate* 1.
- Kelemen, P.B., Matter, J.M., Teagle, D.A.H., Coggon, J.A., the Oman Drilling Project Science Team, 2020a. Site BT1: fluid and mass exchange on a subduction zone plate boundary. In: Kelemen, P.B., Matter, J.M., Teagle, D.A.H., Coggon, J.A., et al. (Eds.), Proceedings of the Oman Drilling Project. International Ocean Discovery Program, College Station, TX.
- Kelemen, P.B., McQueen, N., Wilcox, J., Renforth, P., Dipple, G., Vankeuren, A.P., 2020b. Engineered carbon mineralization in ultramafic rocks for CO₂ removal from air: review and new insights. *Chem. Geol.* 119628.
- Kelemen, P.B., Carlos de Obeso, J., Leong, J.A., Godard, M., Okazaki, K., Kotowski, A.J., Manning, C.E., Ellison, E.T., Menzel, M.D., Urai, J.L., Hirth, G., Rioux, M., Stockli, D. F., Lafay, R., Beinlich, A.M., Coggon, J.A., Warsi, N.H., Matter, J.M., Teagle, D.A.H., Harris, M., Michibayashi, K., Takazawa, E., Al Sulaimani, Z., the Oman Drilling Project Science Team, 2022. Listvenite formation during mass transfer into the leading edge of the Mantle Wedge: initial results from Oman Drilling Project Hole BT1B. *J. Geophys. Res. Solid Earth* 127 e2021JB022352.
- Kerrick, D.M., Connolly, J.A.D., 2001. Metamorphic devolatilization of subducted marine sediments and the transport of volatiles into the Earth's mantle. *Nature* 411, 293.
- Kim, J., Kimura, Y., Puchala, B., Yamazaki, T., Becker, U., Sun, W., 2023. Dissolution enables dolomite crystal growth near ambient conditions. *Science* 382, 915–920.
- King, H.E., Plümper, O., Putnis, A., 2010. Effect of Secondary Phase Formation on the Carbonation of Olivine. *Environ. Sci. Technol.* 44, 6503–6509.
- Klein, F., Garrido, C.J., 2011. Thermodynamic constraints on mineral carbonation of serpentinized peridotite. *Lithos* 126, 147–160.
- Klein, F., McCollom, T.M., 2013. From serpentinization to carbonation: new insights from a CO₂ injection experiment. *Earth Planet. Sci. Lett.* 379, 137–145.
- Klein, F., Goldsby, D.L., Lin, J., Andreani, M., 2022. Carbonation of Serpentinite in Creeping Faults of California. *Geophys. Res. Lett.* 49 e2022GL099185.
- Klein, F., Schroeder, T., John, C.M., Davis, S., Humphris, S.E., Seewald, J.S., Sichel, S., Bach, W., Brunelli, D., 2024. Mineral carbonation of peridotite fueled by magmatic degassing and melt impregnation in an oceanic transform fault. *Proc. Natl. Acad. Sci.* 121, e2315662121.
- Koziol, A.M., Newton, R.C., 1998. Experimental determination of the reaction; magnesite + enstatite = forsterite + CO₂ in the ranges 6–25 kbar and 700–1100 degrees C. *Am. Mineral.* 83, 213–219.
- Kumari, W.G.P., Ranjith, P.G., 2019. Sustainable development of enhanced geothermal systems based on geotechnical research – a review. *Earth Sci. Rev.* 199, 102955.
- Lacinska, A.M., Styles, M.T., 2013. Silicified serpentinite – a residuum of a Tertiary palaeo-weathering surface in the United Arab Emirates. *Geol. Mag.* 150, 385–395.
- Lacinska, A.M., Styles, M.T., Bateman, K., Wagner, D., Hall, M.R., Gowing, C., Brown, P. D., 2016. Acid-dissolution of antigorite, chrysotile and lizardite for ex situ carbon capture and storage by mineralisation. *Chem. Geol.* 437, 153–169.
- Lacinska, A.M., Styles, M.T., Bateman, K., Hall, M., Brown, P.D., 2017. An experimental study of the carbonation of serpentinite and partially serpentinized peridotites. *Front. Earth Sci.* 5, 37.
- Leong, J.A., de Obeso, J.C., Manning, C.E., Kelemen, P.B., 2023. Thermodynamic constraints on the fate of carbon mobilized from subducted sediments in the overlying mantle wedge. *Earth Planet. Sci. Lett.* 623, 118424.
- Lindahl, I., Nilsson, L.P., 2008. Geology of the soapstone deposits of the Linnajavri area, Hamarøy, Nordland, north Norwegian Caledonides—Norway's largest reserves of soapstone. In: Slagstad, T. (Ed.), *Geology for Society*, Geological Survey of Norway Special Publication, 11, pp. 19–35.
- Lisabeth, H.P., Zhu, W., Kelemen, P.B., Ilgen, A., 2017. Experimental evidence for chemo-mechanical coupling during carbon mineralization in ultramafic rocks. *Earth Planet. Sci. Lett.* 474, 355–367.
- Macdonald, A.H., Fyfe, W.S., 1985. Rate of serpentinization in seafloor environments. *Tectonophysics* 116, 123–135.
- Malvoisin, B., Baumgartner, L.P., 2021. Mineral dissolution and precipitation under stress: model formulation and application to metamorphic reactions. *Geochim. Geophys. Geosyst.* 22 e2021GC009633.
- Malvoisin, B., Auzende, A.-L., Kelemen, P.B., 2021. Nanostructure of serpentinisation products: Importance for water transport and low-temperature alteration. *Earth Planet. Sci. Lett.* 576, 117212.
- Manning, C.E., Shock, E.L., Sverjensky, D., 2013. The chemistry of carbon in aqueous fluids at crustal and uppermantle conditions: experimental and theoretical constraints. *Rev. Mineral. Geochem.* 75, 109–148.
- Martyn, J.E., Johnson, G.I., 1986. Geological setting and origin of fuchsite-bearing rocks near Menzies, Western Australia. *Aust. J. Earth Sci.* 33, 1–18.
- Matter, J.M., Kelemen, P.B., 2009. Permanent storage of carbon dioxide in geological reservoirs by mineral carbonation. *Nat. Geosci.* 2, 837–841.
- McCollom, T.M., Seewald, J.S., 2007. Abiotic synthesis of organic compounds in Deep-Sea hydrothermal environments. *Chem. Rev.* 107, 382–401.
- McDonough, W.F., 1990. Constraints on the composition of the continental lithospheric mantle. *Earth Planet. Sci. Lett.* 101, 1–18.
- Menzel, M.D., Garrido, C.J., López Sánchez-Vizcaíno, V., Marchesi, C., Hidas, K., Escayola, M.P., Delgado Huertas, A., 2018. Carbonation of mantle peridotite by CO₂-rich fluids: the formation of listvenites in the Advocate ophiolite complex (Newfoundland, Canada). *Lithos* 323, 238–261.
- Menzel, M.D., Garrido, C.J., López Sánchez-Vizcaíno, V., 2020. Fluid-mediated carbon release from serpentinite-hosted carbonates during dehydration of antigorite-serpentinite in subduction zones. *Earth Planet. Sci. Lett.* 531, 115964.
- Menzel, M.D., Urai, J.L., de Obeso, J.C., Kotowski, A., Manning, C.E., Kelemen, P.B., Kettermann, M., Jesus, A.P., Harigane, Y., the Oman Drilling Project Phase 1 Science, T., 2020b. Brittle deformation of carbonated peridotite—insights from listvenites of the Samail Ophiolite (Oman Drilling Project Hole BT1B). *J. Geophys. Res. Solid Earth* 125 e2020JB020199.
- Menzel, M.D., Urai, J.L., Ukar, E., Decrausaz, T., Godard, M., 2022a. Progressive veining during peridotite carbonation: insights from listvenites in Hole BT1B, Samail ophiolite (Oman). *Solid Earth* 13, 1191–1218.

- Menzel, M.D., Urai, J.L., Ukar, E., Hirth, G., Schwedt, A., Kovács, A., Kibkalo, L., Kelemen, P.B., 2022b. Ductile deformation during carbonation of serpentinized peridotite. *Nat. Commun.* 13, 3478.
- Mervine, E.M., Humphris, S.E., Sims, K.W.W., Kelemen, P.B., Jenkins, W.J., 2014. Carbonation rates of peridotite in the Samail Ophiolite, Sultanate of Oman, constrained through ¹⁴C dating and stable isotopes. *Geochim. Cosmochim. Acta* 126, 371–397.
- Miller, Q.R.S., Schaeff, H.T., Kaszuba, J.P., Gadikota, G., McGrail, B.P., Rosso, K.M., 2019. Quantitative review of olivine carbonation kinetics: reactivity trends, mechanistic insights, and research frontiers. *Environ. Sci. Technol. Lett.* 6, 431–442.
- Molly, E.W., 1959. Platinum deposits of Ethiopia. *Econ. Geol.* 54, 467–477.
- Moore, D.E., Rymer, M.J., 2007. Talc-bearing serpentinite and the creeping section of the San Andreas fault. *Nature* 448, 795–797.
- Moussa, H.E., Azer, M.K., Abou El Maaty, M.A., Maurice, A.E., Yanni, N.N., Akarish, A.I. M., Elnazer, A.A., Elsagheer, M.A., 2021. Carbonation of Neoproterozoic mantle section and formation of gold-bearing listvenite in the Northern Nubian Shield. *Lithos* 406–407, 106525.
- Müller, R.D., Mather, B., Dutkiewicz, A., Keller, T., Merdith, A., Gonzalez, C.M., Gorczyk, W., Zahirovic, S., 2022. Evolution of Earth's tectonic carbon conveyor belt. *Nature* 605, 629–639.
- Nasir, S., Al Sayigh, A.R., Al Harthy, A., Al-Khribash, S., Al-Jaaidi, O., Musllam, A., Al-Mishwat, A., Al-Bu'saidi, S., 2007. Mineralogical and geochemical characterization of listwaenite from the Samail Ophiolite, Oman. *Geochemistry* 67, 213–228.
- NOAA, 2023. Carbon Cycle Greenhouse Gases - Trends in CO₂. NOAA Earth System Research Laboratories, Global Monitoring Laboratory, Boulder, Colorado, USA. <https://gml.noaa.gov/ccgg/trends/global.html> last accessed: 04/12/2023.
- Noël, J., Godard, M., Oliot, E., Martinez, I., Williams, M., Boudier, F., Rodriguez, O., Chaduteau, C., Escario, S., Gouze, P., 2018. Evidence of polygenetic carbon trapping in the Oman Ophiolite: petro-structural, geochemical, and carbon and oxygen isotope study of the Wadi Dima harzburgite-hosted carbonates (Wadi Tayin massif, Sultanate of Oman). *Lithos* 323, 218–237.
- Nosouhian, N., Torabi, G., Arai, S., 2016. Amphibole-bearing listwaenites from the Paleozoic Bayazeh ophiolite (Central Iran). *Ital. J. Geosci.* 135, 109–119.
- Oelkers, E.H., Declercq, J., Saldi, G.D., Gislason, S.R., Schott, J., 2018. Olivine dissolution rates: a critical review. *Chem. Geol.* 500, 1–19.
- Oelkers, E.H., Gislason, S.R., Kelemen, P.B., 2023. Moving subsurface carbon mineral storage forward. *Carbon Capture Sci. Technol.* 6, 100098.
- Ohnmacht, W., 1974. Petrogenesis of Carbonate-orthopyroxenites (Sagvandites) and related rocks from Troms, Northern Norway. *J. Petrol.* 15, 303–324.
- Okamoto, A., Oyanagi, R., Yoshida, K., Uno, M., Shimizu, H., Satish-Kumar, M., 2021. Rupture of wet mantle wedge by self-promoting carbonation. *Commun. Earth Environ.* 2, 151.
- Okazaki, K., Michibayashi, K., Hatakeyama, K., Abe, N., Johnson, K.T.M., Kelemen, P.B., the Oman Drilling Project Science, T., 2021. Major mineral fraction and physical properties of carbonated peridotite (listvenite) from ICDP Oman Drilling Project Hole BT1B inferred from X-Ray CT core images. *J. Geophys. Res. Solid Earth* 126 e2021JB022719.
- Oskierski, H.C., Dlugogorski, B.Z., Jacobsen, G., 2013. Sequestration of atmospheric CO₂ in chrysotile mine tailings of the Woodsreef Asbestos Mine, Australia: quantitative mineralogy, isotopic fingerprinting and carbonation rates. *Chem. Geol.* 358, 156–169.
- Osselin, F., Pichavant, M., Champallier, R., Ulrich, M., Raimbourg, H., 2022a. Reactive transport experiments of coupled carbonation and serpentinization in a natural serpentinite. Implication for hydrogen production and carbon geological storage. *Geochim. Cosmochim. Acta* 318, 165–189.
- Osselin, F., Soulaire, C., Fauguerolles, C., Gaucher, E.C., Scaillet, B., Pichavant, M., 2022b. Orange hydrogen is the new green. *Nat. Geosci.* 15, 765–769.
- Paukert, A.N., Matter, J.M., Kelemen, P.B., Shock, E.L., Havig, J.R., 2012. Reaction path modeling of enhanced in situ CO₂ mineralization for carbon sequestration in the peridotite of the Samail Ophiolite, Sultanate of Oman. *Chem. Geol.* 330–331, 86–100.
- Peng, W., Zhang, L., Menzel, M.D., Vitale Brovarone, A., Tumiati, S., Shen, T., Hu, H., 2020. Multistage CO₂ sequestration in the subduction zone: Insights from exhumed carbonated serpentinites, SW Tianshan UHP belt, China. *Geochim. Cosmochim. Acta* 270, 218–243.
- Peuble, S., Andreani, M., Godard, M., Gouze, P., Barou, F., Van de Moortele, B., Mainprice, D., Reynard, B., 2015a. Carbonate mineralization in percolated olivine aggregates: linking effects of crystallographic orientation and fluid flow. *Am. Mineral.* 100, 474–482.
- Peuble, S., Godard, M., Luquot, L., Andreani, M., Martinez, I., Gouze, P., 2015b. CO₂ geological storage in olivine rich basaltic aquifers: new insights from reactive-percolation experiments. *Appl. Geochem.* 52, 174–190.
- Peuble, S., Andreani, M., Gouze, P., Pollet-Villard, M., Reynard, B., Van de Moortele, B., 2018. Multi-scale characterization of the incipient carbonation of peridotite. *Chem. Geol.* 476, 150–160.
- Peuble, S., Godard, M., Gouze, P., Leprovost, R., Martinez, I., Shilobreeva, S., 2019. Control of CO₂ on flow and reaction paths in olivine-dominated basements: an experimental study. *Geochim. Cosmochim. Acta* 252, 16–38.
- Plank, T., Manning, C.E., 2019. Subducting carbon. *Nature* 574, 343–352.
- Plümpner, O., Wallis, D., Teuling, F., Moulas, E., Schmalholz, S.M., Amiri, H., Müller, T., 2022. High-magnitude stresses induced by mineral-hydration reactions. *Geology* 50, 1351–1355.
- Power, I.M., Wilson, S.A., Dipple, G.M., 2013. Serpentinite carbonation for CO₂ sequestration. *Elements* 9, 115–121.
- Power, I.M., Harrison, A.L., Dipple, G.M., Wilson, S.A., Barker, S.L.L., Fallon, S.J., 2019. Magnesite formation in playa environments near Atlin, British Columbia, Canada. *Geochim. Cosmochim. Acta* 255, 1–24.
- Putnis, A., 2015. Transient porosity resulting from fluid–mineral interaction and its consequences. *Rev. Mineral. Geochem.* 80, 1–23.
- Putnis, A., 2021. Fluid–mineral interactions: controlling coupled mechanisms of reaction, mass transfer and deformation. *J. Petrol.* 62, egab092.
- Putnis, A., Putnis, C.V., 2007. The mechanism of reequilibration of solids in the presence of a fluid phase. *J. Solid State Chem.* 180, 1783–1786.
- Qiu, T., Zhu, Y., 2015. Geology and geochemistry of listwaenite-related gold mineralization in the Sayi gold deposit, Xinjiang, NW China. *Ore Geol. Rev.* 70, 61–79.
- Qiu, T., Zhu, Y., 2018. Listwaenite in the Sartohay ophiolitic mélange (Xinjiang, China): a genetic model based on petrology, U–Pb chronology and trace element geochemistry. *Lithos* 302–303, 427–446.
- Quesnel, B., Gautier, P., Cathelineau, M., Boulvais, P., Couteau, C., Drouillet, M., 2016. The internal deformation of the Peridotite Nappe of New Caledonia: a structural study of serpentine-bearing faults and shear zones in the Koniombo Massif. *J. Struct. Geol.* 85, 51–67.
- Rielli, A., Boschi, C., Dini, A., 2022. Tectonically driven carbonation of serpentinite by mantle CO₂: genesis of the Castiglione cello magnesite deposit in the Ligurian ophiolite of Central Tuscany (Italy). *Ore Geol. Rev.* 149, 105022.
- Robinson, P.T., Malpas, J., Zhou, M.-F., Ash, C., Yang, J.-S., Bai, W.-J., 2005. Geochemistry and Origin of Listwanites in the Sartohay and Luobusa Ophiolites, China. *Int. Geol. Rev.* 47, 177–202.
- Roedder, E., Bodnar, R.J., 1980. Geologic pressure determinations from fluid inclusion studies. *Annu. Rev. Earth Planet. Sci.* 8, 263–301.
- Røyne, A., Jamtveit, B., 2015. Pore-scale controls on reaction-driven fracturing. *Rev. Mineral. Geochem.* 80, 25–44.
- Rudge, J.F., Kelemen, P.B., Spiegelman, M., 2010. A simple model of reaction-induced cracking applied to serpentinization and carbonation of peridotite. *Earth Planet. Sci. Lett.* 291, 215–227.
- Saldi, G.D., Daval, D., Morvan, G., Knauss, K.G., 2013. The role of Fe and redox conditions in olivine carbonation rates: an experimental study of the rate limiting reactions at 90 and 150 °C in open and closed systems. *Geochim. Cosmochim. Acta* 118, 157–183.
- Sanna, A., Uibu, M., Caramanna, G., Kuusik, R., Maroto-Valer, M., 2014. A review of mineral carbonation technologies to sequester CO₂. *Chem. Soc. Rev.* 43, 8049–8080.
- Scambelluri, M., Bebout, G.E., Belmonte, D., Gilio, M., Campomenosi, N., Collins, N., Crispini, L., 2016. Carbonation of subduction-zone serpentinite (high-pressure ophiocarbonate; Ligurian Western Alps) and implications for the deep carbon cycling. *Earth Planet. Sci. Lett.* 441, 155–166.
- Schandl, E.S., Gorton, M.P., 2012. Hydrothermal alteration and CO₂ metasomatism (natural carbon sequestration) of komatiites in the south-western Abitibi greenstone belt. *Can. Mineral.* 50, 129–146.
- Schandl, E.S., Naldrett, A.J., 1992. CO₂ metasomatism of serpentinites, south of Timmins, Ontario. *Can. Mineral.* 30, 93–108.
- Scharf, A., Bailey, C.M., Bolhar, R., Mattern, F., Ring, U., 2022. Post-obduction listwaenite genesis in the Oman Mountains inferred from structural analysis and U–Pb carbonate dating. *Earth Planet. Sci. Lett.* 595, 117756.
- Scheller, E.L., Swindle, C., Grotzinger, J., Barnhart, H., Bhattacherjee, S., Ehlmann, B.L., Farley, K., Fischer, W.W., Greenberger, R., Ingalls, M., Martin, P.E., Osorio-Rodriguez, D., Smith, B.P., 2021. Formation of Magnesium Carbonates on Earth and Implications for Mars. *J. Geophys. Res. Planets* 126 e2021JE006828.
- Schreyer, W., Ohnmacht, W., Mannchen, J., 1972. Carbonate-orthopyroxenites (sagvandites) from Troms, northern Norway. *Lithos* 5, 345–364.
- Schroeder, T., Bach, W., Jöns, N., Jöns, S., Monien, P., Klügel, A., 2015. Fluid circulation and carbonate vein precipitation in the footwall of an oceanic core complex, Ocean Drilling Program Site 175, Mid-Atlantic Ridge. *Geochem. Geophys. Geosyst.* 16, 3716–3732.
- Schwartz, S., Guillot, S., Reynard, B., Lafay, R., Debret, B., Nicollet, C., Lanari, P., Auzende, A.L., 2013. Pressure-temperature estimates of the lizardite/antigorite transition in high pressure serpentinites. *Lithos* 178, 197–210.
- Schwarzenbach, E.M., Früh-Green, G.L., Bernasconi, S.M., Alt, J.C., Plas, A., 2013. Serpentinization and carbon sequestration: a study of two ancient peridotite-hosted hydrothermal systems. *Chem. Geol.* 351, 115–133.
- Sendula, E., Lamadrid, H.M., Rimstidt, J.D., Steele-MacInnis, M., Sublett, D.M., Aradi, L. E., Szabó, C., Caddick, M.J., Zajacz, Z., Bodnar, R.J., 2021. Synthetic Fluid Inclusions XXIV. In situ Monitoring of the Carbonation of Olivine Under Conditions Relevant to Carbon Capture and Storage Using Synthetic Fluid Inclusion Micro-Reactors: Determination of Reaction Rates. *Front. Climate* 3.
- Sieber, M.J., Hermann, J., Yaxley, G.M., 2018. An experimental investigation of C–O–H fluid-driven carbonation of serpentinites under forearc conditions. *Earth Planet. Sci. Lett.* 496, 178–188.
- Sieber, M.J., Yaxley, G.M., Hermann, J., 2020. Investigation of Fluid-driven carbonation of a hydrated, forearc mantle wedge using serpentinite cores in high-pressure experiments. *J. Petrol.* 61.
- Sieber, M.J., Yaxley, G.M., Hermann, J., 2022. COH-fluid induced metasomatism of peridotites in the forearc mantle. *Contrib. Mineral. Petrol.* 177, 44.
- Snæbjörnsdóttir, S.O., Sigfússon, B., Marieni, C., Goldberg, D., Gislason, S.R., Oelkers, E. H., 2020. Carbon dioxide storage through mineral carbonation. *Nat. Rev. Earth Environ.* 1, 90–102.
- Soret, M., Agard, P., Dubacq, B., Plunder, A., Yamato, P., 2017. Petrological evidence for stepwise accretion of metamorphic soles during subduction infancy (Semai ophiolite, Oman and UAE). *J. Metamorph. Geol.* 35, 1051–1080.

- Spandler, C., Hartmann, J., Faure, K., Mavrogenes, J.A., Arculus, R.J., 2008. The importance of talc and chlorite “hybrid” rocks for volatile recycling through subduction zones; evidence from the high-pressure subduction melange of New Caledonia. *Contrib. Mineral. Petrol.* 155, 181–198.
- Stanger, G., 1985. Silicified serpentinite in the Semail nappe of Oman. *Lithos* 18, 13–22.
- Steeffel, C.I., DePaolo, D.J., Lichtner, P.C., 2005. Reactive transport modeling: an essential tool and a new research approach for the Earth sciences. *Earth Planet. Sci. Lett.* 240, 539–558.
- Steele, A., Benning, L.G., Wirth, R., Schreiber, A., Araki, T., McCubbin, F.M., Fries, M.D., Nittler, L.R., Wang, J., Hallis, L.J., Conrad, P.G., Conley, C., Vitale, S., O'Brien, A.C., Riggi, V., Rogers, K., 2022. Organic synthesis associated with serpentinization and carbonation on early Mars. *Science* 375, 172–177.
- Stünitz, H., Neufeld, K., Heilbronner, R., Finstad, A.K., Konopásek, J., Mackenzie, J.R., 2020. Transformation weakening: diffusion creep in eclogites as a result of interaction of mineral reactions and deformation. *J. Struct. Geol.* 139, 104129.
- Sverjensky, D.A., 2019. Thermodynamic modeling of fluids from surficial to Mantle Conditions. *J. Geol. Soc. Lond.* 176, 348–374.
- Sverjensky, D.A., Harrison, B., Azzolini, D., 2014. Water in the deep Earth: the dielectric constant and the solubilities of quartz and corundum to 60 kb and 1200 °C. *Geochim. Cosmochim. Acta* 129, 125–145.
- Tarling, M.S., Smith, S.A.F., Scott, J.M., Rooney, J.S., Viti, C., Gordon, K.C., 2019. The internal structure and composition of a plate-boundary-scale serpentinite shear zone: the Livingstone Fault, New Zealand. *Solid Earth* 10, 1025–1047.
- Templeton, A.S., Ellison, E.T., Kelemen, P.B., Leong, J., Boyd, E.S., Colman, D.R., Matter, J.M., 2024. Low-temperature hydrogen production and consumption in partially-hydrated peridotites in Oman: implications for stimulated geological hydrogen production. *Front. Geochem.* 2.
- Ternieten, L., Früh-Green, G.L., Bernasconi, S.M., 2021a. Carbon geochemistry of the active serpentinization site at the Wadi Tayin Massif: insights from the ICDP Oman Drilling Project: phase II. *J. Geophys. Res. Solid Earth* 126 e2021JB022712.
- Ternieten, L., Früh-Green, G.L., Bernasconi, S.M., 2021b. Distribution and sources of Carbon in Serpentinized Mantle Peridotites at the Atlantis Massif (IODP Expedition 357). *J. Geophys. Res. Solid Earth* 126 e2021JB021973.
- Tiraboschi, C., Tumiati, S., Sverjensky, D., Pettke, T., Ulmer, P., Poli, S., 2017. Experimental determination of magnesia and silica solubilities in graphite-saturated and redox-buffered high-pressure COH fluids in equilibrium with forsterite + enstatite and magnesite + enstatite. *Contrib. Mineral. Petrol.* 173, 2.
- Tominaga, M., Beinlich, A., Lima, E.A., Tivey, M.A., Hampton, B.A., Weiss, B., Harigane, Y., 2017. Multi-scale magnetic mapping of serpentinite carbonation. *Nat. Commun.* 8, 1870.
- Tominaga, M., Beinlich, A., Lima, E.A., Pruett, P., Vento, N.R., Weiss, B.P., 2023. High-Resolution Magnetic-Geochemical Mapping of the Serpentinized and Carbonated Atlin Ophiolite, British Columbia: Toward Establishing Magnetometry as a Monitoring Tool for In Situ Mineral Carbonation. *Geochem. Geophys. Geosyst.* 24 e2022GC010730.
- Tumiati, S., Tiraboschi, C., Miozzi, F., Vitale-Brovarone, A., Manning, C.E., Sverjensky, D.A., Milani, S., Poli, S., 2020. Dissolution susceptibility of glass-like carbon versus crystalline graphite in high-pressure aqueous fluids and implications for the behavior of organic matter in subduction zones. *Geochim. Cosmochim. Acta* 273, 383–402.
- Tutolo, B.M., Mildner, D.F.R., Gagnon, C.V.L., Saar, M.O., Seyfried Jr., W.E., 2016. Nanoscale constraints on porosity generation and fluid flow during serpentinization. *Geology* 44, 103–106.
- Ueda, H., Sawaki, Y., Maruyama, S., 2017. Reactions between olivine and CO₂-rich seawater at 300 °C: implications for H₂ generation and CO₂ sequestration on the early Earth. *Geosci. Front.* 8, 387–396.
- Ulrich, M., Muñoz, M., Guillot, S., Cathelineau, M., Picard, C., Quesnel, B., Boulvais, P., Couteau, C., 2014. Dissolution-precipitation processes governing the carbonation and silicification of the serpentinite sole of the New Caledonia ophiolite. *Contrib. Mineral. Petrol.* 167, 952.
- Uno, M., Koyanagawa, K., Kasahara, H., Okamoto, A., Tsuchiya, N., 2022. Volatile-consuming reactions fracture rocks and self-accelerate fluid flow in the lithosphere. *Proc. Natl. Acad. Sci.* 119 e2110776118.
- Urai, J.L., Feenstra, A., 2001. Weakening associated with the diasporite-corundum dehydration reaction in metabauxites: an example from Naxos (Greece). *J. Struct. Geol.* 23, 941–950.
- van Keken, P.E., Wilson, C.R., 2023. An introductory review of the thermal structure of subduction zones: III—Comparison between models and observations. *Prog. Earth Planet. Sci.* 10, 57.
- van Noort, R., Spiers, C.J., Drury, M.R., Kandianis, M.T., 2013. Peridotite dissolution and carbonation rates at fracture surfaces under conditions relevant for in situ mineralization of CO₂. *Geochim. Cosmochim. Acta* 106, 1–24.
- Wang, J.-Y., Santosh, M., 2019. Eoarchean to Mesoarchean crustal evolution in the Dharwar craton, India: evidence from detrital zircon U-Pb and Hf isotopes. *Gondwana Res.* 72, 1–14.
- Wyllie, P.J., Huang, W.L., Otto, J., Byrnes, A.P., 1983. Carbonation of peridotites and decarbonation of siliceous dolomites represented in the system CaO-MgO-SiO₂-CO₂ to 30 kbar. *Tectonophysics* 100, 359–388.
- Zhang, L., Yang, J., Robinson, P.T., Xiong, F., Chen, Y., Lai, S., Chen, M., 2015. Origin of Listwanite in the Luobusa Ophiolite, Tibet, Implications for Chromite Stability in Hydrothermal Systems. *Acta Geol. Sin. - Engl. Ed.* 89, 402–417.
- Zheng, X., Cordonnier, B., Zhu, W., Renard, F., Jamtveit, B., 2018. Effects of confinement on reaction-induced fracturing during hydration of periclase. *Geochem. Geophys. Geosyst.* 19, 2661–2672.
- Zhu, W., Fusses, F., Lisabeth, H., Xing, T., Xiao, X., De Andrade, V., Karato, S.-I., 2016. Experimental evidence of reaction-induced fracturing during olivine carbonation. *Geophys. Res. Lett.* 43, 9535–9543.